

**NONLINEAR DYNAMICS AND SYSTEMS THEORY**

An International Journal of Research and Surveys

Volume 21                      Number 3                      2021

**CONTENTS**

**PERSONAGE IN SCIENCE**

Academician A.A. Martynyuk. To the 80th Birthday Anniversary..... 225

Design and Analysis of Continuous Positive Airway Pressure Valve  
Using a 3D Printing and Computational Fluid Dynamic..... 229

*S. Bentouati, Mohamed Islem Soualhi,  
Abdellah Abdellah El-Hadj and Hamid Yeklef*

Asymptotic Stability of Some Class of Affine Nonlinear Control  
Systems through Partial Feedback Linearization..... 238

*Firman, Syamsuddin Toaha, Muh Nur*

Dynamical Behaviors of Fractional-Order Selkov Model and Its  
Discretization ..... 246

*T. Houmor, H. Zerimeche and A. Berkane*

DTC-SVM Sensorless Control of Five-Phase Induction Motor Based  
on Two Different Rotor Speed Estimation Approaches ..... 262

*B. S. Khaldi, A. Kouzou, M. O. Mahmoudi and D. Boukhetala*

A Dynamic Contact Problem for Elasto-Viscoplastic Piezoelectric  
Materials with Normal Compliance, Normal Damped Response  
and Damage ..... 280

*L. Maiza, T. Hadj Ammar and M. Said Ameur*

Trajectory Tracking of Coordinated Multi-Robot Systems using  
Nonlinear Model Predictive Control..... 303

*H. Purnawan, S. Subchan, D. Adzkiya and T. Asfihani*

Flow and Heat Transfer of a Non-Newtonian Power-Law Fluid over  
a Non-Linearly Stretching Sheet with Thermal Radiation and Aligned  
Magnetic Field ..... 315

*A. Rani, P. Singh and Mani Mala*

Mathematical Study of a Modified SEIR Model for the Novel  
SARS-Cov-2 Coronavirus ..... 326

*Abdelhamid Zaghdani*

NONLINEAR DYNAMICS & SYSTEMS THEORY

Volume 21, No. 3, 2021

# Nonlinear Dynamics and Systems Theory

**An International Journal of Research and Surveys**

**EDITOR-IN-CHIEF A.A.MARTYNYUK**

*S.P.Timoshenko Institute of Mechanics  
National Academy of Sciences of Ukraine, Kiev, Ukraine*

**MANAGING EDITOR I.P.STAVROULAKIS**

*Department of Mathematics, University of Ioannina, Greece*

**REGIONAL EDITORS**

P.BORNE, Lille, France  
M.FABRIZIO, Bologna, Italy  
*Europe*

M.BOHNER, Rolla, USA  
HAO WANG, Edmonton, Canada  
*USA and Canada*

T.A.BURTON, Port Angeles, USA  
C.CRUIZ-HERNANDEZ, Ensenada, Mexico  
*USA and Latin America*

M.ALQURAN, Irbid, Jordan  
*Jordan and Middle East*

K.L.TEO, Perth, Australia  
*Australia and New Zealand*

# Nonlinear Dynamics and Systems Theory

An International Journal of Research and Surveys

## EDITOR-IN-CHIEF A.A.MARTYNYUK

The S.P.Timoshenko Institute of Mechanics, National Academy of Sciences of Ukraine,  
Nesterov Str. 3, 03680 MSP, Kiev-57, UKRAINE / e-mail: journalndst@gmail.com

## MANAGING EDITOR I.P.STAVROULAKIS

Department of Mathematics, University of Ioannina  
451 10 Ioannina, HELLAS (GREECE) / e-mail: ipstav@cc.uoi.gr

## ADVISORY EDITOR A.G.MAZKO

Institute of Mathematics of NAS of Ukraine, Kiev (Ukraine)  
e-mail: mazko@imath.kiev.ua

## REGIONAL EDITORS

M.ALQURAN (Jordan), e-mail: marwan04@just.edu.jo  
P.BORNE (France), e-mail: Pierre.Borne@ec-lille.fr  
M.BOHNER (USA), e-mail: bohner@mst.edu  
T.A.BURTON (USA), e-mail: taburton@olympen.com  
C. CRUZ-HERNANDEZ (Mexico), e-mail: ccruz@cicese.mx  
M.FABRIZIO (Italy), e-mail: mauro.fabrizio@unibo.it  
HAO WANG (Canada), e-mail: hao8@ualberta.ca  
K.L.TEO (Australia), e-mail: K.L.Teo@curtin.edu.au

## EDITORIAL BOARD

Aleksandrov, A.Yu. (Russia)	Jafari, H. (South African Republic)
Artstein, Z. (Israel)	Khusainov, D.Ya. (Ukraine)
Awrejcewicz, J. (Poland)	Kloedon, P. (Germany)
Benrejeb, M. (Tunisia)	Kokologiannaki, C. (Greece)
Braiek, N.B. (Tunisia)	Krishnan, E.V. (Oman)
Chen Ye-Hwa (USA)	Limarchenko, O.S. (Ukraine)
D'Anna, A. (Italy)	Nguang Sing Kiong (New Zealand)
De Angelis, M. (Italy)	Okninski, A. (Poland)
Denton, Z. (USA)	Peterson, A. (USA)
Vasundhara Devi, J. (India)	Radziszewski, B. (Poland)
Djemai, M. (France)	Shi Yan (Japan)
Dshalalow, J.H. (USA)	Sivasundaram, S. (USA)
Eke, F.O. (USA)	Sree Hari Rao, V. (India)
Gajic Z. (USA)	Staicu V. (Portugal)
Georgiou, G. (Cyprus)	Stavrakakis, N.M. (Greece)
Herlambang T. (Indonesia)	Vatsala, A. (USA)
Honglei Xu (Australia)	Zuyev, A.L. (Germany)
Izobov, N.A. (Belarussia)	

## ADVISORY COMPUTER SCIENCE EDITORS

A.N.CHERNIENKO and A.S.KHOROSHUN, Kiev, Ukraine

## ADVISORY LINGUISTIC EDITOR

S.N.RASSHYVALOVA, Kiev, Ukraine

## INSTRUCTIONS FOR CONTRIBUTORS

**(1) General.** Nonlinear Dynamics and Systems Theory (ND&ST) is an international journal devoted to publishing peer-refereed, high quality, original papers, brief notes and review articles focusing on nonlinear dynamics and systems theory and their practical applications in engineering, physical and life sciences. Submission of a manuscript is a representation that the submission has been approved by all of the authors and by the institution where the work was carried out. It also represents that the manuscript has not been previously published, has not been copyrighted, is not being submitted for publication elsewhere, and that the authors have agreed that the copyright in the article shall be assigned exclusively to InforMath Publishing Group by signing a transfer of copyright form. Before submission, the authors should visit the website:

<http://www.e-ndst.kiev.ua>

for information on the preparation of accepted manuscripts. Please download the archive Sample\_NDST.zip containing example of article file (you can edit only the file Samplefilename.tex).

**(2) Manuscript and Correspondence.** Manuscripts should be in English and must meet common standards of usage and grammar. To submit a paper, send by e-mail a file in PDF format directly to

Professor A.A. Martynyuk, Institute of Mechanics,  
Nesterov str.3, 03057, MSP 680, Kiev-57, Ukraine  
e-mail: journalndst@gmail.com

or to one of the Regional Editors or to a member of the Editorial Board. Final version of the manuscript must typeset using LaTeX program which is prepared in accordance with the style file of the Journal. Manuscript texts should contain the title of the article, name(s) of the author(s) and complete affiliations. Each article requires an abstract not exceeding 150 words. Formulas and citations should not be included in the abstract. AMS subject classifications and key words must be included in all accepted papers. Each article requires a running head (abbreviated form of the title) of no more than 30 characters. The sizes for regular papers, survey articles, brief notes, letters to editors and book reviews are: (i) 10-14 pages for regular papers, (ii) up to 24 pages for survey articles, and (iii) 2-3 pages for brief notes, letters to the editor and book reviews.

**(3) Tables, Graphs and Illustrations.** Each figure must be of a quality suitable for direct reproduction and must include a caption. Drawings should include all relevant details and should be drawn professionally in black ink on plain white drawing paper. In addition to a hard copy of the artwork, it is necessary to attach the electronic file of the artwork (preferably in PCX format).

**(4) References.** Each entry must be cited in the text by author(s) and number or by number alone. All references should be listed in their alphabetic order. Use please the following style:

Journal: [1] H. Poincare, Title of the article. *Title of the Journal* **volume**  
(issue) (year) pages. [Language]

Book: [2] A.M. Lyapunov, *Title of the Book*. Name of the Publishers, Town, year.

Proceeding: [3] R. Bellman, Title of the article. In: *Title of the Book*. (Eds.).  
Name of the Publishers, Town, year, pages. [Language]

**(5) Proofs and Sample Copy.** Proofs sent to authors should be returned to the Editorial Office with corrections within three days after receipt. The corresponding author will receive a sample copy of the issue of the Journal for which his/her paper is published.

**(6) Editorial Policy.** Every submission will undergo a stringent peer review process. An editor will be assigned to handle the review process of the paper. He/she will secure at least two reviewers' reports. The decision on acceptance, rejection or acceptance subject to revision will be made based on these reviewers' reports and the editor's own reading of the paper.

# NONLINEAR DYNAMICS AND SYSTEMS THEORY

An International Journal of Research and Surveys  
Published by InforMath Publishing Group since 2001

Volume 21

Number 3

2021

## CONTENTS

### PERSONAGE IN SCIENCE

- Academician A.A. Martynyuk. To the 80th Birthday Anniversary . . . . 225
- Design and Analysis of Continuous Positive Airway Pressure Valve  
Using a 3D Printing and Computational Fluid Dynamic . . . . . 229  
*S. Bentouati, Mohamed Islem Soualhi,  
Abdellah Abdellah El-Hadj and Hamid Yeklef*
- Asymptotic Stability of Some Class of Affine Nonlinear Control  
Systems through Partial Feedback Linearization . . . . . 238  
*Firman, Syamsuddin Toaha, Muh Nur*
- Dynamical Behaviors of Fractional-Order Selkov Model and Its  
Discretization . . . . . 246  
*T. Houmor, H. Zerimeche and A. Berkane*
- DTC-SVM Sensorless Control of Five-Phase Induction Motor Based  
on Two Different Rotor Speed Estimation Approaches . . . . . 262  
*B. S. Khaldi, A. Kouzou, M. O. Mahmoudi and D. Boukhetala*
- A Dynamic Contact Problem for Elasto-Viscoplastic Piezoelectric  
Materials with Normal Compliance, Normal Damped Response  
and Damage . . . . . 280  
*L. Maiza, T. Hadj Ammar and M. Said Ameer*
- Trajectory Tracking of Coordinated Multi-Robot Systems using  
Nonlinear Model Predictive Control . . . . . 303  
*H. Purnawan, S. Subchan, D. Adzkiya and T. Asfihani*
- Flow and Heat Transfer of a Non-Newtonian Power-Law Fluid over  
a Non-Linearly Stretching Sheet with Thermal Radiation and Aligned  
Magnetic Field . . . . . 315  
*A. Rani, P. Singh and Mani Mala*
- Mathematical Study of a Modified SEIR Model for the Novel  
SARS-Cov-2 Coronavirus . . . . . 326  
*Abdelhamid Zaghdani*

*Founded by A.A. Martynyuk in 2001.*

*Registered in Ukraine Number: KB No 5267 / 04.07.2001.*

# NONLINEAR DYNAMICS AND SYSTEMS THEORY

An International Journal of Research and Surveys

*Impact Factor from SCOPUS for 2019: SJR – 0.328, SNIP – 0.591 and CiteScore – 1.4*

**Nonlinear Dynamics and Systems Theory** (ISSN 1562–8353 (Print), ISSN 1813–7385 (Online)) is an international journal published under the auspices of the S.P. Timoshenko Institute of Mechanics of National Academy of Sciences of Ukraine and Curtin University of Technology (Perth, Australia). It aims to publish high quality original scientific papers and surveys in areas of nonlinear dynamics and systems theory and their real world applications.

## AIMS AND SCOPE

**Nonlinear Dynamics and Systems Theory** is a multidisciplinary journal. It publishes papers focusing on proofs of important theorems as well as papers presenting new ideas and new theory, conjectures, numerical algorithms and physical experiments in areas related to nonlinear dynamics and systems theory. Papers that deal with theoretical aspects of nonlinear dynamics and/or systems theory should contain significant mathematical results with an indication of their possible applications. Papers that emphasize applications should contain new mathematical models of real world phenomena and/or description of engineering problems. They should include rigorous analysis of data used and results obtained. Papers that integrate and interrelate ideas and methods of nonlinear dynamics and systems theory will be particularly welcomed. This journal and the individual contributions published therein are protected under the copyright by International InforMath Publishing Group.

## PUBLICATION AND SUBSCRIPTION INFORMATION

**Nonlinear Dynamics and Systems Theory** will have 4 issues in 2021, printed in hard copy (ISSN 1562–8353) and available online (ISSN 1813–7385), by InforMath Publishing Group, Nesterov str., 3, Institute of Mechanics, Kiev, MSP 680, Ukraine, 03057. Subscription prices are available upon request from the Publisher, EBSCO Information Services (<mailto:journals@ebSCO.com>), or website of the Journal: <http://e-ndst.kiev.ua>. Subscriptions are accepted on a calendar year basis. Issues are sent by airmail to all countries of the world. Claims for missing issues should be made within six months of the date of dispatch.

## ABSTRACTING AND INDEXING SERVICES

Papers published in this journal are indexed or abstracted in: Mathematical Reviews / MathSciNet, Zentralblatt MATH / Mathematics Abstracts, PASCAL database (INIST–CNRS) and SCOPUS.



## PERSONAGE IN SCIENCE

# Academician A.A. Martynyuk

*to the 80th Birthday Anniversary*

March 6, 2021 marked the 80th anniversary of the birth and 57 years of scientific activity of the famous Ukrainian scientist, Head of the Department of Process Stability of the S.P. Tymoshenko Institute of Mechanics of the National Academy of Sciences of Ukraine (NAS of Ukraine), Doctor of Physical and Mathematical Sciences, Professor Anatoliy Andriyovych Martynyuk.

A.A. Martynyuk was born in 1941 in the village of Ganzhalivka, Cherkasy region, in the family of a railway worker. He graduated from the Faculty of Physics and Mathematics of Cherkasy State Pedagogical Institute.

He has been working at the Institute of Mechanics of the National Academy of Sciences of Ukraine as the Head of the Department of Process Stability from 1978 to the present (in 1973 - 1977 A.A. Martyniuk worked at the Institute of Mathematics of the National Academy of Sciences of Ukraine).

He defended his Ph.D. (1967) and doctoral (1973) theses and was awarded the title of professor (1985).

He was elected a Corresponding Member of the National Academy of Sciences of Ukraine (1988), and then Academician of the National Academy of Sciences of Ukraine (2009).

Detailed biographical data are given in article <sup>1</sup> and book <sup>2</sup>.

During 2011 – 2020, A.A. Martynyuk was carrying out significant work related to the preparation for publication of generalized monographs and books. Namely:

\* Books XXVI, XXVII present the results of the development of the direct Lyapunov method - the stability study of systems with uncertain values of parameters, which are described by continuous, pulse and singularly perturbed equations, as well as dynamic equations on a time scale;

\* Book XXVIII describes the methods of qualitative analysis of the perturbed motion of systems, the behavior of which is described by equations containing a small parameter;

\* In book XXIX, on the basis of the matrix-valued Lyapunov function, a direct method for studying the motion stability of systems described by nonlinear equations under structural perturbations of parameters has been developed;

\* Book XXX is the second edition of the book of the same name, published in 1989 by Marcel Dekker Inc., USA. The second edition is supplemented by the estimation of solutions to nonlinear systems on the basis of nonlinear integral inequalities, the criterion

<sup>1</sup>Academician A.A. Martynyuk (*to the seventieth anniversary of his birth*) // *Nonlinear Dynamics and Systems Theory*. — 2011. — **11**, 1. — P. 1 - 5.

<sup>2</sup>A.A. Martynyuk. *Revisiting the Past with Neither Indifference nor Resentment*. — Kiev: Phoenix, 2014. — 139 p.

of asymptotic stability for nonlinear autonomous comparison systems and the replacement of Chapter 5, which is devoted to the application of general methods described in the book;

\* Monograph XXXI is the first in the world mathematical literature, which deals with the development of methods for studying the stability of solutions of dynamic equations on a time scale;

\* In monograph XXXII, the equations of perturbed motion with multivalued right-hand parts are considered. To study the stability of the set of solutions of such systems, a new variant of the direct Lyapunov method was developed on the basis of a matrix-valued auxiliary function;

\* Book XXXIII presents the results of the stability analysis of hybrid systems: on a time scale, with aftereffect, in metric space. The dynamics of shock systems is studied on the basis of new qualitative methods of analysis of such systems;

\* Book XXXIV is an educational and encyclopedic edition, 12 chapters of which contain a summary of classical and modern results of the theory of motion stability and their application in mechanics. The book is based on the original results of the authors, which were published in 1969 - 2019.

Along with his intensive scientific research (A.A. Martynyuk is the author (co-author) of more than 450 journal publications and 34 monographs and books in English, Chinese and Russian), he is active in publishing. He did a great job as the editor of the International Series of Scientific Monographs "Stability and Control: Theory, Methods and Applications" at Gordon and Breach Science Publishers (UK). Between 1992 and 2002, 22 volumes of scientific monographs by the scientists from 10 countries were published in this series.

In 2001, A.A. Martynyuk founded the International Scientific Journal "Nonlinear Dynamics and Systems Theory" and is its editor.

In 2006, he founded a new International series of scientific monographs, textbooks and lecture courses entitled "Stability, Oscillation and Optimization of Systems" at Cambridge Scientific Publishers (UK) and is its editor together with Professor P. Borne (France) ) and Professor C. Cruz-Hernandez (USA). So far, 11 volumes of this series have been published.

A.A. Martynyuk is a member of the editorial boards of three Ukrainian journals: "Applied Mechanics", "Nonlinear Oscillations" and "Electronic Modeling" and two English-language journals: "Journal of Applied Mathematics and Stochastic Analysis" (USA) and "Differential Equations and Dynamical Systems" (Germany).

A.A. Martynyuk prepared 28 candidates and 4 doctors of physical and mathematical sciences. He is the Deputy Chairman of the National Committee for Theoretical and Applied Mechanics of Ukraine.

In 2008, A.A. Martynyuk was awarded the State Prize of Ukraine in the field of science and technology.

The editorial board of the Journal "Nonlinear Dynamics and Systems Theory" sincerely congratulates Anatoliy Andriyovych on his jubilee, wishes him health and new successes in his multifaceted activity.

### List of Monographs and Books by A.A. Martynyuk (Continued)<sup>3</sup>

<sup>3</sup> The titles I-XXV were published in the Journal *Nonlinear Dynamics and Systems Theory*, Vol. 11, issue 1, 2011.

XXVI. Uncertain Dynamical Systems. Stability and Motion Control, (with Yu.A. Martynyuk-Chernienko and Sun Zhen qi), Bending: Science Press, 2011. – 237 p. (translation from Russian into Chinese).

XXVII. Uncertain Dynamical Systems. Stability and Motion Control, (with Yu.A. Martynyuk-Chernienko), Boca Raton: CRC Press, 2012. — 296 p.

XXVIII. Weakly Connected Nonlinear Systems. Boundedness and Stability of Motion, (with L. Chernetskaya, and V.Martynyuk), Boca Raton: CRC Press, 2013. — 212 p.

XXIX. Stability Analysis of Nonlinear Systems under Structural Perturbations, (with V.G. Miladzhnov), Cambridge: Cambridge Scientific Publishers, 2014. — 253 p.

XXX. Stability Analysis of Nonlinear Systems, Second Edition (with, V. Lakshmikantham and S. Leela), Cham: Springer International Publishing Switzerland, 2015. — 329 p.

XXXI. Stability Theory for Dynamic Equations on Time Scales, Cham: Springer International Publishing Switzerland, 2016. — 223 p.

XXXII. Qualitative Analysis of Set-Valued Differential Equations, Cham: Springer Nature Switzerland, 2019. — 198 p.

XXXIII. Dynamics and Stability of Motion of Shock and Hybrid Systems, (with B. Radziszewski and A. Szadkowski), Warsaw: de Gruyter/SCIENDO, 2019. — 193 p.

XXXIV. Stability: Elements of the Theory and Applications with Examples, (with B. Radziszewski and A. Szadkowski), Warsaw: de Gruyter/SCIENDO, 2020. — 328 p.

#### List of Papers by A.A. Martynyuk (Continued)<sup>4</sup>

146. Asymptotic stability criterion for nonlinear monotonic systems and its applications (Review). Int. Appl. Mech., vol. 47, No. 5, 2011. — pp. 475–534.

147. On stabilization of systems with aftereffect by impulse disturbances. Dopov. Nat. Acad. Nauk Ukr. — 2012, No. 9. — pp. 62–65.

148. Instability of motion under interval initial conditions. Dopov. Nat. Acad. Nauk Ukr. — 2013, No. 11. — pp. 55–60.

149. On the stability of motion under interval initial conditions. Dopov. Nat. Acad. Nauk Ukr. — 2013, No. 1. — pp. 47–52.

150. On the stability of an impulse system with aftereffect with respect to two measures. Nonlinear Oscillations. — 2013. — 16, No. 4. — pp. 538–556.

151. On the stability of the trajectories of the set of difference equations. Dopov. Nat. Acad. Nauk. — 2014, No. 5. — pp. 65–69.

152. Direct Lyapunov method on time scales. Communications in Applied Analysis. — 2013, 17, No. 3 and 4. — pp. 483–502.

153. Novel bounds for solutions of nonlinear differential equations. Appl. Math. — 2015, No. 6. pp. 182–194.

154. On stability with respect to two measures of a system of equations with fractional derivatives. Nonlinear Oscillations. — 2015. — 18, No. 2. — pp. 238–244.

155. Elements of the theory of stability of hybrid systems (Review). Int. Appl. Mech., vol. 51, No. 3, 2015. — pp. 243–302.

<sup>4</sup>The titles 1–129 were published in the Journal *Nonlinear Dynamics and Systems Theory*, Vol. 6, issue 1, 2006, and the titles 130–145 were published in the Journal *Nonlinear Dynamics and Systems Theory*, Vol. 11, issue 1, 2011.

156. Analysis of a set of trajectories of generalized standard systems: Averaging technique. *Nonlinear Dynamics and Systems Theory*. — 2017 — 17, No. 1. — pp. 29–41.
157. Constructive estimates of Lyapunov V-function for perturbed equations of motion. *Int. Appl. Mech.*, vol. 53, No. 5, 2017 — pp. 588–594.
158. Deviation of a set of trajectories from a state of equilibrium. *Dopov. Nat. Acad. Nauk Ukr.* — 2017, No. 10. — pp. 10–15.
159. Invariance of solutions to a family of regularized equations. *Dopov. Nat. Acad. Nauk Ukr.* — 2017, No. 12. — pp. 3–7.
160. Fractional-like derivative of Hukuhara and its properties. *Dopov. Nat. Acad. Nauk Ukr.* — 2019, No. 4. — pp. 10–16.
161. On application of mixed Minkowski volumes in qualitative theory of set differential equations. *Global and Stochastic Analysis*. — 2018. Vol. 5. No. 1. — pp. 39–44.
162. Hyers-Ulam-Rassias-stability conditions for families of equations. *Dopov. Nat. Acad. Nauk Ukr.* — 2017, No. 8. — pp. 11–16.
163. Comparison principle and estimates of Lyapunov functions for nonlinear systems. *Dopov. Nat. Acad. Nauk Ukr.* — 2018, No. 9. — pp. 3–11.
164. Dynamic analysis of the set trajectories of a family of equations of motion based on Minkowski mixed volumes. *Int. Appl. Mech.*, vol. 54, No. 4, 2018 — pp. 418–430.
165. Estimation of the Lyapunov function on solutions of quasilinear fractional-like systems. *Dopov. Nat. Acad. Nauk Ukr.* — 2020, No. 11. — pp. 3–8.
166. A.M. Lyapunov's direct method based on matrix auxiliary functions: 40 years of development (review). *Int. Appl. Mech.* — 2020, No. 3, vol. 56, — pp. 3–75.

**Editorial board of the Journal**  
*Nonlinear Dynamics and Systems Theory*



# Design and Analysis of Continuous Positive Airway Pressure Valve Using a 3D Printing and Computational Fluid Dynamic

S. Bentouati<sup>1\*</sup>, Mohamed Islem Soualhi<sup>2</sup>, Abdellah Abdellah El-Hadj<sup>1</sup>  
and Hamid Yeklef<sup>3</sup>

<sup>1</sup> *Laboratory of Mechanics, Physics, Mathematical Modeling (LMP2M), University of Medea, Medea 26000, Algeria.*

<sup>2</sup> *Hospital of Ouargla, Intensive Care Unit, Algeria.*

<sup>3</sup> *Hospital Mohamed Boudiaf of Medea, Medical Equipment Maintenance Service, Algeria.*

Received: March 10, 2021; Revised: May 5, 2021

**Abstract:** The non-invasive ventilatory support in the Coronavirus (COVID-19) treatment uses also a mask as an interface between the medical device and the patient. The choice of this interface is one of the fundamental elements for the successful implementation of these techniques. The use of suitable equipment is also essential for their success, especially in continuous positive pressure with the mask (CPAP-continuous positive airway pressure) or during non-invasive two-level pressure ventilation. The criteria such as the ease of use and the required performance must be brought together in the medical equipment. With this aim, we will design a new version of the CPAP valve using the 3D printer, we used also the ANSYS software for the analysis and computation of the flow (CFD).

**Keywords:** *continuous positive airway pressure system; non-invasive ventilation; 3-dimensional printing; computational fluid dynamic.*

**Mathematics Subject Classification (2010):** 93A10, 93C95, 70K99.

---

\* Corresponding author: <mailto:bentouati.smain@gmail.com>

## 1 Introduction

Ventilation is the only known treatment available for people with pulmonary failure caused by COVID-19. The resuscitation machines, that are at the disposal of hospitals, are complex and very expensive. Their availability is far from being close enough to meet the large number of patients received. For example, in our intensive care unit (in Medea, Algeria) we have around 7 machines that are currently functioning. So, given a large number of coronavirus patients that threaten to overwhelm our medical services, critically ill patients without ventilation treatment are at risk of losing their lives. To prevent this, we have designed CPAP (Continuous Positive Airway Pressure) valves, which help with artificial ventilation. The ventilatory assistance applied to patients in acute respiratory distress by NIV (non-invasive ventilation) is a very effective technique to avoid tracheal intubation [1,2]. In this pandemic situation, the decathlon face mask (diving mask) is transformed to be used for medical purposes. We used it as the interface between the patient with coronavirus (Covid-19) and the valve we designed. It is therefore integrated in the kit shown in Figure 1. This valve is used to maintain continuous positive pressure throughout the respiratory cycle (during inspiration and expiration), which keeps the lungs open. NIV is an essential therapeutic mode in resuscitation and the evaluation of its practical use is very important and gives good results when controlling APE (Acute Pulmonary Edema) [3-5].



**Figure 1:** Yellow CPAP valve integrated in the kit, including, in particular, a pressure gauge (OHMEDA) and a ball flow meter which can vary from 0 to 30 l/min.

For the operation of the CPAP breathing valve, the quantity of oxygen arriving in an annular chamber is accelerated to the speed of sound as it passes through the microcannulas. This generates a high velocity flow in the center of the tube, which creates a zone of turbulence with the effect of separating the patient's respiratory volume (lungs and dead volume) from the outside air, without creating an airflow for the patient. It is the patient who will call for an air-oxygen mixture during inspiration. As we can see in Figure 2, the CPAP valve, which we manufactured in our laboratory using a 3D printer, is open on the atmospheric air side and works according to the Venturi effect. The turbulence zone acts as a virtual two-way valve that keeps the lungs under pressure during inspiration and creates a brake at expiration [6].

Finally, in this work, we will design a new version of the CPAP valve using the 3D

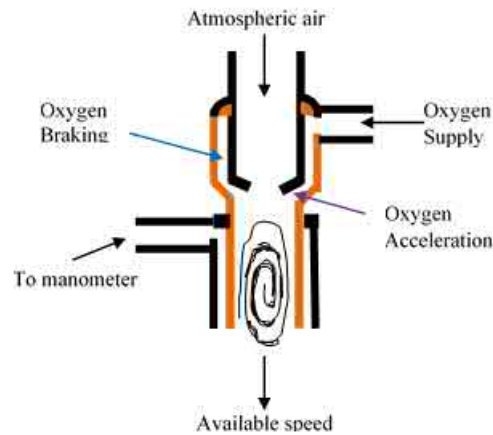


**Figure 2:** Diagram of the Boussignac CPAP System.

printer, the ANSYS software will be used for the analysis of the flow and the optimization of the parameters of this valve.

## 2 The CPAP Treatment Principle

For respiratory failure, the CPAP offers pupil oxygen levels, so it is attached to a flow of  $O_2$ , see Figure 3. In our case,  $O_2$  is delivered to the patient by means of a diving mask, and the expiratory pressures are set above atmospheric pressure, therefore patients will breathe spontaneously during CPAP. The therapeutic use of CPAP is based on the delivery of high  $O_2$  flow ( $FiO_2$  from 35% to 90%) creating positive pressures of the respiratory tract which attract the open alveoli during the expiratory phase of the respiration allowing a longer time for exchanged gases. This results in physiological effects at high flow [7].

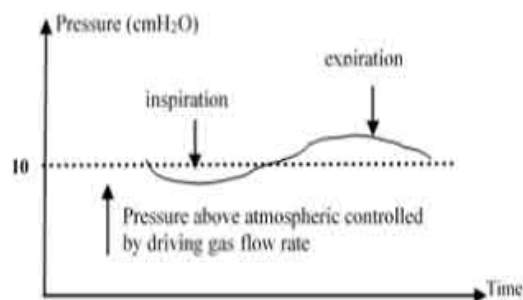


**Figure 3:** Profile of CPAP [7].

### 3 The CPAP Valve Design

CPAP is a ventilatory mode allowing to maintain in the airways a pressure higher than atmospheric pressure at the end of expiration [8, 9]. In spontaneous ventilation, the name is CPAP. In pre-hospital care, spontaneous positive pressure ventilation is indicated mainly in hemodynamic pulmonary edema (OAP) [10,11] when it is not possible to obtain a correct haematosis despite the  $\text{FiO}_2$  of 100% (at least 70%) and when one wishes to avoid the tracheal intubation, and it is also indicated in patients with coronavirus (Covid-19). The non-invasive ventilation mode of this CPAP valve makes it possible to maintain airway permeability under positive pressure throughout the respiratory cycle, thus improving haematosis and decreasing respiratory work, this technique was first described and applied in 1930 for the treatment of OAP [12]. As you can see in Figure 4, the CPAP valve, which we made in our laboratory using a 3D printer, is open and works according to the Venturi effect [13,14]. Figure 5 shows a section view of the CPAP valve.



**Figure 4:** Representation of the CPAP valve that we manufactured (the left image: before assembly, the center image: complete assembly of the valve, the right image: comparison with the original valve).

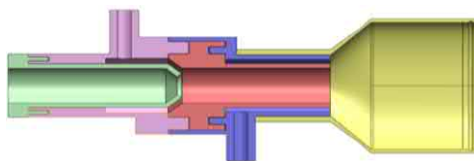


**Figure 5:** Detailed section view of the CPAP valve.

### 4 CFD Simulation

In this study, a finite volume method with ANSYS CFD is used to solve the set of equations system. We use one phase fluid flow instead of 3 phases (air,  $\text{O}_2$ ,  $\text{CO}_2$ ) in order to simplify the calculations. The fluid flow is considered to be turbulent. The standard  $k-\varepsilon$  turbulence model has been widely used by researchers in many flow phenomena. The

$k - \varepsilon$  model is based on the Reynolds averaged Navier-Stokes (RANS) model. Supplementary terms of the Reynolds stresses are obtained, which require additional equations to solve them. This model uses two transport equations for turbulent kinetic energy ( $k$ ) and its dissipation ( $\varepsilon$ ) to solve for these terms. The governing equations for unsteady incompressible flow of a Newtonian fluid are given by [15]

$$\frac{\partial u_i}{\partial x_i} = 0, \tag{1}$$

$$\frac{\partial(\rho u_i u_j)}{\partial x_j} = \frac{\partial \rho}{\partial x_i} + \frac{\partial}{\partial x_j} \left[ \mu \left( \frac{\partial u_i}{\partial x_j} + \frac{\partial u_j}{\partial x_i} - \frac{2}{3} \delta_{ij} \frac{\partial u_i}{\partial x_i} \right) \right]. \tag{2}$$

The equations of the turbulent kinetic energy ( $k$ ) and its dissipation ( $\varepsilon$ ) are shown in Equations (3) and (4) as below:

$$\frac{\partial}{\partial x_j} (\rho k x_j) = \frac{\partial}{\partial x_j} \left[ \left( \mu + \frac{\mu_t}{\sigma_k} \right) \frac{\partial k}{\partial x_j} \right] + G_k + G_b - \rho \varepsilon, \tag{3}$$

$$\frac{\partial}{\partial x_j} (\rho \varepsilon u_i) = \frac{\partial}{\partial x_j} \left[ \left( \mu + \frac{\mu_t}{\sigma_\varepsilon} \right) \frac{\partial \varepsilon}{\partial x_j} \right] + C_{1\varepsilon} \varepsilon \frac{\varepsilon}{k} (G_k + C_{3\varepsilon} G_b) - C_{2\varepsilon} \frac{\varepsilon^2}{k} \rho \varepsilon. \tag{4}$$

The term  $G_k$  represents the generation of turbulence kinetic energy due to the mean of velocity gradients, which is given as  $G_k = \mu_t S^2$  for the standard ( $k\varepsilon$ ) model, where the modulus of the mean rate of strain tensor  $S$  is given as  $S = 2S_{ij}^2$ .  $S_{ij}$  is the symmetric deformation tensor equal to  $\frac{1}{2} (u_{ij} + u_{ji})$ . The term of  $G_b$  is the generation of turbulence produced by buoyancy. On the other hand,  $C_{1\varepsilon}$ ,  $C_{2\varepsilon}$ ,  $C_{3\varepsilon}$ ,  $\sigma_k$  and  $\sigma_\varepsilon$  are constants whose values are 1.44, 1.92, 0.09, 1, and 1.3, respectively, [16, 17].

#### 4.1 Boundaries and boundary conditions

Figure 6 shows the mesh of the domain of interest and the different boundary conditions. There are two inlets. The turbulent intensity was set at 5% and the turbulent viscosity ratio was set as 10 (default values of fluent). The outlet was set as a pressure outlet, and the gauge pressure was set at 0 Pa, which means that the static pressure is equal to ambient pressure. In addition, the backflow turbulence intensity is 5% and the turbulent viscosity ratio is 10. The walls assumed no slip conditions and they were set to be stationary, as they do not move during the fluid flow.

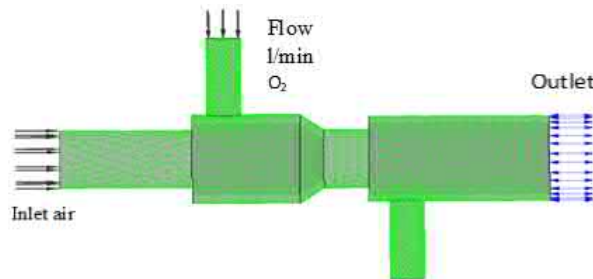


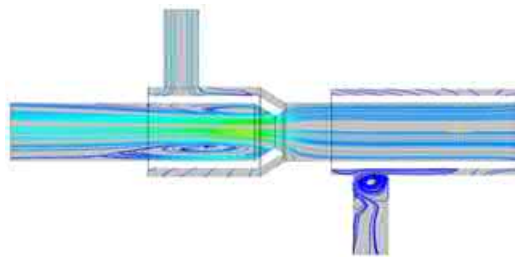
**Figure 6:** Mesh with boundary conditions.

## 4.2 Discretization schemes and algorithms

For this CFD problem, the finite volume method (FVM) scheme was implemented and utilised. A structural meshing technique is used to discretize the fluid domain. The set of the obtained RANS equations with boundary conditions are solved at each node of the mesh. The SIMPLEC algorithm (Semi-Implicit Method for Pressure Linked Equations-Consistent) is adopted in this study to calculate the pressures and velocities for the solution [18–21]. The solution is also affected by spatial discretization. For this purpose, the second order is used for pressure and momentum, and the first order is used for turbulent kinetic energy and its dissipation rate.

## 4.3 Numerical analysis results

Results of numerical simulations are presented in the following figures. Figure 7 shows the stream lines at the central plane at 4s.



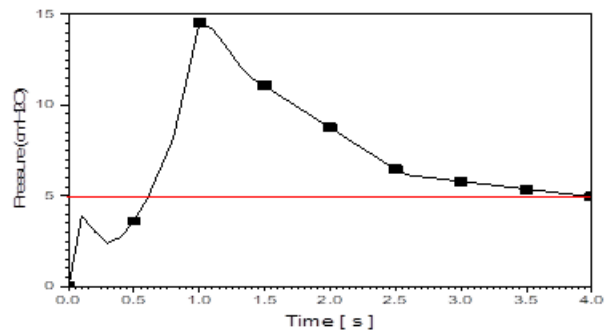
**Figure 7:** Streamlines at central plane at the time of 4s.

Figure 8 shows the simulation result of the pressure generated by the CPAP valve using the ANSYS CFD software. The pressure evolution during one cycle of breathing is presented here. A lot of physical parameters are introduced with a really very long computation time just to have this curve. So, we can see clearly the pressure which rises to around  $15\text{cmH}_2\text{O}$ , then drops back to  $5\text{cmH}_2\text{O}$ . However, in practice (Figure 9(b)), the pressure remains stable at around  $7.5\text{ cmH}_2\text{O}$  during the inspiration stage.

## 5 Experimental Test of CPAP

As shown in Figure 9, in the resuscitation service in our region, we are testing our CPAP valve at the MEDEA hospital with pure oxygen via a ball flow meter that can vary from 0 to 20 l/min of brand (MedilineR), a manometer pressure (OHMEDA) indicating the pressure variation between inspiration and expiration to measure the positive expiratory pressure (PEEP).

To pass to expiration, the pressure of the gases exhaled by the patient must exceed the adjustment pressure of this valve indicated via the manometer. In fact, this pressure is proportional to the flow of oxygen. Hence, we have chosen to carry out our measurements by varying different  $\text{O}_2$  levels in order to have a simple approach close to clinical values, Table 1 below indicates the  $\text{O}_2$  flow rate required to achieve the desired PEEP pressures. We have compared, in Table 1, the practical results between the original Boussignac valve and our designed valve made in the laboratory using a 3D printer. First, we notice



**Figure 8:** Pressure history at the outlet.

that the third column (our valve) reports good results. It is very important to note that the ICU doctors affirm that these results are very important at breathing difficulties.



**Figure 9:** CPAP valve integrated into the kit including a Decathlon mask, a flowmeter connected to the wall-mounted O<sub>2</sub> and a pressure gauge (the left image (a) with the original valve), (the center or the right image (b) and (c)) is indicating the variation in expiratory and inspiratory pressure).

O <sub>2</sub> flow required(lit/min)	PEEP original valve(cmH <sub>2</sub> O)	PEEP obtained(cmH <sub>2</sub> O)
10	3	2
15	8	5.5
20	10	7.5

**Table 1:** Comparison of PEEP for experimental and numerical results for different O<sub>2</sub> flows.

## 6 Conclusion

In the present work, we have designed and fabricated a CPAP valve. In addition, a numerical study by the ANSYS software is done. The turbulent fluid flow is analysed in order to optimize the parameters provided by the valve. The tests that we have carried out experimentally in the MEDEA hospital, have given a satisfactory result. Finally, the valve we designed is easy to use in the intensive care unit with the advantage of providing proven respiratory support in VIN with a positive pressure. The PEEP is adjustable from 2 to 7.5 cmH<sub>2</sub>O corresponding to the oxygen flow of 10 to 20l/min, respectively, according to the needs of patients with coronavirus (Covid-19).

## Acknowledgment

The authors wish to thank the DGRSDT/MESRS, Algeria, for their financial support of this study.

## References

- [1] E. Mark, N. Stefano and B. Schonhofer. *Non-invasive Vebtilation and Weaning. Principal and Practice*. CRC Press, 2nd edition, 2018.
- [2] G. Bellani, N. Patroniti, M. Greco, G. Foti and A. Pesenti. The use of helmets to deliver non-invasive continuous positive airway pressure in hypoxemic acute respiratory failure. *Minerva Anesthesiol* **74** (2008) 651–656.
- [3] F. Templier, F. Dolveck, M. Baer, F. Fernandez, M. Chauvin and D. Fletcher. Laboratory testing measurement of FIO<sub>2</sub> delivered by Boussignac CPAP system with an input of 100% oxygen. *Annales Franaises d'Anesthésie et de Réanimation* **22** (2003) 103–107.
- [4] A. Mateos-Rodriguez and J. Ortega-Anselmi Francisco. Alternative CPAP methods for the treatment of secondary serious respiratory failure due to pneumonia by COVID-19. *Medicina Clinica* **156** (2) (2021) 55–60. <https://doi.org/10.1016/j.medcli.2020.09.006>.
- [5] A. Paganoa, G. Portaa, et al. Non-invasive CPAP in mild and moderate ARDS secondary to SARS-CoV2. *Respiratory Physiology and Neurobiology* (2020) Sep; 280: 103489. [doi.org/10.1016/j.resp.2020.103489](https://doi.org/10.1016/j.resp.2020.103489).
- [6] B. Giacomo, F. Ester, S. Luigi, C. Nicolo and P. Antonio. An improved Boussignac device for the delivery of non-invasive CPAP: the SUPER-Boussignac. *Intensive Care Med.* **35** (2009) 1094–1099. DOI 10.1007/s00134-009-1403-x.
- [7] G. Esmond and C. Mikelson. *Non-Invasive Respiratory Support Techniques, Oxygen Therapy, Non-Invasive Ventilation and CPAP*. Wiley-Blackwell Publ., 2009.
- [8] F. Moritz, J. Benichou, et al. Boussignac continuous positive airway pressure device in the emergency care of acute cardiogenic pulmonary oedema: a randomized pilot study. *Eur. J. Emerg. Med.* **10** (3) (2003) 204–208.
- [9] F. Templier, F. Dolveck, F. Baer, M. Chauvin and D. Fletcher. Boussignac continuous positive airway pressure system: pratical use in a prehospital medical care unit. *Eur. J. Emerg. Med.* **10** (2) (2003) 87–93.
- [10] A.D. Bersten, A.W. Holt, A.E. Vedig and G.A. Skowronski. Treatment of severe cardiogenic pulmonary edema with continuous positive airway pressure delivered by face mask. *N. Engl. J. Med.* **325** (26) (1991) 1825–1830.
- [11] M. Lin, Y.F. Yang, H.T. Chiang, M.S. Chang, B.N. Chiang and M.D. Cheitlin. Reappraisal of continuous positive airway pressure therapy in acute cardiogenic pulmonary edema: short-term results and long-term follow-up. *Chest* **107** (5) (1995) 1379–1386.

- [12] E. L’Her. Non-invasive ventilation in acute respiratory distress. Réanimation et urgence médicales, CHU de la Cavale-Blanche, 29609 Brest cedex, France Article Original. 31-12-2004. ITBM-RBM **26** (2005) 41–50.
- [13] D. Isabey, G. Boussignac and A. Harf. Effect of air entrainment on airway pressure during endotracheal gas injection. *Appl. Physiol.* **67** (1989) 771–779.
- [14] B. Vallet, J. Leclerc, E. Plaisance and P. Goldstein. Intérêt de la ventilation non invasive au cours de l’insuffisance respiratoire aigüe, utilisation potentielle en médecine préhospitalière. In Sfar, editor. Médecine d’urgence 1998. 40e congrès national d’anesthésie et de réanimation. Paris: Elsevier, 1998. P. 133–148.
- [15] B.E. Launder and D.B. Spalding. *Lectures in Mathematical Models of Turbulence*. Academic Press, London, England. 1972.
- [16] D. Khelfi, A. Abdellah El-Hadj and N. Ait-Messaoudene. Modelling of a 3D plasma thermal spraying and the effect of the particle injection angle. *Revue des Energies Renouvelables CISM*, 2008.
- [17] D.C. Wilcox. *Turbulence Modeling for CFD*. La Canada, CA, DCW Industries, Inc., 1993.
- [18] H.K. Versteeg and W. Malalasekera. *An Introduction to Computational Fluid Dynamics – The Finite Volume Method*. Addison-Wesley-Longman, 1995. ISBN: 978-0-582-21884-0.
- [19] A.V. Artiukh, M.V. Sidorov and S.M. Lamtyugova. R-Functions and Nonlinear Galerkin Method for Solving the Nonlinear Stationary Problem of Flow around Body of Revolution. *Nonlinear Dynamics and Systems Theory* **21** (2) (2021) 138-149.
- [20] A. Najafi and B. Raeisy. Boundary Stabilization of a Plate in Contact with a Fluid. *Nonlinear Dynamics and Systems Theory* **12** (2) (2012) 193-205.
- [21] W. Parandyk, D. Lewandowski and J. Awrejcewicz. Mathematical Modeling of the Hydro-Mechanical Fluid Flow System on the Basis of the Human Circulatory System. *Nonlinear Dynamics and Systems Theory* **15** (1) (2015) 50-62.



# Asymptotic Stability of Some Class of Affine Nonlinear Control Systems through Partial Feedback Linearization

Firman \*, Syamsuddin Toaha, Muh Nur

*Department of Mathematics, Faculty of Mathematics and Natural Science, Hasanuddin University, Indonesia*

Received: March 8, 2021; Revised: May 10, 2021

**Abstract:** The problem of asymptotic stability for some class of nonlinear control systems, where the relative degree of the system is well defined, with relative degree being 1 and  $n - 1$ ,  $n$  is the dimension of the system, is addressed in this paper. To solve the problem, we will design an input control. For the design of input controls, the system will be transformed through partial feedback linearization such that the zero dynamic of the system with respect to a new state is asymptotically stable and the new state is a linear combination of state variables.

**Keywords:** *relative degree of system; partial feedback linearization; zero dynamic; asymptotic stability.*

**Mathematics Subject Classification (2010):** 93C10, 93D20.

## 1 Introduction

In the analysis for nonlinear control systems, there is no general method which can be applied to any nonlinear control system in designing the control input for solving the stability problems. Therefore, in general, the researchers describe some particular nonlinear classes only. Recently, stability problems for nonlinear control systems have been intensively investigated. J. Naiborhu and K. Shimizu [1] proposed a dynamic feedback control for the asymptotic stability of a nonlinear class, where its unforced dynamic is asymptotically stable. In 2004, P. Chen et al. [2] and L. Diao et al. [3] introduced the problem of stability through system transformation, where the transformation of the system is made through dynamic feedback. One of popular methods for solving stability

---

\* Corresponding author: <mailto:firman.math11@gmail.com>

problems is the input-output linearization method. Some researchers studied the stability problems of a nonlinear control system using the input-output linearization method, for example, Ricardo Marino and Patrizio Tomei [4] discussed the stability of a lower triangular nonlinear control system. Its stability control was the dynamic feedback of order  $n + 2(r - 1)$  ( $n$  is the system order,  $r$  is the relative degree). Results on stabilization of nonlinear lower triangular systems with uncertainties in the output feedback form have been presented in [5] and [6]. In [7], J. Naiborhu et al. discussed the asymptotic stability problem for a nonlinear class, where its control's design used exact linearization. Furthermore, in [8], the authors have addressed the problem of stabilization for a class of nonlinear control systems with the relative degree of the system being not well defined. Then, in [9], the authors have introduced the problem of stabilization for a class of nonlinear systems with uncertainty.

In this paper, we will investigate asymptotic stability of some class of affine nonlinear control systems, with the relative degrees of the system being 1 and  $n - 1$ . For the design of input controls, the system will be transformed through partial feedback linearization.

## 2 Problem Formulation

Consider the affine nonlinear control system

$$\dot{x}(t) = f_1(x(t)) + f_2(x(t))u, \tag{1}$$

where  $x(t) \in \mathcal{R}^n$ ,  $u(t) \in \mathcal{R}$ .  $f_1 : D \rightarrow \mathcal{R}^n$ ,  $f(\vec{0}) = \vec{0}$  and  $f_2 : D \rightarrow \mathcal{R}^n$  are sufficiently smooth in a domain  $D \subset \mathcal{R}^n$ .

Let a state  $y(t) = f_3(x(t))$ ,  $f_3 : D \rightarrow \mathcal{R}$  be sufficiently smooth in a domain  $D \subset \mathcal{R}^n$ ,  $f_3(\vec{0}) = 0$ .

According to [10], if we have

$$y^{(\rho)}(t) = L_{f_1}^\rho f_3(x) + L_{f_2} L_{f_1}^{\rho-1} f_3(x)u, \tag{2}$$

with  $L_{f_2} L_{f_1}^k f_3(x) = 0, k = 0, 1, 2, \dots, \rho - 2$ ,  $L_{f_2} L_{f_1}^{\rho-1} f_3(x) \neq 0$ , for all  $x \in D_0$ , then the relative degree of the system with respect to the state  $y$  is  $\rho$ ,  $1 < \rho < n$ , in a region  $D_0 \subset D$ , where  $L_{f_2} L_{f_1}^k f_3(x) = \frac{\partial(L_{f_1}^k f_3)}{\partial x} f_2(x)$ ,  $L_{f_1}^k f_3(x) = L_{f_1} L_{f_1}^{k-1} f_3(x) = \frac{\partial(L_{f_1}^{k-1} f_3(x))}{\partial x} f_1(x)$ ,  $\dots$ ,  $L_{f_1}^2 f_3(x) = \frac{\partial(L_{f_1} f_3(x))}{\partial x} f_1(x)$ ,  $L_{f_1} f_3(x) = \frac{\partial f_3(x)}{\partial x} f_1(x)$ ,  $L_{f_1}^0 f_3(x) = f_3(x)$ .

Let the relative degree of the system (1) with respect to the state  $y$  be  $\rho$ . By partial feedback linearization, the system (1) with respect to the state  $y$  can be transformed to

$$\dot{z}_k = z_{k+1}, k = 1, 2, \dots, \rho - 1, \tag{3}$$

$$\dot{z}_\rho = f(z) + g(z)u, \tag{4}$$

$$\dot{z}_{\rho+1} = q_{\rho+1}(z), \tag{5}$$

⋮

$$\dot{z}_n = q_n(z) \tag{6}$$

with the Jacobian matrix of  $z(x)$  being nonsingular at a point  $x_0$ ,  $z = (z_1, z_2, \dots, z_n)$ ,  $y = z_1$ .

Consider the system (5)-(6). If  $z_1 = 0$  for all  $t$ , then the system (5)-(6) is said to be zero dynamic with respect to the state  $y = z_1$ .

The following theorem describes the asymptotic stability of the nonlinear system (see [11]).

**Theorem 2.1** *Consider a system*

$$\dot{\chi} = f(\chi, \nu), \quad (7)$$

$$\dot{\nu} = g(\nu) \quad (8)$$

and suppose that  $\dot{\nu} = g(\nu)$  has an asymptotically stable equilibrium at  $\nu = 0$ . If  $\dot{\chi} = f(\chi, 0)$  has an asymptotically stable equilibrium at  $\chi = 0$ , then the system (7)-(8) has an asymptotically stable equilibrium at  $(\chi, \nu) = (0, 0)$ .

In order to use Theorem 1, we need to choose the state variable such that the zero dynamic of the system (1) is asymptotically stable. In this paper, we present asymptotic stability of some class of affine nonlinear control systems, where the relative degree of the system (1) is well defined, with the relative degree being 1 and  $n - 1$ ,  $n$  is the dimension of the system. For a class of affine nonlinear control systems with the relative degree of the system being 1, the input control design is needed so that the zero dynamic of the system is asymptotically stable. Next, for a class of affine nonlinear control systems with the relative degree of the system being  $n - 1$ , to achieve the stability, we will design an input control when the zero dynamic of the system is asymptotically stable.

### 3 Main Results

First, we will investigate the asymptotic stability for an affine nonlinear control system in the following form:

$$\dot{x} = Ax + \tau u, \quad x(t) \in \mathcal{R}^n, \quad \tau \in \mathcal{R}^n, \quad u(t) \in \mathcal{R}, \quad (9)$$

with

$$A = \begin{pmatrix} 0 & 1 & \dots & 0 \\ \vdots & \vdots & \ddots & \vdots \\ 0 & 0 & \dots & 1 \\ 1 & 0 & \dots & 0 \end{pmatrix}$$

and  $\tau_1 = \tau_2 = \dots = 0$ ,  $\tau_{n-1} = -\alpha_1$ ,  $\alpha_1 > 0$ ,  $\tau_n = \alpha_2 + \phi(x_1)$ ,  $\alpha_2 > 0$ ,  $\phi(0) = 0$ .

The following theorem states that the new state variable of the system (9) can be chosen such that the zero dynamic of the system (9) is asymptotically stable.

**Theorem 3.1** *Suppose the nonlinear system as in equation (9). Then there exists a state variable  $y = a_0x_1 + a_1x_2 + \dots + a_{n-2}x_{n-1} + a_{n-1}x_n$  such that the relative degree of the system (9) with respect to the state  $y$  is 1. Furthermore, the zero dynamic for the system (9) with respect to the state  $y$  is asymptotically stable.*

**Proof.** Let  $y = a_0x_1 + a_1x_2 + a_2x_3 + \dots + a_{n-2}x_{n-1} + a_{n-1}x_n$ . We have

$$\dot{y} = a_0x_2 + a_1x_3 + a_2x_4 + \dots + a_{n-2}x_n + a_{n-1}x_1 + (a_{n-1}(\alpha_2 + \phi(x_1)) - a_{n-2}\alpha_1)u.$$

Thus, the relative degree of the system (9) with respect to the state  $y$  is 1, with  $a_{n-1}(\alpha_2 + \phi(x_1)) - a_{n-2}\alpha_1 \neq 0$ .

Furthermore, the partial feedback linearization is

$$\dot{y} = v, \tag{10}$$

$$\dot{\eta}_1 = \eta_2, \tag{11}$$

$$\dot{\eta}_2 = \eta_3, \tag{12}$$

$$\vdots \tag{13}$$

$$\dot{\eta}_{n-2} = \eta_{n-1}, \tag{14}$$

$$\dot{\eta}_{n-1} = x_n - \alpha_1 u, \tag{15}$$

where  $\eta_1 = x_1, \eta_2 = x_2, \dots, \eta_{n-1} = x_{n-1}$ .

We will choose the input control  $u$  such that the zero dynamic is asymptotically stable. Next, we choose  $v = -k_1 a_0 x_1 - k_2 a_1 x_2 - k_3 a_2 x_3 - \dots - k_n a_{n-1} x_n$ , with  $a_{n-1} = 1$ . We have

$$\begin{aligned} u &= \frac{a_0 x_1 \left(-k_1 - \frac{-1}{a_0}\right) + a_1 x_2 \left(-k_2 - \frac{-a_0}{a_1}\right) + \dots + a_{n-1} x_n (-k_n - a_{n-2})}{\alpha_2 + \phi(x_1) - \alpha_1} \\ &= \frac{-\beta(a_0 x_1 + a_1 x_2 + a_2 x_3 + \dots + x_n)}{\alpha_2 + \phi(x_1) - a_{n-2} \alpha_1}, \end{aligned} \tag{16}$$

where  $\beta = k_1 + \frac{1}{a_0} = k_2 + \frac{a_0}{a_1} = k_3 + \frac{a_1}{a_2} = \dots = k_n + a_{n-2}$ .

Next, if  $y(t) = 0, \forall t$ , then the zero dynamic of the system (9) with respect to the state  $y$  is

$$\dot{\eta}_1 = \eta_2, \tag{17}$$

$$\dot{\eta}_2 = \eta_3, \tag{18}$$

$$\vdots \tag{19}$$

$$\dot{\eta}_{n-2} = \eta_{n-1}, \tag{20}$$

$$\dot{\eta}_{n-1} = -a_0 \eta_1 - a_1 \eta_2 - a_2 \eta_3 - \dots - a_{n-2} \eta_{n-1}. \tag{21}$$

From Eqs. (17)–(21), it can be written

$$\dot{\eta} = \mathcal{A}_1 \eta,$$

where  $\eta = (\eta_1, \eta_2, \dots, \eta_{n-1})^T$  and

$$\mathcal{A}_1 = \begin{pmatrix} 0 & 1 & \dots & 0 \\ \vdots & \vdots & \ddots & \vdots \\ 0 & 0 & \dots & 1 \\ -a_0 & -a_1 & \dots & -a_{n-2} \end{pmatrix}.$$

If we choose  $a_0, a_1, \dots, a_{n-2}$  such that all the root of the characteristic polynomial of the matrix  $\mathcal{A}_1$   $p(\lambda) = a_0 + a_1 \lambda + \dots + a_{n-2} \lambda^{n-2} + \lambda^{n-1}$  have negative real part, then the zero dynamic of system (9) with respect to the state  $y$  is asymptotically stable. Hence, there exists the state variable  $y = a_0 x_1 + a_1 x_2 + \dots + a_{n-1} x_n$  such that the zero dynamic of the system (9) with respect to the state  $y$  is asymptotically stable.

**Proposition 3.1** Consider system (9) with the state  $y = a_0x_1 + a_1x_2 + \dots + a_{n-1}x_n$ . Chose  $a_{n-1} = 1$  and  $a_0, a_1, \dots, a_{n-2}$  such that the polynomial

$$p(\lambda) = a_0 + a_1\lambda + \dots + a_{n-2}\lambda^{n-2} + \lambda^{n-1} \tag{22}$$

is Hurwitz. If we choose the new input  $v$  as in Eq. (10) such that  $\dot{y} = v$  has an asymptotically stable equilibrium at  $y = 0$ , then at using the input control in Eq.(16), the system (10)-(15) has an asymptotically stable equilibrium at  $(y, \eta) = (0, 0)$ . Furthermore, the system (9) has an asymptotically stable equilibrium at  $x = 0$ .

Next, the affine nonlinear control system is considered in the following form:

$$\dot{x} = Mx + \tau u + \theta(x_1), x(t) \in \mathcal{R}^n, u(t) \in \mathcal{R}, \tag{23}$$

with  $\theta(x_1) \in C^\infty(\mathcal{R}^n)$ ,  $\theta(0) = 0$ ,  $\tau = (0, 0, \dots, 0, \tau_{n-1}, \tau_n)^T$ ,  $\tau_{n-1} \neq 0$ ,

$$\tau_{n-1} = -\tau_n, M = \begin{pmatrix} 0 & 1 & 0 & \dots & 0 \\ 0 & 0 & 1 & \dots & 0 \\ \vdots & \vdots & \vdots & \ddots & \vdots \\ 0 & 0 & 0 & \dots & 1 \\ 0 & 0 & 0 & \dots & 0 \end{pmatrix}, \theta_1(x_1) + \theta_2(x_1) + \dots + \theta_n(x_1) = 0.$$

**Theorem 3.2** Suppose the nonlinear system as in equation (23). Let the state variables  $y = \alpha x_1 + x_2 + \dots + x_n$ ,  $\alpha \neq 1$ . Then the relative degree of the system (23) with respect to the state  $y$  is  $n - 1$ . Furthermore, the zero dynamic for the system (23) with respect to the state  $y$  is asymptotically stable.

**Proof.** Let  $y = ax$ ,  $a = (\alpha, 1, \dots, 1)$ ,  $x = (x_1, x_2, \dots, x_n)^T$ ,  $\alpha \neq 1$ . We have

$$\dot{y} = a\dot{x} = aMx + a\theta(x_1), \tag{24}$$

$$\ddot{y} = aM^2x + aM\theta(x_1) + a\frac{d\theta}{dt}, \tag{25}$$

$$\vdots \tag{26}$$

$$y^{(n-2)} = aM^{(n-2)}x + aM^{(n-3)}\theta(x_1) + \dots + aM(\theta(x_1))^{(n-4)} + a(\theta(x_1))^{(n-3)}, \tag{27}$$

$$y^{(n-1)} = aM^{(n-1)}x + aM^{(n-2)}\theta(x_1) + \dots + aM(\theta(x_1))^{(n-3)} + a(\theta(x_1))^{(n-2)} + b_n(1 - \alpha)u. \tag{28}$$

Thus, the relative degree of the system (23) with respect to the state  $y$  is  $n - 1$ . Furthermore, the linearized input state for system (23) with respect to the state  $y = z_1$  is

$$\dot{z}_k = z_{k+1}, k = 1, 2, \dots, n - 2, \tag{29}$$

$$\dot{z}_{n-1} = f(z, \eta) + g(z, \eta)u, \tag{30}$$

$$\dot{\eta} = \dot{x}_1 + \dot{x}_2 + \dots + \dot{x}_n = \eta - x_1 \tag{31}$$

with  $f(z, \eta) = aM^{(n-1)}x + aM^{(n-2)}\theta(x_1) + \dots + aM(\theta(x_1))^{(n-3)} + a(\theta(x_1))^{(n-2)}$ ,  $g(z, \eta) = b_n(1 - \alpha)$ ,  $\alpha \neq 1$ ,  $z = (z_1, z_2, \dots, z_{n-1})$ .

Furthermore, we will investigate the stability of the zero dynamic of the system (23) with respect to the state  $y = z_1$ . Consider

$$\eta\dot{\eta} = \eta(\eta - x_1) = \eta^2 - \eta\left(\frac{z_1 - \eta}{\alpha - 1}\right). \tag{32}$$

If  $z_1 = 0$  and  $0 < \alpha < 1$ , then

$$\eta\dot{\eta} = \frac{\alpha\eta^2}{\alpha - 1} < 0. \tag{33}$$

Therefore, the zero dynamic of the system (23) with respect to the state  $y = z_1$  is asymptotically stable.

Consider the system (29)-(31). If we choose the input control

$$u = \frac{1}{g(z, \eta)} (-f(z, \eta) - c_0z_1 - c_1z_2 - \dots - c_{n-2}z_{n-1}), \tag{34}$$

then we have the normal form of the system (23) with respect to the state  $y = z_1$

$$\dot{z} = \mathcal{B}z, \tag{35}$$

$$\dot{\eta} = q(z, \eta), \tag{36}$$

with

$$\mathcal{B} = \begin{pmatrix} 0 & 1 & \dots & 0 \\ \vdots & \vdots & \ddots & \vdots \\ 0 & 0 & \dots & 1 \\ -c_0 & -c_1 & \dots & -c_{n-2} \end{pmatrix},$$

$\dot{\eta} = q(z, \eta)$  in Eq.(31). In particular, the matrix  $\mathcal{B}$  has a characteristic polynomial

$$p(\lambda) = c_0 + c_1\lambda + \dots + c_{n-2}\lambda^{n-2} + \lambda^{n-1}. \tag{37}$$

Because the zero dynamic of the system (23) with respect to the state  $y = z_1$  has an asymptotically stable equilibrium at  $\omega = 0$  and if we choose  $c_0, c_1, \dots, c_{n-2}$  such that all the roots of the polynomial  $p(\lambda)$  have negative real part, then the system (29)-(31) has an asymptotically stable equilibrium at  $(z, \eta) = (0, 0)$ .

**Proposition 3.2** *Consider the zero dynamic of the system (23) with respect to the state  $y = z_1$ . Let all the roots of the polynomial in Eq.(37) have negative real part. Then, at using the input control in Eq.(34), the system (29)-(31) has an asymptotically stable equilibrium at  $(z, \eta) = (0, 0)$ .*

**Example 3.1** Suppose the nonlinear control system is

$$\dot{x}_1 = x_2, \tag{38}$$

$$\dot{x}_2 = x_3 - \alpha_1 u, \tag{39}$$

$$\dot{x}_3 = x_1 + (\alpha_2 + x_1^2) u. \tag{40}$$

Let  $y = c_0x_1 + c_1x_2 + x_3$ . Then  $\dot{y} = c_0x_2 + c_1x_3 + x_1 + (\alpha_2 + x_1^2 - c_1\alpha_1)u$ .

Thus, if  $\alpha_2 > c_1\alpha_1$ , the relative degree is one for all  $x$ . Then, according to (16), the input control is

$$u(t) = \frac{-\beta(c_0x_1 + c_1x_2 + c_2x_3 + x_4)}{\alpha_2 + x_1^2 - c_1\alpha_1} \tag{41}$$

with  $\beta = k_1 + \frac{1}{c_0} = k_2 + \frac{c_0}{c_1} = k_3 + c_1$ . If we choose  $k_1, k_2, k_3 > 0$  and  $c_0, c_1$  such that all roots of the polynomial  $p(\lambda) = c_0 + c_1\lambda + \lambda^2$  are Hurwitz, then the system (38)-(40) has an asymptotically stable equilibrium at  $(x_1, x_2, x_3) = (0, 0, 0)$ .

Simulation result is shown in Fig.1a for constants  $k_1 = \frac{59}{6}, k_2 = \frac{44}{5}, k_3 = 5, c_0 = 6, c_1 = 5$ . The initial value  $x_1(0) = -1, x_2(0) = 2, x_3(0) = -3$ .

**Example 3.2** Suppose the nonlinear control system is

$$\dot{x}_1 = x_2 + x_1^2, \quad (42)$$

$$\dot{x}_2 = x_3 - u + x_1^2, \quad (43)$$

$$\dot{x}_3 = u - 2x_1^2. \quad (44)$$

The relative degree of the system (42)-(44) with respect to the state  $y = \alpha x_1 + x_2 + x_3$  is 2,  $0 < \alpha < 1$ . The system (42)-(44) can be transformed to

$$\begin{aligned} \dot{z}_1 &= z_2, \\ \dot{z}_2 &= f(z, \eta) + g(z, \eta)u, \\ \dot{\eta} &= \eta - \left( \frac{z_1 - \eta}{\alpha - 1} \right), \end{aligned} \quad (45)$$

with  $y = z_1, f(z, \eta) = \alpha x_3 + (\alpha - 2)x_1^2 + 2(\alpha - 1)x_1x_2 + 2(\alpha - 1)x_1^3, g(z, \eta) = 1 - \alpha$ .

Thus, the zero dynamic of the system (42)-(44) with respect to the state  $y = z_1$  is asymptotically stable. Then, according to (34), the input control is

$$u = \frac{1}{1 - \alpha} (-a(z, \eta) - c_0 z_1 - c_1 z_2). \quad (46)$$

If we choose  $c_0, c_1$  such that all roots of the polynomial  $p(\lambda) = c_0 + c_1\lambda + \lambda^2$  have negative real part, then the system (42)-(44) has an asymptotically stable equilibrium at  $(x_1, x_2, x_3) = (0, 0, 0)$ .

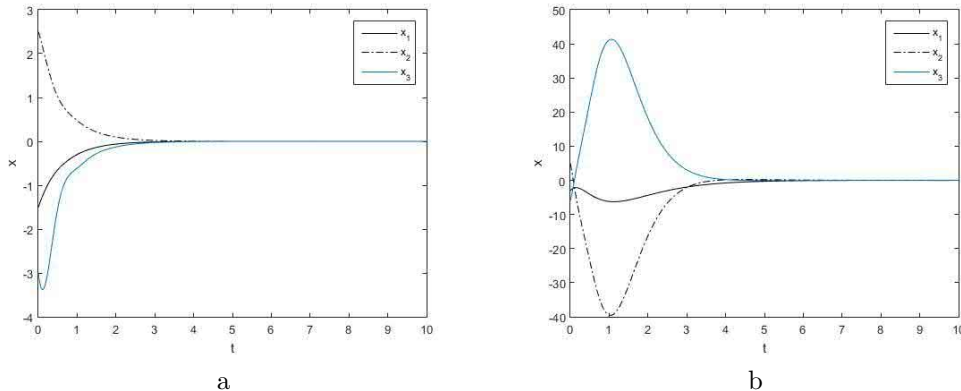


**Figure 1:** a) simulation result for Example 3.1, b) simulation result for Example 3.2.

Simulation result is shown in Fig.1b for constants  $\alpha = 0,5, c_0 = 6, c_1 = 5$ . The initial value  $x_1(0) = -3, x_2(0) = 5, x_3(0) = -6$ .

#### 4 Conclusion

In this paper, we have investigated asymptotic stability of some class of affine nonlinear control systems through partial feedback linearization. For a class of affine nonlinear control systems with the relative degree of the system (9) with respect to the state  $y$  being 1, the input control is designed so that the zero dynamic of the system (9) is asymptotically stable. Next, for a class of affine nonlinear control systems with the relative degree of the system (23) with respect to the state  $y$  being  $n - 1$ , the input control is designed when the zero dynamic of the system (9) is asymptotically stable, where the state  $y$  is the linear combination of the state variables.

#### Acknowledgment

The research is supported by PDU-LPPM UNHAS Program 2020.

#### References

- [1] J. Naiborhu and K. Shimizu. Direct Gradient Descent Control for Global Stabilization of General Nonlinear Control System. *IEEE Trans. Fundamental* **E83-A** (3) (2000) 516-523.
- [2] P. Chen, X. Ye and H. Qin. Stabilization of a Class of Non-Minimum Phase Nonlinear Systems by Dynamic Output Feedback. In: *Proceeding of 8th International Conference on Control, Automation, Robotics and Vision*. China, 2004, 1206–1211.
- [3] L. Diao and M. Guay. Output Feedback Stabilization of Uncertain Non-Minimum Phase Nonlinear Systems. In: *American Control Conf.*, 2004, 3671–3676.
- [4] Riccardo Marino and Patrizio Tomei. A Class of Globally Output Feedback Stabilizable Nonlinear Nonminimum Phase Systems. *IEEE Transactions on Automatic Control* **50** (12) (2005) 2097-2101.
- [5] Z. Li, Z. Chen and Z. Dan Yuan. The Stability Analysis and Control of a Class of Non-Minimum Phase Nonlinear Systems. *International Journal of Nonlinear Science* **3** (2) (2007) 103-110.
- [6] N. Wang, W. Xu and F. Chen. Adaptive global output feedback stabilisation of some non-minimum phase nonlinear uncertain systems. *IET Control Theory* **2** (2) (2008) 117-125.
- [7] J. Naiborhu, Firman and K. Mu'tamar. Particle Swarm Optimization in the Exact Linearization Technique for Output Tracking of Non-Minimum Phase Nonlinear Systems. *Applied Mathematical Science* **7** (1) (2013) 5427-5442.
- [8] Firman, J. Naiborhu and Roberd Saragih. Modification of a Steepest Descent Control for Output Tracking of Some Class Non-Minimum Phase Nonlinear Systems. *Applied Mathematics and Computation* **269** (2015) 497-506.
- [9] Firman, J. Naiborhu, Roberd Saragih and W.I. Supto. Output Tracking of Some Class Non-Minimum Phase Nonlinear Uncertain Systems. *Nonlinear Dynamics and Systems Theory* **7** (4) (2017) 347-356.
- [10] H.K. Khalil. *Nonlinear Systems*. Prentice Hall, Upper Saddle River, New Jersey, 2002.
- [11] A. Isidori. *Nonlinear Control Systems: An Introduction*. Springer, Berlin, Heidelberg, 1989.



# Dynamical Behaviors of Fractional-Order Selkov Model and Its Discretization

T. Houmor<sup>1\*</sup>, H. Zerimeche<sup>2</sup> and A. Berkane<sup>1</sup>

<sup>1</sup> *Department of Mathematics, Constantine 1 University, 25000, Algeria.*

<sup>2</sup> *Laboratory of Mathematics and their Interactions, Abdelhafid Boussouf University Center, Mila, Algeria.*

Received: November 22, 2020; Revised: May 16, 2021

**Abstract:** In this work, we study the dynamics of a fractional-order Selkov model, which is a classical mathematical model describing glycolysis, and its corresponding discretized version. First, non-negativity, existence and uniqueness of the solution for the model are discussed. We also investigate the local stability and the existence of a Hopf bifurcation. The discrete fractional-order model is shown to exhibit very rich behaviors and when considering the step size as a control parameter, a flip bifurcation, Neimark-Sacker bifurcation and chaos are obtained. Finally, numerical simulations are carried out to verify the correctness of the theoretical results obtained.

**Keywords:** *fractional order; Selkov model; local stability; bifurcations; discretization.*

**Mathematics Subject Classification (2010):** 34A08, 34A34, 34C23, 65P20.

## 1 Introduction

Glycolysis is the first step in the breakdown of glucose to extract energy for cellular metabolism, it is present in nearly all living organisms. After many years of experimental observations, Higgins [1] was the first to use mathematical modelling to understand the process, he presented a model to explain sustained oscillations in the yeast glycolytic system. His model, however, has no limit cycle for those values of its parameters with which self oscillations are observed experimentally. In 1968, Selkov [2] introduced an alternative mathematical model able to well reproduce the glycolytic oscillations in yeast, it was shown that the Selkov model exhibits a Hopf bifurcation and thus there exist parameter values for which it has a periodic solution. This model has sparked a number

---

\* Corresponding author: [mailto:tarek\\_houmor@umc.edu.dz](mailto:tarek_houmor@umc.edu.dz)

of further complementary studies. Results on the uniqueness and global attractivity of the glycolytic oscillations were obtained by d’Onofrio [3]. Vervevko et al. [4] studied the influence of periodic influx of glycolytic oscillations within the forced Selkov system, in this work the quasi-periodic oscillations and chaos were obtained. In [5], several properties of the dynamics of the solutions of the model were established, an analysis of the Poincaré compactification of the system was given to study unbounded solutions. Artés et al. [6] described the global dynamics in the Poincaré disc of the Selkov and Higgins-Selkov models.

On the other hand, fractional calculus, defined as a generalisation of ordinary differentiation and integration to arbitrary non-integer order, has gained a considerable importance during the past four decades and longer due to its use in many fields in natural science and engineering applications such as neurons [7], finance systems [8, 9], biological systems [10, 11], chemical systems [12], nuclear magnetic resonance [13] and so on. The main advantage of fractional-order differential equation models is that they are naturally related to systems with memory, which exist in most biological systems, and it allows greater degree of freedom than integer-order systems. Moreover, it was shown that the stability region of the fractional-order models is greater than the stability region of the integer-order ones.

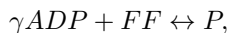
In this paper, we investigate the dynamic behaviors of the fractional-order Selkov model and its corresponding discretized version. First, we prove different mathematical results such as non-negativity, existence and uniqueness of the solution for the model. We also study the local stability of the unique equilibrium point and the existence of a Hopf bifurcation. We implement a predictor-corrector scheme to do numerical simulations and to illustrate our analytical findings. The discrete fractional-order model is shown to exhibit very rich behaviors. A flip bifurcation, Neimark-Sacker bifurcation and chaos are obtained.

## 2 Description of the Model

In [2], Selkov proposed the following simplified system:

$$\begin{aligned} \frac{dx}{dt} &= 1 - xy^\gamma, \\ \frac{dy}{dt} &= \alpha y (xy^{\gamma-1} - 1) \end{aligned} \tag{1}$$

with the initial conditions  $x(0) > 0$ ,  $y(0) > 0$ . The quantities  $x(t)$  and  $y(t)$  represent dimensionless concentrations of ATP and ADP at time  $t$ , respectively, while  $t$  is a dimensionless time variable.  $\gamma > 1$  is the stoichiometric parameter of the reaction



the parameter  $\alpha$  is a positive real number.

Selkov showed that the above planar system has only one equilibrium  $E = (1, 1)$  in a finite part of the  $(x, y)$  phase plane, the characteristic equation in the neighbourhood of  $E$  is

$$\begin{vmatrix} -1 - \lambda & -\gamma \\ \alpha & \alpha(\gamma - 1) - \lambda \end{vmatrix} = 0,$$

its roots are

$$\lambda_{1,2} = \frac{1}{2} \{ \alpha(\gamma - 1) - 1 \pm \sqrt{[\alpha(\gamma - 1) - 1]^2 - 4\alpha} \}.$$

Then  $E$  is a stable node at  $0 < \alpha \leq \alpha_1$ , a stable focus at  $\alpha_1 < \alpha < \alpha_0$ , an unstable focus at  $\alpha_0 < \alpha < \alpha_2$  and an unstable node at  $\alpha_2 \leq \alpha < \infty$ , where

$$\alpha_0 = \frac{1}{\gamma - 1} \quad \text{and} \quad \alpha_{1,2} = \left( \frac{\sqrt{\gamma} \pm 1}{\gamma - 1} \right)^2, \quad (\alpha_1 < \alpha_2). \quad (2)$$

Moreover, if we consider the real part of the eigenvalues as a function of  $\alpha$ , then it passes through zero when  $\alpha = \alpha_0$  and its derivative with respect to  $\alpha$  at that point is non-zero. Thus a Hopf bifurcation occurs. The first Lyapunov number  $\sigma$  of the bifurcation is found to be  $\sigma = -\frac{3\pi(\gamma - 1)^{\frac{1}{2}}}{4}(\gamma^2(\gamma - 1) + 1) < 0$ . Thus the Hopf bifurcation is non-degenerate and supercritical [5].

**Remark 2.1** Selkov showed that the investigation of system (1) in infinity by means of the Poincaré transformations [14] provides that this system has, in a positive quadrant of infinity, two more equilibrium states:  $E_1 = (\infty, 0)$  and  $E_2 = (0, \infty)$ , which explains that some orbits may be unbounded. Here, we will consider only the equilibrium  $E = (1, 1)$  in a finite part of the  $(x, y)$  phase plane.

The system considered in what follows is

$$\begin{aligned} {}_0^c D_t^q x &= 1 - xy^\gamma, \\ {}_0^c D_t^q y &= \alpha y (xy^{\gamma-1} - 1), \end{aligned} \quad (3)$$

where  ${}_0^c D_t^q$  is the Caputo fractional derivative with the fractional order  $q$  ( $0 < q \leq 1$ ). The main advantage of Caputo's approach is that the initial conditions for the fractional differential equations with Caputo derivatives take the similar form as for the integer-order differential equations. We therefore study the system (3) with the same initial conditions  $x(0) > 0$ ,  $y(0) > 0$  as in (1).

### 3 Non-Negativity, Existence and Uniqueness

Since  $x$  and  $y$  are the concentrations of ATP and ADP in living cells, respectively, we are only interested in solutions that are non-negative. To prove the non-negativity of our system, we shall use the following results.

**Lemma 3.1** [15] Suppose that  $x(t) \in C[a, b]$  and  $D_a^q x(t) \in C(a, b]$  with  $0 < q \leq 1$ . The Generalized Mean Value Theorem states that

$$x(t) = x(a) + \frac{1}{\Gamma(q)} (D_a^q x)(\xi) \cdot (t - a)^q,$$

where  $a \leq \xi \leq t$ ,  $\forall t \in (a, b]$ .

**Corollary 3.1** [15] Suppose that  $x(t) \in C[a, b]$  and  ${}_0^c D_a^q x(t) \in C(a, b]$  with  $0 < q \leq 1$ . Then the following conditions hold:

1. If  ${}_0^c D_a^q x(t) \geq 0$ ,  $\forall t \in (a, b)$ , then  $x(t)$  is a non-decreasing function for each  $t \in [a, b]$ .
2. If  ${}_0^c D_a^q x(t) \leq 0$ ,  $\forall t \in (a, b)$ , then  $x(t)$  is a non-increasing function for each  $t \in [a, b]$ .

We can now state the following theorem.

**Theorem 3.1** *All solutions of system (3) with the initial conditions  $x(0) \geq 0$  and  $y(0) \geq 0$  are non-negative.*

**Proof.** We will prove that  $x(t) \geq 0$  for all  $t \geq 0$ . Suppose that the statement is not true, then there is a constant  $t_1 > 0$  such that

$$\begin{cases} x(t) > 0, & 0 \leq t < t_1, \\ x(t_1) = 0, \\ x(t_1^+) < 0. \end{cases} \tag{4}$$

Substituting the second equation of system (4) into the first equation of (3) gives

$${}_0^c D_t^q x(t)|_{t=t_1} = 1. \tag{5}$$

According to Corollary 3.1 we have  $x(t_1^+) \geq 0$ , which contradicts the fact that  $x(t_1^+) < 0$ . Therefore, we have  $x(t) \geq 0, \forall t \geq 0$ . Using the same argument we show that  $y(t) \geq 0, \forall t \geq 0$ .  $\square$

Now, we study the existence and uniqueness of the solution of our system (3). We have the following lemma due to [16].

**Lemma 3.2** *Consider the system*

$${}_0^c D_t^q x(t) = f(t, x), \quad t > t_0,$$

*with the initial condition  $x_{t_0}$ , where  $0 \leq q \leq 1, f : [t_0, \infty) \times \Omega \rightarrow \mathbb{R}^n, \Omega \subset \mathbb{R}^n$ . If  $f(t, x)$  satisfies the locally Lipschitz condition with respect to  $x$ , then there exists a unique solution of the above system on  $[t_0, \infty) \times \Omega$ .*

We also need to use the following technical lemma.

**Lemma 3.3** *Let  $x$  and  $y$  be two positive real numbers and  $\gamma \geq 1$ , then*

$$|x^\gamma - y^\gamma| \leq \gamma(\sup(x, y))^{\gamma-1}|x - y|.$$

**Theorem 3.2** *We consider system (3) with the initial conditions  $x(0) = x_0$  and  $y(0) = y_0$  in the region  $[0, \infty) \times \Omega$ , where  $\Omega = \{(x, y) \in \mathbb{R}^2 / \max\{|x|, |y|\} \leq M\}$  for sufficiently large  $M$ . This initial value problem has a unique solution.*

**Proof.** Let us define the functions  $f_1(x, y) = 1 - xy^\gamma$  and  $f_2(x, y) = \alpha y(xy^{\gamma-1} - 1)$ . Further, we define  $F = (f_1, f_2)^T$  and  $X = (x, y)^T$ , then the differential equation can be written as  ${}_0^c D_t^q X = F(X)$ .

We show that the function  $F : \Omega \rightarrow \mathbb{R}^2$  is locally Lipschitz. Denote  $X_1 = (x_1, y_1)$  and  $X_2 = (x_2, y_2)$ . Then for any  $X_1, X_2 \in \Omega$  we have

$$\begin{aligned} \|F(X_1) - F(X_2)\| &= |f_1(x_1, y_1) - f_1(x_2, y_2)| + |f_2(x_1, y_1) - f_2(x_2, y_2)| \\ &= |x_1 y_1^\gamma - x_2 y_2^\gamma| + \alpha |x_1 y_1^\gamma - x_2 y_2^\gamma - y_1 + y_2| \\ &\leq (1 + \alpha) |x_1 y_1^\gamma - x_2 y_2^\gamma| + \alpha |y_1 - y_2|, \end{aligned}$$

noticing that

$$|x_1 y_1^\gamma - x_2 y_2^\gamma| = \frac{1}{2} [(x_1 - x_2)(y_1^\gamma + y_2^\gamma) + (x_1 + x_2)(y_1^\gamma - y_2^\gamma)]$$

and using the triangle inequality and Lemma 3.3 we have

$$\begin{aligned}
\|F(X_1) - F(X_2)\| &\leq \\
&\leq \frac{1+\alpha}{2} [|x_1 - x_2| |y_1^\gamma + y_2^\gamma| + |x_1 + x_2| |y_1^\gamma - y_2^\gamma|] + \alpha |y_1 - y_2| \\
&\leq \frac{1+\alpha}{2} [|x_1 - x_2| |y_1^\gamma + y_2^\gamma| + \gamma (\sup(y_1, y_2))^{\gamma-1} |x_1 + x_2| |y_1 - y_2|] + \alpha |y_1 - y_2| \\
&\leq (1+\alpha)M^\gamma |x_1 - x_2| + ((1+\alpha)\gamma M^\gamma + \alpha) |y_1 - y_2| \\
&\leq L \|X_1 - X_2\|,
\end{aligned}$$

where  $L = (1+\alpha)\gamma M^\gamma + \alpha$ . Thus  $F(X)$  satisfies the Lipschitz condition with respect to  $X$ , following Lemma 3.2, there exists a unique solution  $X(t)$  of system (3) with the initial condition  $X(0) = (x(0), y(0))$ .  $\square$

#### 4 Local Stability and Hopf Bifurcation

The system (3) has only one equilibrium state  $E$  with coordinates  $\bar{x} = \bar{y} = 1$ . Linearising the system about this point leads to the Jacobian matrix

$$J = \begin{bmatrix} -1 & -\gamma \\ \alpha & \alpha(\gamma - 1) \end{bmatrix},$$

the characteristic equation is then

$$\begin{vmatrix} -1 - \lambda & -\gamma \\ \alpha & \alpha(\gamma - 1) - \lambda \end{vmatrix} = 0,$$

its roots are

$$\lambda_{1,2} = \frac{1}{2} \{ \alpha(\gamma - 1) - 1 \pm \sqrt{[\alpha(\gamma - 1) - 1]^2 - 4\alpha} \}.$$

The system (3) is said to be locally asymptotically stable [17] around the equilibrium point  $(\bar{x}, \bar{y})$  if

$$|\arg(\lambda_i)| > \frac{q\pi}{2}, \quad i = 1, 2.$$

Hence it follows that

- If  $0 < \alpha \leq \alpha_1$ :  $\lambda_{1,2}$  are real negative eigenvalues,  $E$  is asymptotically stable for all  $q \in (0, 1]$ .
- If  $\alpha_1 < \alpha < \alpha_2$ :  $\lambda_{1,2}$  are complex conjugate eigenvalues,  $E$  is asymptotically stable if and only if  $|\arg(\lambda_{1,2})| > \frac{q\pi}{2}$ , that is,  $0 < q < q^*$ , where

$$q^* = \frac{2}{\pi} \left| \arctan \sqrt{\frac{4\alpha}{[\alpha(\gamma - 1) - 1]^2 - 1}} \right|.$$

- If  $\alpha \geq \alpha_2$   $\lambda_{1,2}$  are real positive eigenvalues,  $E$  is unstable for all  $q \in (0, 1]$ ,

where  $\alpha_0$ ,  $\alpha_1$  and  $\alpha_2$  are defined as in (2).

Stability region of the fractional-order Selkov model for  $\gamma = 2$  in the  $(\alpha - q)$  plane is shown in Fig. 1. The stable and unstable regions are separated by the curve of equation

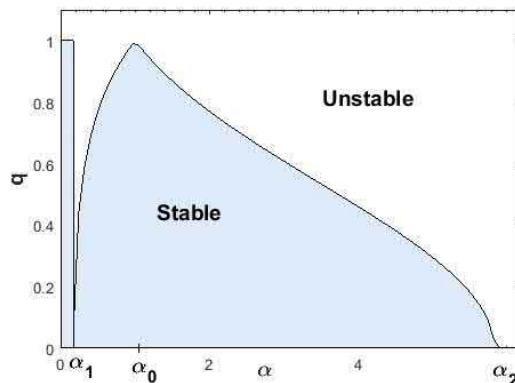


**Figure 1:** Stability region of the fractional-order Selkov model for  $\gamma = 2$ .

$q(\alpha) = \frac{2}{\pi} \left| \arctan \sqrt{\frac{4\alpha}{[\alpha(\gamma - 1) - 1]^2} - 1} \right|$ . A Hopf bifurcation occurs when the system has a pair of complex conjugate eigenvalues of the Jacobian matrix at an equilibrium point and when the stability of the equilibrium point changes from stable to unstable as the bifurcation parameter crosses a critical value. From the results of local stability, we observe that the order of derivatives has an effect on the stability of model (3). Thus, we can choose the order to be the bifurcation parameter. There are some studies that considered the existence of the Hopf bifurcations in fractional-order systems [18–20]. In this study, we use the conditions for the existence of a Hopf bifurcation which were introduced by Xiang Li and Ranchao Wu [20].

**Theorem 4.1** [20] *When the bifurcation parameter  $q$  passes through the critical value  $q^* \in (0, 1)$ , fractional-order system (3) undergoes a Hopf bifurcation at the equilibrium point if the following conditions hold:*

(a) *the Jacobian matrix of the system (3) at the equilibrium point has a pair of complex conjugate eigenvalues  $\lambda_{1,2}$ , where  $\mathcal{R}e(\lambda_{1,2}) > 0$ ;*

(b)  *$m(q^*) = 0$ , where  $m(q) = \frac{q\pi}{2} - \min_{1 \leq i \leq 2} |\arg(\lambda_i)|$ ;*

(c)  *$\left. \frac{dm(q)}{dq} \right|_{q=q^*} \neq 0$ .*

If  $\alpha_0 < \alpha < \alpha_2$ , then the Jacobian matrix of the system (3) at the equilibrium point has a pair of complex conjugate eigenvalues  $\lambda_{1,2}$ , where  $\mathcal{R}e(\lambda_{1,2}) > 0$ . Hence, condition (a) in Theorem 4.1 holds. Moreover, when the bifurcation parameter takes the critical value  $q = q^*$ , we obtain  $m(q^*) = 0$  which is the condition (b) of the theorem.

Finally, from the definition of  $m(q)$ , we have  $\left. \frac{dm(q)}{dq} \right|_{q=q^*} = \frac{\pi}{2} \neq 0$ . This implies that condition (c) holds. Therefore, from Theorem 4.1 model (3) undergoes a Hopf bifurcation at the equilibrium point  $E = (1, 1)$  when the bifurcation parameter passes through the critical value  $q^*$ , where  $\alpha_0 < \alpha < \alpha_2$ .

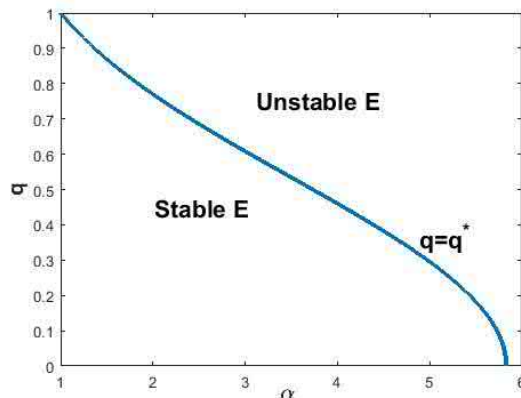


**Figure 2:** The Hopf bifurcation curve  $q = q^*$  separates the stability region of  $E$  into the stable and unstable regions for  $\gamma = 2$  and  $\alpha_0 < \alpha < \alpha_2$ .

**Remark 4.1** An important difference between the Hopf bifurcation in the integer- and the fractional-order system is that in the integer-order system the limit cycle can be a solution for this system, but in the fractional-order system, the limit cycle can not be a solution of the system and the trajectories approach a limit cycle. In [21], the authors proved that there are no periodic solutions in fractional-order systems. Thus, there is no self-sustained solutions in the fractional-order Selkov model.

## 5 Discretized Fractional-Order Selkov Model and Its Analysis

In this section, we investigate some dynamical behavior of the discretized fractional-order Selkov system (3). The discretization process can be done in the following manner [22,23]. Assume that  $x(0) = x_0$  and  $y(0) = y_0$  are the initial conditions of system (3). The discretization with a piecewise constant argument is given as

$$\begin{aligned} {}_0^c D_t^q x &= 1 - x([t/s]s)y^\gamma([t/s]s), \\ {}_0^c D_t^q y &= \alpha y([t/s]s) (x([t/s]s)y^{\gamma-1}([t/s]s) - 1). \end{aligned} \quad (6)$$

We suppose that  $t \in [0, s)$ , hence  $t/s \in [0, 1)$ . So, we have

$$\begin{aligned} {}_0^c D_t^q x &= 1 - x_0 y_0^\gamma, \\ {}_0^c D_t^q y &= \alpha y_0 (x_0 y_0^{\gamma-1} - 1), \end{aligned} \quad (7)$$

whose solution becomes

$$\begin{aligned} x_1(t) &= x_0 + I_0^q (1 - x_0 y_0^\gamma), \\ &= x_0 + \frac{t^q}{q\Gamma(q)} (1 - x_0 y_0^\gamma), \\ y_1(t) &= y_0 + I_0^q (\alpha y_0 (x_0 y_0^{\gamma-1} - 1)), \\ &= y_0 + \frac{t^q}{q\Gamma(q)} (\alpha y_0 (x_0 y_0^{\gamma-1} - 1)), \end{aligned} \quad (8)$$

where  $I_0^q = \frac{1}{\Gamma(q)} \int_0^t (t - \tau)^{q-1} d\tau$ ,  $q > 0$ .

In the second step, we assume  $t \in [s, 2s)$  so that  $t/s \in [1, 2)$  and obtain

$$\begin{aligned} {}_0^c D_t^q x &= 1 - x(s)y^\gamma(s), \\ {}_0^c D_t^q y &= \alpha y(s) (x(s)y^{\gamma-1}(s) - 1). \end{aligned} \tag{9}$$

The solution of this equation is

$$\begin{aligned} x_2(t) &= x_1(s) + I_s^q (1 - x_1(s)y_1^\gamma(s)), \\ &= x_1(s) + \frac{(t - s)^q}{q\Gamma(q)} (1 - x_1(s)y_1^\gamma(s)), \\ y_2(t) &= y_1(s) + I_s^q (\alpha y_1(s) (x_1(s)y_1^{\gamma-1}(s) - 1)), \\ &= y_1(s) + \frac{(t - s)^q}{q\Gamma(q)} (\alpha y_1(s) (x_1(s)y_1^{\gamma-1}(s) - 1)), \end{aligned} \tag{10}$$

where  $I_s^q = \frac{1}{\Gamma(q)} \int_s^t (t - \tau)^{q-1} d\tau$ ,  $q > 0$ .

Repeating the discretization process  $n$  times, we have

$$\begin{aligned} x_{n+1}(t) &= x_n(ns) + \frac{(t - ns)^q}{q\Gamma(q)} (1 - x_n(ns)y_n^\gamma(ns)), \\ y_{n+1}(t) &= y_n(ns) + \frac{(t - ns)^q}{q\Gamma(q)} (\alpha y_n(ns) (x_n(ns)y_n^{\gamma-1}(ns) - 1)), \end{aligned} \tag{11}$$

where  $t \in [ns, (n + 1)s)$ . Making  $t \rightarrow (n + 1)s$ , we obtain the corresponding fractional discrete model of the continuous fractional model (3) as

$$\begin{aligned} x_{n+1} &= x_n + \frac{s^q}{q\Gamma(q)} (1 - x_n y_n^\gamma), \\ y_{n+1} &= y_n + \frac{s^q}{q\Gamma(q)} (\alpha y_n (x_n y_n^{\gamma-1} - 1)). \end{aligned} \tag{12}$$

It should be noticed that if the fractional parameter  $q$  converges to one in equation (12), we have the forward Euler discretization of system (3).

### 5.1 Stability of the fixed point of the discretized system

In this subsection, we study the asymptotic stability of the fixed points of the model (12). By solving the equations  $x_{n+1} = x_n = x$  and  $y_{n+1} = y_n = y$ , we can easily find that (12) has the same unique fixed point as in the fractional-order system (3) given by  $E = (1, 1)$  for every parameter value  $\alpha$  and step size  $s$ . To investigate the stability of the fixed point of model (12), we need the following lemma [24].

**Lemma 5.1** *Let  $F(\lambda) = \lambda^2 - Tr\lambda + Det$ . Suppose that  $F(1) > 0$ ,  $\lambda_1$  and  $\lambda_2$  are the two roots of  $F(\lambda)$ . Then*

- (i)  $|\lambda_1| < 1$  and  $|\lambda_2| < 1$  if and only if  $F(-1) > 0$  and  $Det < 1$ .
- (ii)  $|\lambda_1| < 1$  and  $|\lambda_2| > 1$  (or  $|\lambda_1| > 1$  and  $|\lambda_2| < 1$ ) if and only if  $F(-1) < 0$ .

- (iii)  $|\lambda_1| > 1$  and  $|\lambda_2| > 1$  if and only if  $F(-1) > 0$  and  $Det > 1$ .
- (vi)  $\lambda_1 = -1$  and  $\lambda_2 \neq 1$  if and only if  $F(-1) = 0$  and  $Tr \neq 0, 2$ .
- (v)  $\lambda_1$  and  $\lambda_2$  are complex and  $|\lambda_1| = |\lambda_2|$  if and only if  $Tr^2 - 4Det < 0$  and  $Det = 1$ .

To distinguish between the different topological types for the fixed point  $E$ , we need the following lemma [25].

**Lemma 5.2** (i) A fixed point  $E$  is called a sink if  $|\lambda_1| < 1$  and  $|\lambda_2| < 1$ , so the sink is locally asymptotically stable.

(ii) A fixed point  $E$  is called a source if  $|\lambda_1| > 1$  and  $|\lambda_2| > 1$ , so the source is locally unstable.

(iii) A fixed point  $E$  is called a saddle if  $|\lambda_1| < 1$  and  $|\lambda_2| > 1$  (or  $|\lambda_1| > 1$  and  $|\lambda_2| < 1$ ), the saddle is locally unstable.

(iv) A fixed point  $E$  is called non-hyperbolic if either  $|\lambda_1| = 1$  or  $|\lambda_2| = 1$ .

**Theorem 5.1** For all  $0 < q \leq 1$  we have the following results:

- If  $0 < \alpha \leq \alpha_1$ , then the fixed point  $E$  is a sink if  $0 < s < s_1$ , a saddle point if  $s_1 < s < s_2$ , and a source if  $s \geq s_2$ .
- If  $\alpha_1 < \alpha < \alpha_0$ , then the fixed point  $E$  is a sink if  $0 < s < s_0$ , non-hyperbolic if  $s = s_0$ , and a source if  $s > s_0$ .
- If  $\alpha \geq \alpha_0$ , then the fixed point  $E$  is a source for all  $s > 0$ ,

where

$$s_0 = \left[ \frac{q\Gamma(q)}{\alpha} (1 - \alpha(\gamma - 1)) \right]^{1/q}$$

$$s_{1,2} = \left[ \frac{q\Gamma(q)}{\alpha} \left( (1 - \alpha(\gamma - 1)) \pm \sqrt{(\alpha(\gamma - 1) - 1)^2 - 4\alpha} \right) \right]^{1/q}, \quad s_1 < s_2.$$

**Proof.** The Jacobian matrix of system (12) at the fixed point  $E$  is

$$J^* = \begin{bmatrix} 1 - \frac{s^q}{q\Gamma(q)} & -\gamma \frac{s^q}{q\Gamma(q)} \\ \alpha \frac{s^q}{q\Gamma(q)} & 1 + \alpha(\gamma - 1) \frac{s^q}{q\Gamma(q)} \end{bmatrix}.$$

The characteristic equation of the Jacobian matrix can be written as

$$\lambda^2 - Tr\lambda + Det = 0,$$

where  $Tr$  is the trace and  $Det$  is the determinant of the Jacobian matrix  $J^*$ , they are given as

$$Tr = 2 + \frac{s^q}{q\Gamma(q)} (\alpha(\gamma - 1) - 1),$$

$$Det = 1 + \frac{s^q}{q\Gamma(q)} (\alpha(\gamma - 1) - 1) + \alpha \left( \frac{s^q}{q\Gamma(q)} \right)^2.$$

$\alpha$	0	$\alpha_1$	$\alpha_0$	$\alpha_2$
Selkov model	Stable Node	Stable Focus	Unstable Focus	Unstable Node
FO Selkov model	LA Stable $\forall q \in (0, 1]$	LA Stable iff $0 < q < q^*$		Unstable $\forall q \in (0, 1]$
Discretized FO Selkov model	a Sink for $0 < s < s_1$ a Saddle for $s_1 < s < s_2$ a Source for $s \geq s_2$ $\forall q \in (0, 1]$	a Sink for $s < s_0$ a Source for $s > s_0$ $\forall q \in (0, 1]$	a Source $\forall s > 0$ $\forall q \in (0, 1]$	

**Table 1:** Comparison of dynamical behaviors of the Selkov model (1) with its corresponding fractional-order system (3) and discretized fractional-order system (12).

Hence, the eigenvalues are

$$\lambda_{1,2} = 1 + \frac{s^q}{2q\Gamma(q)} \left( \alpha(\gamma - 1) - 1 \pm \sqrt{(\alpha(\gamma - 1) - 1)^2 - 4\alpha} \right).$$

We have

$$F(1) = \alpha \left( \frac{s^q}{q\Gamma(q)} \right)^2 > 0, \quad \text{for all } \alpha > 0, s > 0,$$

and

$$F(-1) = 4 + 2 \frac{s^q}{q\Gamma(q)} (\alpha(\gamma - 1) - 1) + \alpha \left( \frac{s^q}{q\Gamma(q)} \right)^2.$$

Applying Lemma 5.1 with some algebraic manipulations, one can obtain the results.  $\square$  A comparison table on dynamical behaviors of the Selkov model (1) with its corresponding fractional-order system (3) and discretized fractional-order system (12) has been given in Table 1.

### 5.2 Bifurcation analysis

The necessary and sufficient conditions ensuring that  $|\lambda_1| < 1$  and  $|\lambda_2| < 2$  are

$$F(1) > 0, \quad F(-1) > 0 \text{ and } Det > 1.$$

The violation of one of these conditions, with the other two being simultaneously fulfilled leads to:

- (i) a fold or transcritical bifurcation (a real eigenvalue that passes through +1). This local bifurcation leads to the stability switching between two different steady states;

- (ii) a flip bifurcation (a real eigenvalue that passes through -1). This local bifurcation entails the birth of a period 2-cycle;
- (iii) a Neimark-Sacker bifurcation (i.e., the modulus of a complex eigenvalue pair that passes through 1). This local bifurcation implies the birth of an invariant curve in the phase plane. The Neimark-Sacker bifurcation is considered to be equivalent to the Hopf bifurcation in continuous time and is indeed the major instrument to prove the existence of quasi-periodic orbits for the map.

In [25], the author presents a complete study of the main types of bifurcations for two-dimensional maps.

Now, we study the bifurcation types of the fixed point  $E$ .

**Theorem 5.2** *The fixed point  $E$  loses its stability*

- (i) *via a flip bifurcation when  $0 < \alpha \leq \alpha_1$  and  $s = s_1$ .*
- (ii) *via a Neimark-Sacker bifurcation when  $\alpha_1 < \alpha < \alpha_0$  and  $s = s_0$ .*

**Proof.**

- (i) When  $0 < \alpha \leq \alpha_1$ , the Jacobian matrix  $J^*$  has a pair of real eigenvalues. At  $s = s_1$ , we have  $\lambda_1 \neq 0$  and  $\lambda_2 = -1$ , thus the model (12) undergoes a flip bifurcation which entails the birth of a period 2-cycle.
- (ii) When  $\alpha_1 < \alpha < \alpha_0$ , the Jacobian matrix  $J^*$  has a pair of complex conjugate eigenvalues. At  $s = s_0$ , the modulus of  $\lambda_{1,2}$  is equal to 1, thus the model (12) undergoes a Neimark-Sacker bifurcation.  $\square$

## 6 Numerical Simulation

In this section, we perform numerical simulation to confirm the above theoretical analysis and to illustrate the dynamics of both the fractional-order Selkov model and its discretization.

There are many numerical methods for solving nonlinear fractional differential equations such as the Adomian decomposition method [26], variational iteration method [27] and homotopy perturbation method [28]. In this study, we use the Adams-type predictor-corrector method [29] for the numerical solution of system (3). This method is a very effective tool to give numerical solutions of fractional-order differential equations.

Without loss of generality, we fix  $\gamma = 2$ , which gives  $\alpha_0 = 1$ ,  $\alpha_1 = 0.17157$  and  $\alpha_2 = 5.8284$ , we choose  $\alpha = 1.2$  (in the interval  $(\alpha_1, \alpha_2)$ ) and we vary the order  $q$ , the step size is considered as 0.01 and the initial point  $x(0) = 1.5$ ,  $y(0) = 1.3$ . Note that for  $\alpha = 1.2$ , there exists a critical value  $q = q^* = 0.9418$  below which the equilibrium point  $E$  is asymptotically stable and above which unstable. The stable behavior of the system is presented in Fig.5(a)-(b) for  $q = 0.92$  ( $< 0.9418$ ) and the unstable behavior of the system for  $q = 0.98$  ( $> 0.9418$ ) is presented in Fig.5(c)-(d). A Hopf bifurcation occurs at  $q = q^*$ .

To illustrate the corresponding discrete system (12) of the fractional-order Selkov system (3), we consider  $q = 0.85$ . Stability of the fixed point depends on the step size  $s$ . First, we take  $\alpha = 0.1$  (in the interval  $(0, \alpha_1)$ ), then the step size  $s$  should be less than  $s_1 = 2.8775$  for  $E$  to be stable and otherwise unstable. The fixed point undergoes

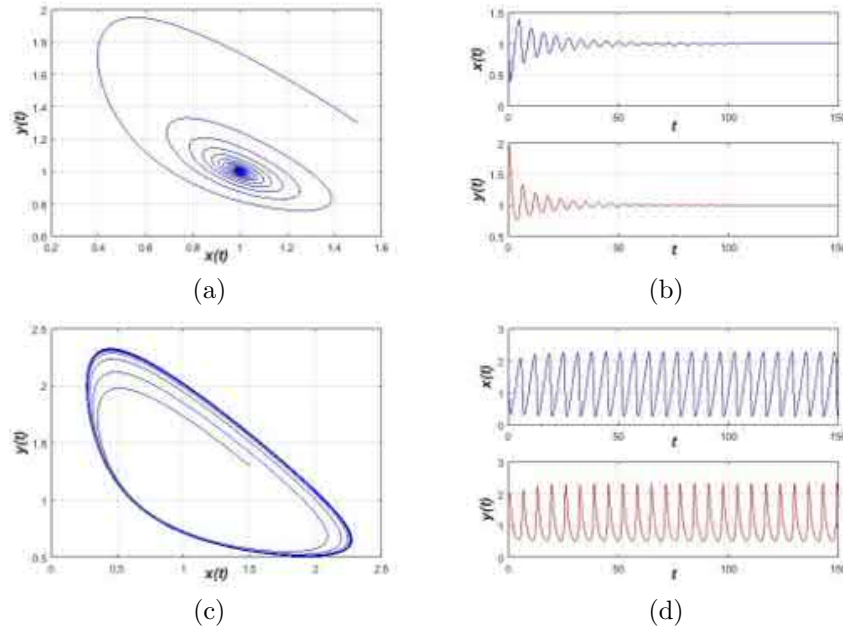
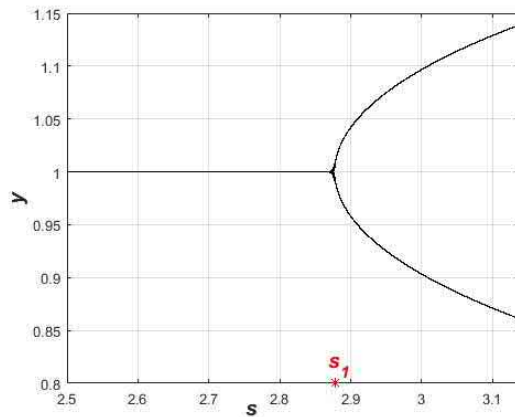


**Figure 3:** Phase portraits and the time series fractional-order Selkov model for (a),(b)  $q = 0.92$ , (c), (d)  $q = 0.98$ .

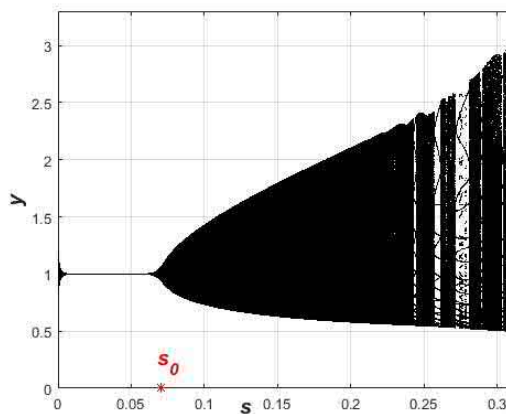
a flip bifurcation (Fig.4(a)) at the critical step size  $s = s_1$ . Now, we take  $\alpha = 0.9$  (in the interval  $(\alpha_1, \alpha_0)$ ), the Jacobian matrix  $J^*$  has a pair of complex conjugate eigenvalues  $\lambda_{1,2} = 0.99409 + 0.11203i$ , where  $|\lambda_{1,2}| = 1$ , for the value of step size  $s = s_0 = 0.07597$  this implies that the system (12) undergoes a Neimark-Saker bifurcation at the fixed point  $E$ . The bifurcation diagram (Fig.4(b)) represents it succinctly. The maximal Lyapunov exponents corresponding to Fig.4(b) are computed and plotted in Fig.4(c), from which we deduce that chaotic behaviors may arise when the step size  $s$  is increasing. Some phase portraits are displayed in Fig.5. It clearly depicts the process of how a smooth invariant closed curve (Fig.5(b)) bifurcates from the stable fixed point  $E$  (Fig.5(a)). When  $s$  exceeds  $s_0 = 0.07597$  (for example,  $s = 0.08$ ), a simple closed curve enclosing the fixed point  $E$  appears. When  $s$  increases, the simple closed curve disappears. The strange attractor of system (12) for  $s = 0.305$  is shown in Fig.5(f).

### 7 Conclusion

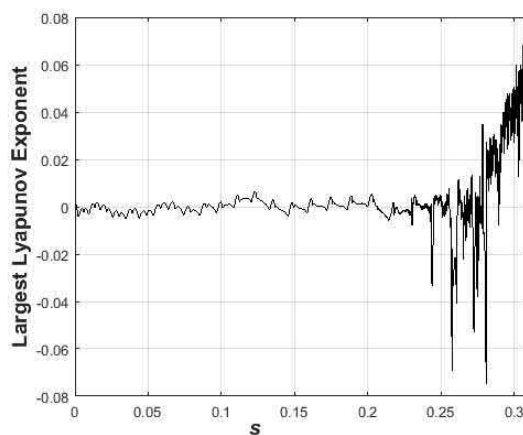
In this work, we have introduced a fractional-order Selkov model and its discretized counterpart. For the fractional-order system we have proved some mathematical results such as non-negativity, existence and uniqueness of the solution. We have also studied the local stability of the equilibrium point and proved the existence of a Hopf bifurcation with respect to the fractional order. Discretization of the fractional-order system was done with piecewise constant arguments and the corresponding dynamics was explored. It is observed that the dynamics of the discrete system depends on both the step size and the fractional order. Existence of the Neimark-Saker and flip bifurcations has been shown both analytically and numerically. It is also observed that the discrete fractional-order



(a)



(b)



(c)

**Figure 4:** (a) Bifurcation diagram of the discrete fractional-order Selkov system (12) for  $q = 0.85$  and  $\alpha = 0.1$ , a flip bifurcation occurs at  $s = s_1 = 2.8775$ ; (b),(c) Bifurcation diagram and the corresponding maximal Lyapunov exponent of system (12) for  $q = 0.85$  and  $\alpha = 0.9$ , a Neimark-Sacker bifurcation occurs at  $s = s_0 = 0.070591$ .

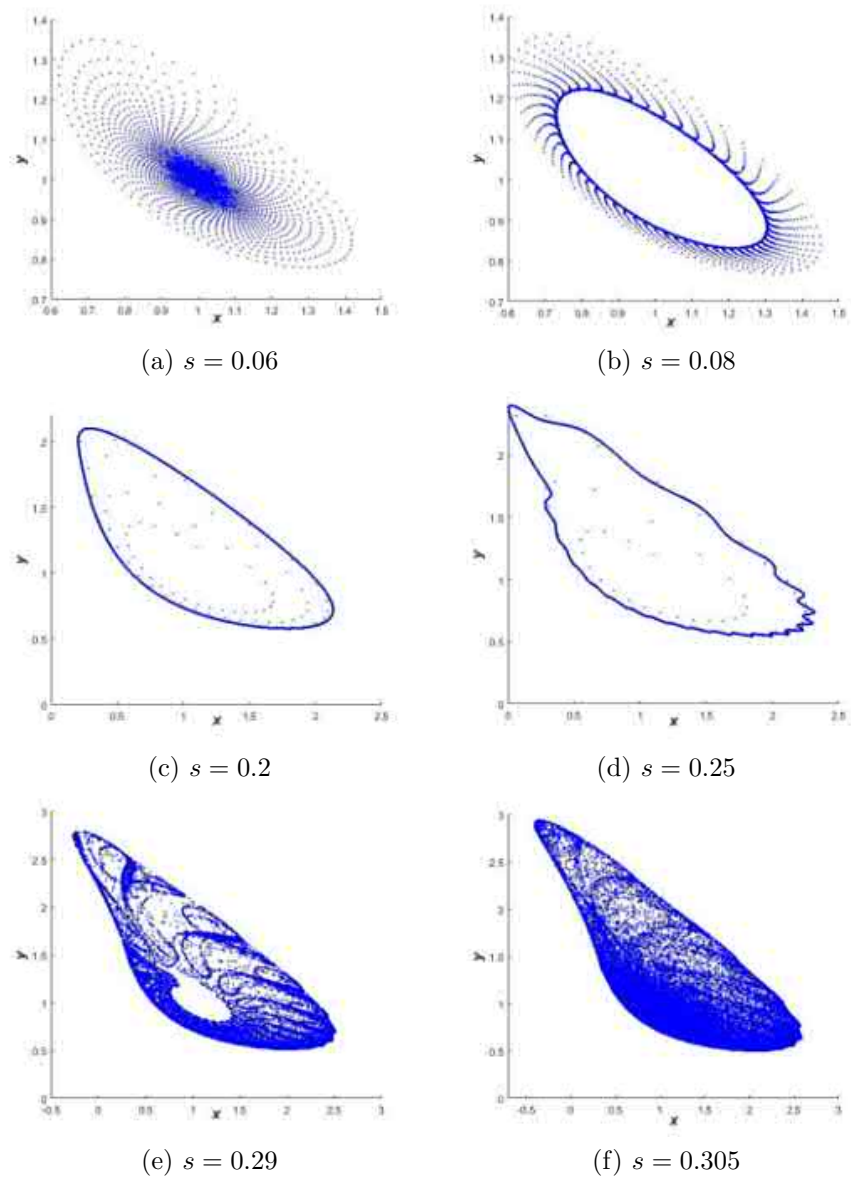


**Figure 5:** Phase portraits of the discretized fractional-order Selkov model for some values of the step size  $s$ .

system shows more complex dynamics as the step size becomes larger. Our simulation results revealed that the discrete system exhibits chaotic dynamics for a larger step size.

## References

- [1] J. Higgins. A chemical mechanism for oscillation of glycolytic intermediates in yeast cells. *Proc. Natl. Acad. Sci. (USA)* **51** (1964) 989–994.
- [2] E.E. Selkov. Self-oscillations in glycolysis. *Eur. J. Biochem* **4** (1968) 79–86.
- [3] A. d’Onofrio. Uniqueness and global attractivity of glycolytic oscillations suggested by Selkov’s model. *J. Math. Chem.* **48** (2010) 339–346.
- [4] D.V. Verveyko, A.Y. Verisokin and E.B. Postnikov. Mathematical model of chaotic oscillations and oscillatory entrainment in glycolysis originated from periodic substrate supply. *Chaos* **27** (2017) 083104.
- [5] P. Brechmann and A.D. Rendall. Dynamics of the selkov oscillator. *Mathematical Biosciences* **306** (2018) 152–159.
- [6] J. C. Artés, J. Llibre and C. Valls. Dynamics of the Higgins-Selkov and Selkov systems. *Chaos Solitons Fractals* **114** (2018) 145–150.
- [7] C. Song and J. Cao. Dynamics in fractional-order neural networks. *Neurocomputing* **142** (2014) 494–498.
- [8] N. Laskin. Fractional market dynamics. *Physica A* **287** (2000) 482–492.
- [9] R. Barkat and T. Menacer. Dynamical Analysis, Stabilization and Discretization of a Chaotic Financial Model with Fractional Order. *Nonlinear Dynamics and Systems Theory*. **20** (3) (2020) 253–266.
- [10] F.A. Rihan. Numerical modeling of fractional-order biological systems. *Abstract and Applied Analysis* **2013** (2013) 1–11 .
- [11] C. Ionescu, A. Lopes, D. Copot, J.A.T. Machado and J.H.T. Bates. The Role of Fractional Calculus in Modelling Biological Phenomena: A review. *Communications in Nonlinear Science and Numerical Simulation* (2017). doi: 10.1016/j.cnsns.2017.04.001.
- [12] M. Sheybak and H. Tajadodi. Numerical Solutions of Fractional Chemical Kinetics System. *Nonlinear Dynamics and Systems Theory*. **19** (1-SI) (2019) 200–208.
- [13] N. Hamri and T. Houmor. Chaotic dynamics of the fractional order nonlinear Bloch system. *Electronic Journal of Theoretical Physics* **8** (25) (2011) 233–244.
- [14] L. Perko. *Differential Equations and Dynamical Systems*. Springer, Heidelberg, 1991.
- [15] M. Odibat and N. T. Shawagfeh. Generalized Taylor’s formula. *Appl.Math.Comput.* **186** (2007) 286-293.
- [16] I. Podlubny. *Fractional Differential Equations*. Academic Press, New York, 1999.
- [17] D. Matignon. Stability result on fractional differential equations with applications to control processing. In: *Comput. Eng. Syst. Appl.*, Lille, France, 1996, 963-968.
- [18] A.S. Deshpande, V. Daftardar-Gejji and Y.V. Sukale. On Hopf bifurcation in fractional dynamical systems. *Chaos Solitons Fractals* **98** (2017) 189–198. <https://doi.org/10.1016/j.chaos.2017.03.034>.
- [19] M. Abdelouahab, N. Hamri and J. Wang. Hopf bifurcation and chaos in fractional-order modified hybrid optical system. *Nonlinear Dynamics* **69** (1-2) (2012) 275–284. <https://doi.org/10.1007/s11071-011-0263-4>.
- [20] X. Li and R. Wu. Hopf bifurcation analysis of a new commensurate fractional-order hyperchaotic system. *Nonlinear Dynamics* **78** (1) (2014) 279–288. <https://doi.org/10.1007/s11071-014-1439-5>.

- [21] M.S. Tavazoei and M. Haeri. A proof for non existence of periodic solutions in time invariant fractional order systems. *Automatica* **45** (8) (2009) 1886–1890.
- [22] A.M.A. El-Sayed and S.M. Salman. On a discretization process of fractional order Riccati's differential equation. *J. Fract. Calc. Appl.* **4** (2013) 251–259.
- [23] A.A. Elsadany and A.E. Matouk. Dynamical behaviors of fractional-order Lotka Volterra predator-prey model and its discretization. *J. Appl. Math. Comput.* **49** (2015) 269–283.
- [24] H.N. Agiza, E.M. Elabbasy, H. EL-Metwally and A.A. Elsadany. Chaotic dynamics of a discrete prey predator model with Holling type II. *Nonlinear Anal. Real World Appl.* **10** (2009) 116–119.
- [25] S. Elaydi. *Discrete Chaos with Applications in Science and Engineering*. (2nd edn.). Chapman and Hall/CRC, Boca Raton, 2008.
- [26] H. Jafari and V. Daftardar-Gejji. Solving a system of nonlinear fractional differential equations using Adomian decomposition. *J. Comput. Appl. Math.* **196** (2) (2006) 644–651. <https://doi.org/10.1016/j.cam.2005.10.017>.
- [27] G. Wu. A fractional variational iteration method for solving fractional nonlinear differential equations. *Comput. Math. Appl.* **61** (8) (2011) 2186–2190. <https://doi.org/10.1016/j.camwa.2010.09.010>.
- [28] J.H. He. Homotopy perturbation technique. *Computer Methods in Applied Mechanics and Engineering* **178** (3-4) (1999) 257–262.
- [29] K. Diethelm, N.J. Ford and A.D. Freed. A predictor-corrector approach for the numerical solution of fractional differential equations. *Nonlinear Dynamics* **29** (1) (2002) 3–22. <https://doi.org/10.1023/A:1016592219341>.



# DTC-SVM Sensorless Control of Five-Phase Induction Motor Based on Two Different Rotor Speed Estimation Approaches

B. S. Khaldi<sup>1,2,\*</sup>, A. Kouzou<sup>1</sup>, M. O. Mahmoudi<sup>2</sup> and D. Boukhetala<sup>2</sup>

<sup>1</sup> *Laboratory of Applied Automation and Industrial Diagnosis, Faculty of Sciences and Technology, Djelfa University, Algeria.*

<sup>2</sup> *Process Control Laboratory, National Polytechnic School, Algiers, Algeria.*

Received: March 9, 2021; Revised: May 20, 2021

**Abstract:** This paper deals with the study and analysis of the five-phase induction motor (FFIM) sensorless control based on the combination of the direct torque control (DTC) technique and the space vector modulation (SVM) technique. Indeed, this sensorless control applied to the FFIM is achieved using two different rotor speed estimation approaches. The first approach is based on the adaptive flux and speed observer for ensuring the estimation of the rotor speed and rotor flux at once. The second approach is performed based on the model reference adaptive system estimator for ensuring the estimation of the rotor speed. The applications of both estimation approaches with the combined techniques for ensuring the sensorless control of the FFIM are presented and analyzed to shed light on their main performances compared with each other based on the main predominant constraints such as the processor computation time and memory size costs, robustness against the machine parameter variation and the accuracy of estimation. The analysis of the results obtained by simulation allows the validation of both approaches in ensuring the sensorless control of the FFIM using the DTC-SVM with some limited differences.

**Keywords:** *direct torque control (DTC); space vector modulation (SVM); stator flux oriented control (SFOC); five-phase induction machine (FFIM); speed sensorless; adaptive observer; model reference adaptive system (MRAS).*

**Mathematics Subject Classification (2010):** 03B52, 93C42, 94D05.

---

\* Corresponding author: <mailto:bs.khaldi@gmail.com>

## 1 Introduction

Multiphase drives have recently gained interest due to their advantages over traditional three-phase drives for high-power applications (e.g., locomotive traction, electric ship propulsion) and/or high-current applications (e.g., electric and hybrid vehicles). Indeed, there are plenty benefits of a greater number of phases such as reducing the inverter per leg power, decreasing the amplitude of torque pulsations in motor drives and lowering the dc-link current harmonics [1]. Another very interesting feature of this kind of machines is their capability to start-up and run even with one or two non-adjacent stator phases under open or short circuit. Hence, it provides high reliability, especially in industrial applications where the stop of the machine has to be avoided during working process.

The technique of torque control of induction motors was developed and presented by I. Takahashi as a direct torque control (DTC) [2], and by M. Depenbrock as a direct self control (DSC) [3]. It is possible to enhance the operating characteristics of not only the motor but also the voltage source inverter (VSI) supplying such drives by using the direct control of the stator flux and torque instead of the traditional current control technique.

The basic principle behind a three-phase ac drive's DTC is to directly and independently control the electromagnetic torque and flux linkage by using six or eight voltage space vectors saved in a lookup table. Since the DTC approach has additional advantages when applied to multiphase machines, in recent years the application of the DTC technique for multiphase machines has received a widespread attention [4–6]. The five-phase induction motor direct torque control can minimize successfully the ripple amplitude of both the stator flux and the torque, allowing a more reliable flux and torque control [7].

The use of the space vector modulation (SVM) retains the transient performance and robustness of the DTC, and decreases the torque ripple of the steady state. At the same time, the switching frequency can also be kept constant and controllable [8]. It can be said that the five-phase inverter can give more flexibility due to its ability to provide 32 space vector voltages, hence the elaboration of the desired torque and flux can be obtained in a more flexible and accurate way compared to its counter-part of three phases.

A large number of studies have been carried out focusing mainly on sensorless drives on a three-phase induction machine to increase the efficiency and reduce cost. Although the cases of the sensorless control of a multiphase motor drive are limited in the literature, nevertheless few documented research activities treat the sensorless control of a five-phase motor as a three-phase case extension. B. S. Khaldi et al. [9] have presented a comparison between a new sensorless method and an adaptive observer for the DTC applied on the five-phase IM. H. Echeikh et al. [10] have proposed an improved sliding mode observer for the sensorless control of a five-phase induction motor. O. Gonzalez et al. [11] have proposed a speed sensorless control of a five-phase induction machine by using an inner loop of the model-based predictive control. In [12], the authors have described the use of 02 speed observers system planes for a five-phase machine supplied by the current source inverter.

It is known that the most popular speed sensorless control is the MRAS technique because of its simple implementation. In some previous works, the MRAS speed estimator is applied for the five-phase induction machine with several schemes such as the scalar control [13], the vector control [14], and the SVM-backstepping control [15]. However, a limited number of works have investigated the direct torque control of a five-phase induction machine.

In this paper, the authors present an extension of the application of the MRAS technique for a three-phase machine to be incorporated with the application of the DTC for a five-phase induction motor for ensuring its sensorless control and compare it with a speed and flux full-order adaptive observer which is used for the same purpose.

The following part of this paper is organized in five sections. Section 2 focuses on the presentation of the modeling of a five-phase induction machine; Section 3 describes in details the direct torque control of a five-phase induction motor and the space vector PWM. In Section 4, the authors present the first observer used for the estimation of the rotor speed and the rotor flux called a speed and flux full-order adaptive observer. Further, in Section 5, the extended application of the MRAS to a five-phase induction motor is presented. Section 6 is dedicated to the results obtained via simulation. This paper ends with a conclusion.

## 2 Modeling of a Five-Phase Induction Machine

In the present paper, the modeling of the five-phase induction machine will be based on some simplifying hypotheses, which can be presented as follows:

- The motor has an unsaturated symmetrical armature.
- The hysteresis and eddy currents are negligible.
- The air gap is of uniform thickness, the slotting effect is neglected.
- The proper and mutual inductances are independent of the currents flowing in the different windings.
- The distribution of the flux along the air gap is assumed to be a sine waveform.
- The skin effect is negligible.
- Considering regular phase shifting between each two sequenced phases, the windings in all phases are supposed to be identical.

The model of the machine is presented in a common reference frame, rotating at an arbitrary angular speed as shown in Fig.1.

The model of the five-phase squirrel cage induction machine can be written in matrix form as follows [16]:

$$\begin{cases} [V_{abcde}^s] = [R_s][I_{abcde}^s] + \frac{d}{dt} [\phi_{abcde}^s], \\ [V_{abcde}^r] = [R_r][I_{abcde}^r] + \frac{d}{dt} [\phi_{abcde}^r] = 0, \end{cases} \quad (1)$$

$$\begin{cases} [\phi_{abcde}^s] = [L_s][I_{abcde}^s] + [L_{sr}][I_{abcde}^r], \\ [\phi_{abcde}^r] = [L_r][I_{abcde}^r] + [L_{rs}][I_{abcde}^s], \end{cases} \quad (2)$$

where

$$\begin{bmatrix} V_{abcde}^s \\ V_{abcde}^r \end{bmatrix} = \begin{bmatrix} V_a^s & V_b^s & V_c^s & V_d^s & V_e^s \\ V_a^r & V_b^r & V_c^r & V_d^r & V_e^r \end{bmatrix}^T, \quad (3)$$

$$\begin{bmatrix} I_{abcde}^s \\ I_{abcde}^r \end{bmatrix} = \begin{bmatrix} I_a^s & I_b^s & I_c^s & I_d^s & I_e^s \\ I_a^r & I_b^r & I_c^r & I_d^r & I_e^r \end{bmatrix}^T, \quad (4)$$

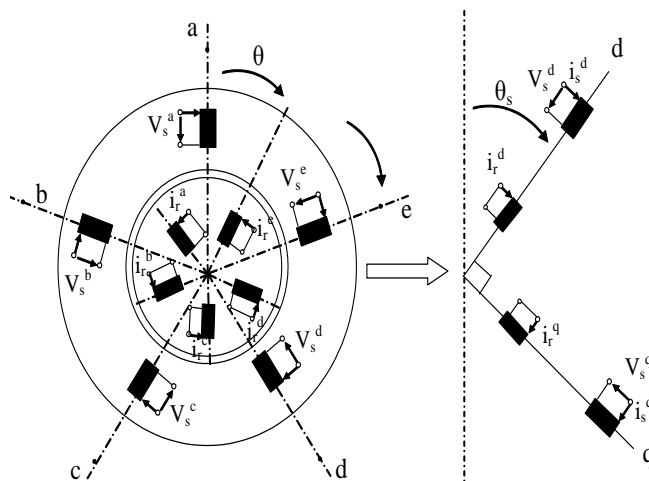


Figure 1: Park transformation applied to the five-phase induction machine.

$$\begin{bmatrix} \phi_{abcde}^s \\ \phi_{abcde}^r \end{bmatrix} = \begin{bmatrix} \phi_a^s & \phi_b^s & \phi_c^s & \phi_d^s & \phi_e^s \\ \phi_a^r & \phi_b^r & \phi_c^r & \phi_d^r & \phi_e^r \end{bmatrix}^T. \quad (5)$$

For the simplification of the model of the machine under study, which is presented in the natural frame abc, the following matrices of transformation are used for the stator and the rotor to obtain the model of the machine in biphasic frames while keeping the power invariant. These matrices are presented as follows:

$$A_s = \sqrt{\frac{2}{5}} \begin{bmatrix} \cos \theta_s & \cos(\theta_s - \alpha) & \cos(\theta_s - 2\alpha) & \cos(\theta_s + 2\alpha) & \cos(\theta_s + \alpha) \\ -\sin \theta_s & -\sin(\theta_s - \alpha) & -\sin(\theta_s - 2\alpha) & -\sin(\theta_s + 2\alpha) & -\sin(\theta_s + \alpha) \\ 1 & \cos(2\alpha) & \cos(4\alpha) & \cos(4\alpha) & \cos(2\alpha) \\ 0 & \sin(2\alpha) & \sin(4\alpha) & -\sin(4\alpha) & -\sin(2\alpha) \\ 1/\sqrt{2} & 1/\sqrt{2} & 1/\sqrt{2} & 1/\sqrt{2} & 1/\sqrt{2} \end{bmatrix}, \quad (6)$$

$$A_r = \sqrt{\frac{2}{5}} \begin{bmatrix} \cos \beta & \cos(\beta - \alpha) & \cos(\beta - 2\alpha) & \cos(\beta + 2\alpha) & \cos(\beta + \alpha) \\ -\sin \beta & -\sin(\beta - \alpha) & -\sin(\beta - 2\alpha) & -\sin(\beta + 2\alpha) & -\sin(\beta + \alpha) \\ 1 & \cos(2\alpha) & \cos(4\alpha) & \cos(4\alpha) & \cos(2\alpha) \\ 0 & \sin(2\alpha) & \sin(4\alpha) & -\sin(4\alpha) & -\sin(2\alpha) \\ 1/\sqrt{2} & 1/\sqrt{2} & 1/\sqrt{2} & 1/\sqrt{2} & 1/\sqrt{2} \end{bmatrix}. \quad (7)$$

Here

$$\theta_s = \int \omega_a dt \text{ and } \beta = \theta_s - \theta = \int (\omega_a - \omega) dt, \quad (8)$$

where  $\alpha = 2\pi/5$ ,  $\beta$  is the instantaneous angular position of the d-axis of the common reference frame,  $\omega_a$  is the arbitrary speed of the selected common reference frame,  $\omega$  is the rotor angular (electrical) speed and  $\theta$  is the instantaneous rotor position. Using these transformations, the equations in the  $d - q - d_1 - q_1 - 0$  domain can be written as

$$[V_{dq_1q_10}^s] = [A_s][V_{abcde}^s], \quad [\phi_{dq_1q_10}^r] = [A_r][\phi_{abcde}^r], \quad (9)$$

$$[V_{dq d_1 q_1 0}^r] = [A_r][V_{abcde}^r], \quad [I_{dq d_1 q_1 0}^s] = [A_s][I_{abcde}^s], \quad (10)$$

$$[\phi_{dq d_1 q_1 0}^s] = [A_s][\phi_{abcde}^s], \quad [I_{dq d_1 q_1 0}^r] = [A_r][I_{abcde}^r]. \quad (11)$$

The stator and rotor voltage equations for the machine in arbitrary reference frame can be written as (the symbol  $p$  stands for  $d/dt$ )

$$\begin{cases} V_{ds} = R_s I_{ds} - \omega_a \phi_{qs} + p\phi_{ds}, & V_{d_1s} = R_s I_{d_1s} + p\phi_{d_1s}, \\ V_{qs} = R_s I_{qs} + \omega_a \phi_{ds} + p\phi_{qs}, & V_{q_1s} = R_s I_{q_1s} + p\phi_{q_1s}, \\ V_{dr} = R_r I_{dr} - (\omega_a - \omega) \phi_{qr} + p\phi_{dr}, & V_{d_1r} = R_r I_{d_1r} + p\phi_{d_1r}, \\ V_{qr} = R_r I_{qr} + (\omega_a - \omega) \phi_{dr} + p\phi_{qr}, & V_{q_1r} = R_r I_{q_1r} + p\phi_{q_1r}. \\ V_{0s} = R_s I_{0s} + p\phi_{0s}, & V_{0r} = R_r I_{0r} + p\phi_{0r}. \end{cases} \quad (12)$$

The flux linkages  $\phi_{ds}$ ,  $\phi_{qs}$ ,  $\phi_{dr}$  and  $\phi_{qr}$  can be written after transformation as

$$\begin{cases} \phi_{ds} = (L_{ls} + L_m) I_{ds} + L_m I_{dr}, & \phi_{d_1s} = L_{ls} I_{d_1s}, \\ \phi_{qs} = (L_{ls} + L_m) I_{qs} + L_m I_{qr}, & \phi_{q_1s} = L_{ls} I_{q_1s}, \\ \phi_{dr} = (L_{lr} + L_m) I_{dr} + L_m I_{ds}, & \phi_{d_1r} = L_{lr} I_{d_1r}, \\ \phi_{qr} = (L_{lr} + L_m) I_{qr} + L_m I_{qs}, & \phi_{q_1r} = L_{lr} I_{q_1r}. \\ \phi_{0s} = L_{ls} I_{0s}, & \phi_{0r} = L_{lr} I_{0r}. \end{cases} \quad (13)$$

In the stationary reference frame, the stator and rotor equations of the five-phase IM can also be obtained as follows:

$$\begin{cases} V_{\alpha s} = R_s I_{\alpha s} + p\phi_{\alpha s}, & V_{d_1s} = R_s I_{d_1s} + p\phi_{d_1s}, \\ V_{\beta s} = R_s I_{\beta s} + p\phi_{\beta s}, & V_{q_1s} = R_s I_{q_1s} + p\phi_{q_1s}, \\ V_{0s} = R_s I_{0s} + p\phi_{0s}, \\ V_{\alpha r} = R_r I_{\alpha r} + \omega \phi_{\beta r} + p\phi_{\alpha r}, & V_{d_1r} = R_r I_{d_1r} + p\phi_{d_1r}, \\ V_{\beta r} = R_r I_{\beta r} - \omega \phi_{\alpha r} + p\phi_{\beta r}, & V_{q_1r} = R_r I_{q_1r} + p\phi_{q_1r}, \\ V_{0r} = R_r I_{0r} + p\phi_{0r}, \end{cases} \quad (14)$$

$$\begin{cases} \phi_{\alpha s} = (L_{ls} + L_m) I_{\alpha s} + L_m I_{\alpha r}, & \phi_{d_1s} = L_{ls} I_{d_1s}, \\ \phi_{\beta s} = (L_{ls} + L_m) I_{\beta s} + L_m I_{\beta r}, & \phi_{q_1s} = L_{ls} I_{q_1s}, \\ \phi_{\alpha r} = (L_{lr} + L_m) I_{\alpha r} + L_m I_{\alpha s}, & \phi_{d_1r} = L_{lr} I_{d_1r}, \\ \phi_{\beta r} = (L_{lr} + L_m) I_{\beta r} + L_m I_{\beta s}, & \phi_{q_1r} = L_{lr} I_{q_1r}, \\ \phi_{0r} = L_{lr} I_{0r}, & \phi_{0s} = L_{ls} I_{0s}. \end{cases} \quad (15)$$

The torque equation can be written as

$$T_e = PL_m (I_{dr} I_{qs} - I_{ds} I_{qr}). \quad (16)$$

Therefore, the difference between the model of the five-phase machine and the model of the three-phase machine is the existence of  $d_1 - q_1$  components in (12)-(15). From equations (12) and (13), it is clear that the components of the rotor and stator in the  $d_1 - q_1$  frame are completely decoupled from the components of  $d - q$  and one from each other. On the other side, the rotor and stator components in  $d_1 - q_1$  are totally decoupled, hence these components do not contribute to the production of the flux or the electromagnetic couple, however they can produce more losses in the machine. Due to the short-circuited rotor winding and star connection of the stator winding, it is supposed further that the five-phase components are balanced in the stator and rotor, the zero sequence components of both the stator and the rotor can be omitted from further consideration.

This means that the five-phase induction machine model would be identical to the three-phase induction machine model. Therefore, as with a three-phase induction machine, the same DTC concepts can be used.

### 3 Direct Torque Control of a Five-Phase Induction Motor

The direct torque control approach was found to be a powerful technique for ensuring a quick dynamic response in the three-phase induction motor, hence it is expected to achieve the same features when applied to the five-phase induction motor which is presented in this section. The DTC approach is based on the vector theory of space voltage [2, 3]. The decoupling of the flux and the torque can be accomplished based on the merits of the used five-phase inverters, which allows obtaining of suitable space voltage vectors among the available switching patterns offered by this kind of inverter.

The DTC control technique was demonstrated in several previous works to be more simple compared to the conventional control techniques such as the field-oriented control, which have been used intensively for the control of many machine topologies. Indeed, the DTC does not use the current controller and PWM signal generators, in contrast, the torque response is greatly improved [17], which makes this technique more attractive to be applied within many topologies of electrical motors such as multi-phase machines.

The five-phase motor is fed by a five-phase voltage source inverter as shown in Fig.2. In this kind of inverter, 32 switching states can be obtained, there are two zero voltage states associated with either, all upper switches are “on” or all bottom switches are “off”. At the same time, there are thirty non-zero active vectors, which are distributed in three concentrated regular decagons, where these active vectors are presenting the difference vertices. The difference between the three decagons is the length of their vertices with constant ratios referring to the inner decagon vertices that can be defined as the golden ratio  $\phi$ ,  $1 : 1.618 : 1.618^2$  (Fig.3).

The SV-PWM is used to produce almost the best sinusoidal phase output voltages, where the most low frequency dominant harmonics have neglected amplitude compared to the fundamental component. In this paper, it is proposed to use only the active vectors, which are located in the two outer decagons presenting the large and medium active vectors. In each switching period, the use of two adjacent medium space vectors with two large active space vectors makes it possible to maintain a zero average value [18], and consequently, providing almost sinusoidal output.

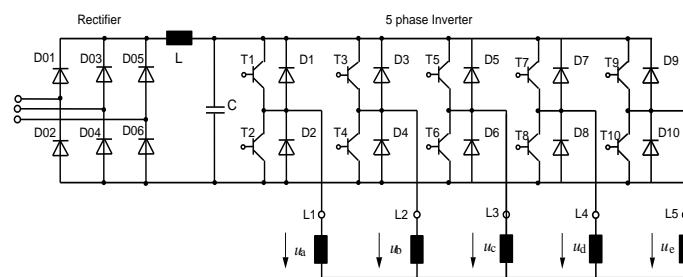


**Figure 2:** Five-phase pulsewidth-modulation inverter.

The stator vector control or the stator flux oriented control (SFOC) is applied to the five-phase induction machine. It is based basically on two types of estimators, which are used to ensure the estimation in real time of the stator flux and the rotor speed. The first one is the adaptative flux and speed observer, and the second one is the MRAS estimator. The principal of the SFOC presented in this paper is illustrated in Fig.4, where

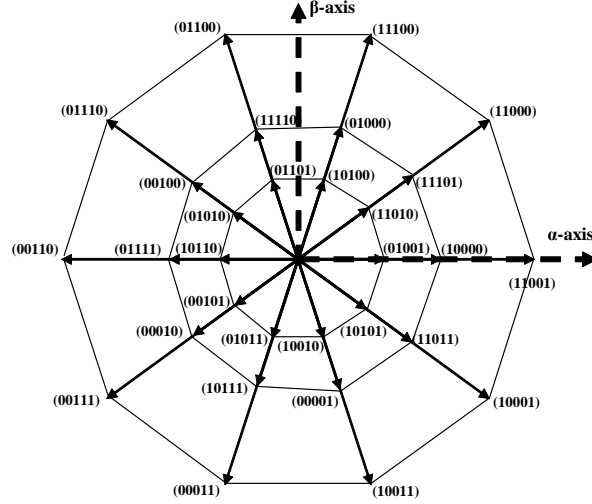


**Figure 3:** Thirty non-zero switching vectors for the five-phase IM motor drive in the  $\alpha - \beta$  plane.

the control can be achieved based on the use of one of the aforementioned estimators as it is indicated in Fig.4.

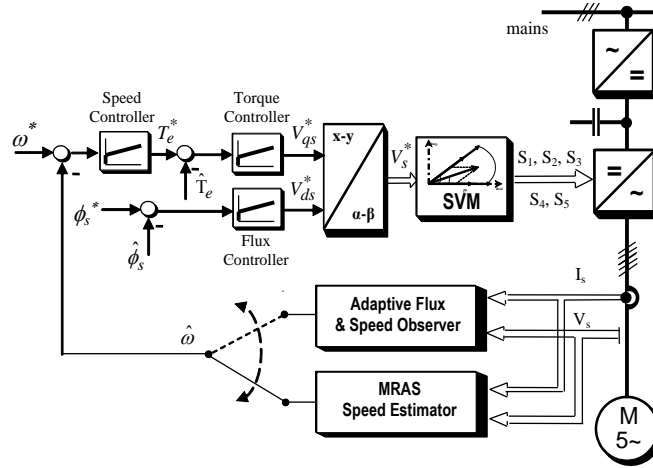


**Figure 4:** Schematic block diagram of the speed sensorless five-phase induction motor.

The mechanical equation of the motor can be expressed as follows:

$$\begin{cases} \frac{J}{P} \frac{d\omega}{dt} = T_e - T_L - \frac{T_f}{P} \omega, \\ T_e = P(\phi_{ds} I_{qs} - \phi_{qs} I_{ds}), \end{cases} \quad (17)$$

where  $T_e$  is the electromagnetic torque developed by the motor in (N.m),  $T_L$  is the load torque in (N.m),  $T_f$  is the friction torque in (N.m) and  $\omega$  is the rotor speed in rad/s.

The voltage stator equation presented in equation (12) can be rewritten in the stator flux coordinate, where the stator linkage flux is aligned with the  $d$  axis, which means that the  $q$  component will be equal to zero ( $\phi_{ds} = \phi_s, \phi_{qs} = 0$ ). Hence, the voltage stator equations become as follows:

$$\begin{cases} V_{ds} = R_s I_{ds} + \frac{d\phi_s}{dt}, \\ V_{qs} = R_s I_{qs} + \omega_a \phi_s, \\ T_e = p\phi_s I_{qs}. \end{cases} \quad (18)$$

From (18), the motor can be expressed as follows:

$$\begin{cases} \frac{d\phi_s}{dt} = V_{ds} - R_s I_{ds}, \\ T_e = \frac{p\phi_s}{R_s} (V_{qs} - \omega_a \phi_s). \end{cases} \quad (19)$$

Indeed, the DTC-SVM is based mainly on the stator flux oriented control (SFOC) and benefits from the use of two PI controllers, the first one is used for the torque control and the second one is used for the flux control. These controllers contribute within a closed loop to providing the reference stator voltages in the  $(d - q)$  frame as shown in Fig.5. Then these obtained voltages are used as the input for the SVPWM technique to generate the different switching patterns [8].

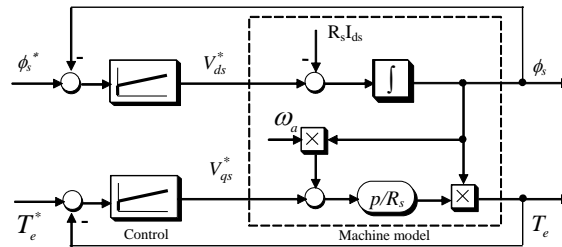


Figure 5: Block diagram of the flux and torque loops.

As shown in Fig.6(a), four active space vectors (two medium vectors and two large vectors) in each sector, will be applied for the production of the desired reference voltage at each sampling time step. Therefore, the main task of the SVPWM techniques is the determination of the times of application of each vector in each sector to synthesize the output voltage vector as required. The four times of application of the four vectors are nominated as  $t_{al}, t_{bl}, t_{am}, t_{bm}$  [18]. These times are calculated based on the following equations and are shown in Fig.6(b).

$$t_a = \frac{|\bar{V}_s^*| \sin(k\pi/5 - \alpha)}{|\bar{V}_l| \sin(\pi/5)} t_s, \quad t_b = \frac{|\bar{V}_s^*| \sin(\alpha - (k - 1)\pi/5)}{|\bar{V}_l| \sin(\pi/5)} t_s, \quad (20)$$

where  $k$  is the sector number ( $k= 1$  to  $10$ ),

$$\begin{aligned} t_{al} &= \frac{|\bar{V}_l|}{|\bar{V}_l| + |\bar{V}_m|} t_a, & t_{am} &= \frac{|\bar{V}_m|}{|\bar{V}_l| + |\bar{V}_m|} t_a, \\ t_{bl} &= \frac{|\bar{V}_l|}{|\bar{V}_l| + |\bar{V}_m|} t_b, & t_{bm} &= \frac{|\bar{V}_m|}{|\bar{V}_l| + |\bar{V}_m|} t_b. \end{aligned} \quad (21)$$

The zero space vector application time is given by  $t_0 = t_s - t_{al} - t_{am} - t_{bl} - t_{bm}$ .

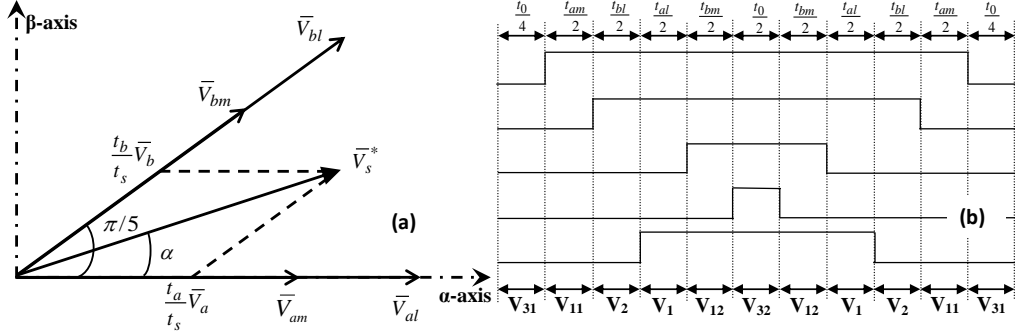


**Figure 6:** (a) Vector time calculation for the five-phase VSI in the first sector, (b) SVPWM switching pattern (the 1<sup>st</sup> sector using large and medium space vector) [18].

#### 4 Speed and Flux Full-Order Adaptive Observer

The stator and rotor equations of the five-phase IM model in the  $\alpha$ - $\beta$  stationary reference frame can be obtained by applying only the Clark transformation to equation (12). The new resulting ones can be written as follows:

$$\begin{cases} V_{\alpha s} = R_s I_{\alpha s} + p\phi_{\alpha s}, & V_{\beta s} = R_s I_{\beta s} + p\phi_{\beta s}, \\ 0 = R_r I_{\alpha r} + \omega\phi_{\beta r} + p\phi_{\alpha r}, & 0 = R_r I_{\beta r} - \omega\phi_{\alpha r} + p\phi_{\beta r}. \end{cases} \quad (22)$$

In the same manner, the magnetic equations of the stator and rotor flux can be rewritten as follows:

$$\begin{cases} \phi_{\alpha s} = L_s I_{\alpha s} + L_m I_{\alpha r}, & \phi_{\alpha r} = L_r I_{\alpha r} + L_m I_{\alpha s}, \\ \phi_{\beta s} = L_s I_{\beta s} + L_m I_{\beta r}, & \phi_{\beta r} = L_r I_{\beta r} + L_m I_{\beta s}. \end{cases} \quad (23)$$

The obtained model of the five-phase IM can be written further in the canonical space state form as follows:

$$\dot{X} = AX + BU, \quad (24)$$

where

$$X = [I_{\alpha s}, I_{\beta s}, \phi_{\alpha r}, \phi_{\beta r}]^T, \quad U = [V_{\alpha s}, V_{\beta s}], \quad (25)$$

$$A = \begin{bmatrix} a & 0 & b & bT_r\omega \\ 0 & a & -bT_r\omega & b \\ \frac{L_m}{T_r} & 0 & -\frac{1}{T_r} & -\omega \\ 0 & \frac{L_m}{T_r} & \omega & -\frac{1}{T_r} \end{bmatrix}, \quad B = \begin{bmatrix} \frac{1}{\sigma L_s} & 0 \\ 0 & \frac{1}{\sigma L_s} \\ 0 & 0 \\ 0 & 0 \end{bmatrix}, \quad (26)$$

$$a = -\frac{1}{\sigma L_s} \left( R_s + \frac{L_m^2}{L_r T_r} \right), \quad b = \frac{L_m}{\sigma L_s T_r L_r}, \quad \sigma = 1 - \frac{L_m^2}{L_s L_r}, \quad T_r = \frac{L_r}{R_r}. \quad (27)$$

A full-order observer is proposed and can be build based on the system of equations (24), where the rotor speed is supposed to be constant within each sampling period, which is considered in this work as an additional assumption to be taken into account. Furthermore, it is important to clarify that this assumption is very realistic and practical as the mechanical time constant is relatively larger compared to the electrical time constant. The operating model of the obtained full-order observer can be presented as follows [19]:

$$\hat{X} = A\hat{X} + BU + G \left( \hat{I}_s - I_s \right), \quad (28)$$

$$\hat{A} = \begin{bmatrix} a & 0 & b & bT_r\hat{\omega} \\ 0 & a & -bT_r\hat{\omega} & b \\ \frac{L_m}{T_r} & 0 & -\frac{1}{T_r} & -\hat{\omega} \\ 0 & \frac{L_m}{T_r} & \hat{\omega} & -\frac{1}{T_r} \end{bmatrix}, \quad I_s = [I_{\alpha s}, I_{\beta s}]^T. \quad (29)$$

The symbol ( $\hat{X}$ ) denotes the estimated values,  $G$  is the observer gain matrix, which is determined by the following equation such that the observer poles are proportional to those of the induction motor (the proportionality constant is  $k$ , and  $k >= 1$ ) [19]:

$$G = \begin{bmatrix} g_1 & g_2 & g_3 & g_4 \\ -g_2 & g_1 & -g_4 & g_3 \end{bmatrix}, \quad (30)$$

where

$$\begin{aligned} g_1 &= (k - 1)(a - 1/T_r), & g_2 &= (k - 1)\hat{\omega}, & g_4 &= -c(k - 1)\hat{\omega}, \\ g_3 &= (k^2 - 1)(ca + L_m/T_r) - c(k - 1)(a - 1/T_r), & c &= \frac{1}{bT_r}. \end{aligned} \quad (31)$$

By using (28) and (29), it is possible to implement a speed estimator, which is able to estimate the rotor speed in real time by using the adaptive state observer shown in Fig.7 [19].

$$\hat{\omega} = K_p (e_{i\alpha s}\hat{\phi}_{\beta r} - e_{i\beta s}\hat{\phi}_{\alpha r}) + K_i \int (e_{i\alpha s}\hat{\phi}_{\beta r} - e_{i\beta s}\hat{\phi}_{\alpha r}) dt, \quad (32)$$

where  $K_p$  and  $K_i$  are arbitrary positive gains.

$$e_{i\alpha s} = I_{\alpha s} - \hat{I}_{\alpha s} \quad \text{and} \quad e_{i\beta s} = I_{\beta s} - \hat{I}_{\beta s}. \quad (33)$$

In this observer, only  $d$  and  $q$  voltage components of the five-phase machine are used since  $d_1$  and  $q_1$  components do not present any significant contribution in the estimation.

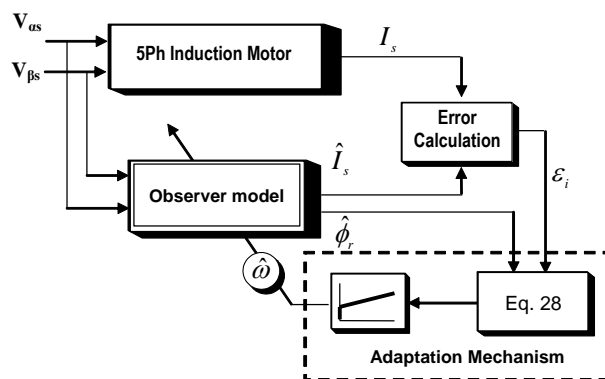


Figure 7: Block diagram of the adaptive flux and speed observer.

### 5 Model Reference Adaptive System MRAS

In this section, the model reference adaptive system technique (MRAS) is used to perform the sensorless direct torque control of the five-phase induction motor using the values resulting from the estimation of the rotor flux and the rotor speed based on the available

measurements of stator currents and voltages. Indeed, this technique possesses simple process of programming and implementation, where it benefits mainly from the advantage of using two decoupled models of the motor under study to ensure the estimation of the required states [15, 20]. The first estimation model called the reference model does not require the computation of the rotor speed, it is rotor speed independent, and it serves in the estimation of the rotor flux based on two inputs, that is, the measured stator current and the controlled stator voltage (measured or computed based on the SVPWM process) at the output side of the inverter. The second model is a tuning model which is called the adaptive (adjustable) model, it requires as an input only the stator measured current and uses the estimated rotor speed to adjust the output which is the adjustable rotor flux. A defined error between the two outputs of the aforementioned model will be used via a PI controller with a simple gain which performs the adaptation process of the proposed MRAS for obtaining the estimated rotor speed. It is worthy here to clarify that the MRAS process is based on the components of the stationary frame  $\alpha$ - $\beta$ .

Based on the equations of rotor flux in (15) and the equation of stator voltages in (14), the derivative of the rotor flux components can be written as follows:

$$\begin{cases} d\phi_{\alpha r}^{(1)} / dt = \frac{L_r}{L_m} (V_{\alpha s} - (R_s + \sigma L_s p) i_{\alpha s}), \\ d\phi_{\beta r}^{(1)} / dt = \frac{L_r}{L_m} (V_{\beta s} - (R_s + \sigma L_s p) i_{\beta s}), \end{cases} \quad (34)$$

where  $\sigma = 1 - \frac{L_m^2}{L_s L_r}$ .

This equation presents the first model, where it is clear that from the measured stator currents ( $i_{\alpha s}, i_{\beta s}$ ) and the stator voltage components ( $v_{\alpha s}, v_{\beta s}$ ) obtained from the output controlled inverter, the two components of the rotor flux ( $\phi_{\alpha s}, \phi_{\beta s}$ ) can be calculated (estimated) as shown in Fig.8. Based on the equations of rotor flux in (15) and the equation of rotor voltages in (14), the derivative of the rotor flux components can be written as follows:

$$\begin{cases} d\phi_{\alpha r}^{(2)} / dt = -\frac{1}{T_r} \phi_{\alpha r}^{(2)} - \hat{\omega}_r \phi_{\beta r}^{(2)} + \frac{L_m}{T_r} i_{\alpha s}, \\ d\phi_{\beta r}^{(2)} / dt = -\frac{1}{T_r} \phi_{\beta r}^{(2)} + \hat{\omega}_r \phi_{\alpha r}^{(2)} + \frac{L_m}{T_r} i_{\beta s}, \end{cases} \quad (35)$$

where  $T_r = \frac{L_r}{R_r}$ .

This equation presents the second model, where it is clear that from only the measured stator currents ( $i_{\alpha s}, i_{\beta s}$ ), the previous estimated rotor speed ( $\hat{\omega}_r$ ) at the MRAS output and the two previous estimated components of the adjustable rotor flux ( $\phi_{\alpha s}, \phi_{\beta s}$ ), the actual two components of the estimated flux can be obtained as shown in Fig.8. The error which is used at the input of the PI controller is defined as follows:

$$e_\phi = \phi_{\beta r}^{(1)} \phi_{\alpha r}^{(2)} - \phi_{\alpha r}^{(1)} \phi_{\beta r}^{(2)}. \quad (36)$$

Finally, the estimated actual speed is obtained as follows:

$$\hat{\omega}_r = k_p e_\phi + k_i \int e_\phi. \quad (37)$$

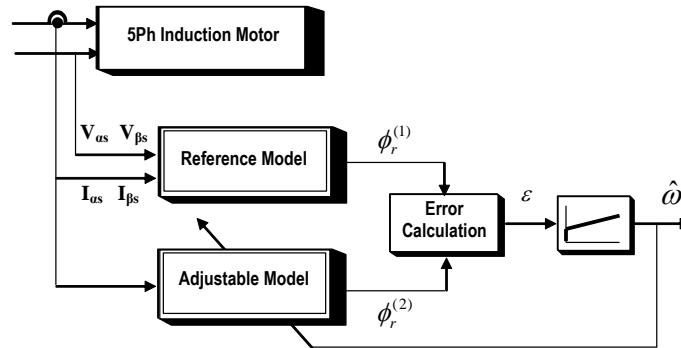


Figure 8: Block diagram of the MRAS speed estimator.

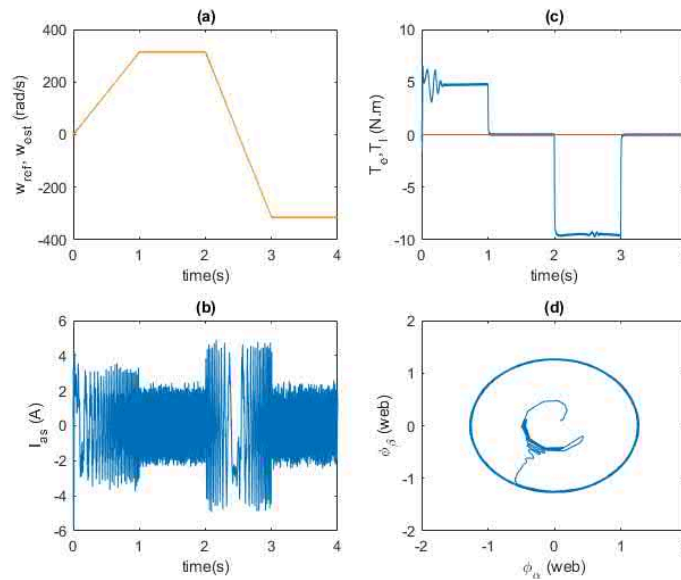
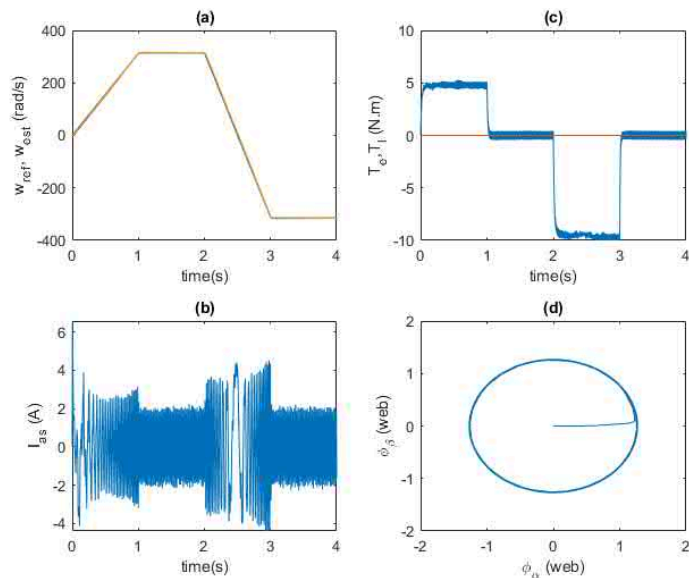


Figure 9: Adaptive observer (speed reverse condition): (a) reference speed, estimated speed, (b) stator current, (c) electromagnetic torque, (d)  $\alpha$  and  $\beta$  axes stator fluxes versus each other.

## 6 Results

In this section, the two investigated speed estimation approaches in combination with the DTC-SVM, which have been presented in the previous sections to ensure the sensorless control of the five-phase induction machine, have been performed via simulation under MATLAB/Simulink. Indeed, the main aim of the presented simulation is the evaluation of the effectiveness and the performances of both approaches in ensuring the dynamic stability of the speed control of the machine being studied under two specific speed profiles within the rated speed range and low speed range.

In these simulations, a profile of the reference speed variation is proposed and contains



**Figure 10:** MRAS estimator (speed reverse condition): (a) reference speed, estimated speed, (b) stator current, (c) electromagnetic torque, (d)  $\alpha$  and  $\beta$  axes stator fluxes versus each other.

the reverse of the speed direction as shown in Figs.9(a) and 10(a) under no-load torque application. The main characteristics of the five-phase induction motor used in these simulations are presented in Table 1.

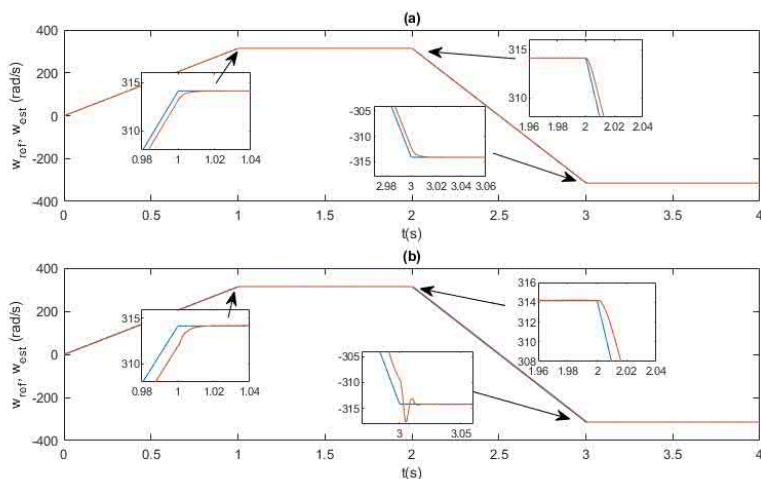


**Figure 11:** Zoom at the point of speed changes for (a) ASO and (b) MRAS.

It can be seen clearly from Fig.9(a) and Fig.10(a) that the reference of the rotor speed profile is the same for both approaches and it includes four main steps, two transient

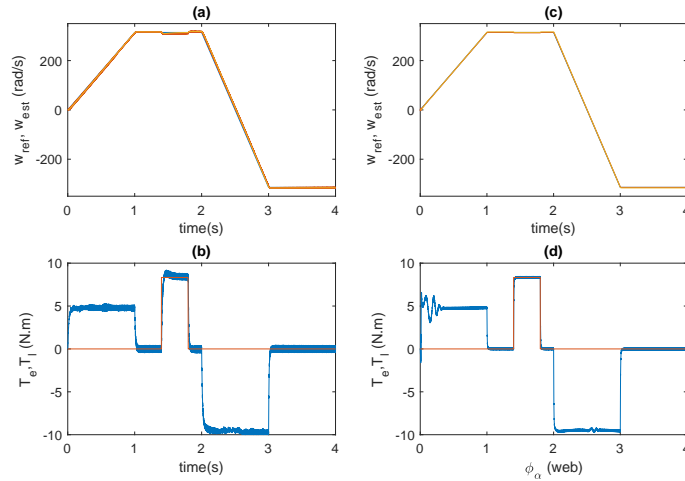


**Figure 12:** Under the load and speed reverse condition 1- MRAS estimator: (a) reference and estimated speed, (b) load and electromagnetic torque; 2- Adaptive observer: (c) reference and estimated speed, (d) load and electromagnetic torque.

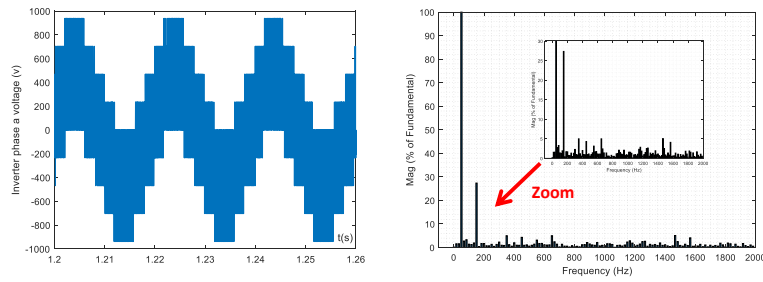


**Figure 13:** Harmonic Spectrum for output voltage using Adaptive Observer.

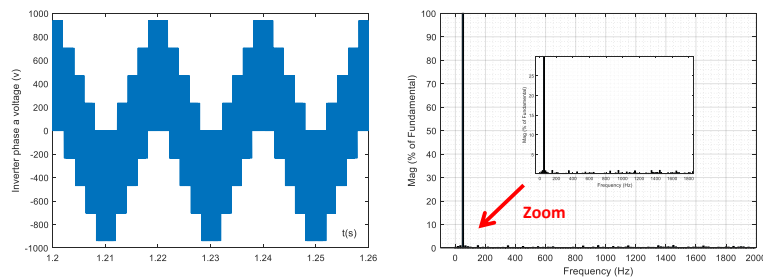


**Figure 14:** Harmonic Spectrum for output voltage using the MRAS estimator.

steps and two steady steps. The first step takes place from 0 s to 1 s, it is the start-up step which is a transient step in the forward direction, where the speed changes from 0 rad/s to its nominal rated speed 1500 rpm (314.15 rad/s electrical).

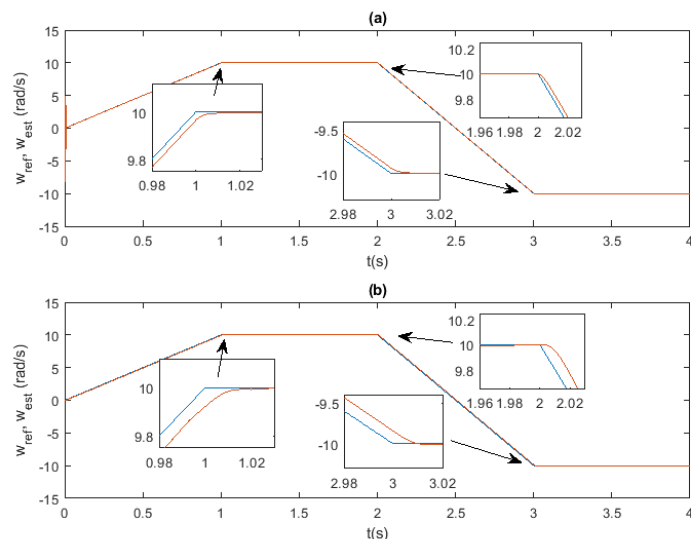


**Figure 15:** Speed reverse condition at low-speed operation: (a) Reference and estimated speed (ASO), (b) Reference and estimated speed (MRAS).

The second step takes place from 1 s to 2 s, it is a steady step where the speed is kept constant at its nominal rated value in the forward direction. The third step is the second transient step in which the speed changes from its nominal rated speed in the forward direction to the same value of speed but in the reverse direction (backward direction) within the interval of time from 2 s to 3 s. The last step is the second steady step, where the speed remains constant in the reverse direction at the nominal rated speed from 3 s to 4 s. It is obvious from Fig.9(a) and Fig.10(a) that in both cases of application of the adaptive speed observer (ASO) and the MRAS, respectively, the rotor speed of the five-phase induction motor follows accurately the reference speed profile with neglected errors within the two steady steps among the imposed four steps of the reference speed profile, while very small errors are noticed during the transient steps for both sensorless control approaches used.

Fig.9(b) and Fig.10(b) show the waveforms of the stator current of phase (a) for both approaches. It is clear that both currents follow the dynamics of the speed profile, where increased currents are noticed during the start-up and speed reverse due to the required electromagnetic torque developed by the induction motor in both cases.

Fig.9(c) and Fig.10(c) show the developed electromagnetic torque in both cases. It is obvious that within the start-up step in the case of MRAS approach, the developed torque reaches the required torque with neither remarkable overshoot nor oscillations. Meanwhile, in the case of ASO, a remarkable overshoot and oscillations can be noticed clearly, which presents a bit drawback compared to the MRAS approach. However, during other steps both approaches dynamics behave in the same way.

Fig.9(d) and Fig.10(d) present the  $\beta$ -axis flux function of the  $\alpha$ -axis, where it can be seen clearly that it has a circular form in both cases with less oscillations due to neglected harmonics components in the flux components following both axes. On the other side, there is no observable impact of the variations of the speed, mainly during the transient

steps, which confirms the enhanced dynamics of both sensorless control approaches used, except the one observed during the start-up for the ASO approach which makes the curve in the flux plan reach the circle a bit later compared to the MRAS approach.

Fig.11 shows the zooms of three regions within the reference profile speed and the estimated rotor speed at the instant of their changes under both approaches of ASO and MRAS, respectively. It can be noticed clearly that the ASO has a little more accurate tracking of the reference speed compared to the MRAS. However, this difference is too limited and it does not affect the real dynamic of the motor in tracking the profile speed.

Fig.12 shows the rotor speed dynamics under the application of both sensorless control approaches with the same aforementioned reference speed profile as in the previous simulations, however, in this simulation a load torque, which is chosen to be equal to the rated nominal load torque of 8.33 N.m, is applied during the first steady step from 1.4 s to 1.8 s. As there is no change in the profile of the reference speed profile, the same dynamics is obtained in the regions where there is no load torque. Indeed, it can be noted that the rotor speed decreases lightly when the load torque is applied in the case of MRAS, and this decrease is neglected in the case of ASO.

Figs.13 and 14 present the waveforms and harmonic spectrums of the inverter output voltage of phase “a” applied to the five-phase induction motor, which are obtained by the application of the SVPWM technique under the ASO and MRAS approaches, respectively. It is clear that the low frequency harmonics have less values in the case of the MRAS approach compared to the ASO approach. This issue does not affect really the stator currents and the developed electromagnetic torque due to the fact that the inductance in each phase serves good enough as a low-pass filter for damping the current ripples and, consequently, the torque ripples. Hence, it can be said that the quality of both obtained voltages is acceptable in practical applications.

The last simulation is dedicated to the low-speed profile within a very limited range from -10 rad/s to 10 rad/s, which is shown in Fig.15. It can be observed that both approaches possess high dynamic performances in ensuring the tracking of the reference speed without failure during all step changes. Hence, it can be concluded that both approaches are valid in ensuring the sensorless control of the five-phase induction machine within a wide range of speed variation with a very little advantage of the MRAS compared to the ASO.

Rated voltage	$U_n = 220$ v	Stator Resistance	$R_s = 10\Omega$
Rated Current	$I_n = 2.1$ A	Rotor Resistance	$R_r = 6.3\Omega$
Stator inductance	$L_s = 0.46$ H	Mutual Inductance	$L_m = 0.42$ H
Rotor Inductance	$L_r = 0.46$ H	Number of poles pairs	$p = 2$
Moment of Inertia	$J = 0.03kg.m^2$	Friction coefficient	$f_r = 0.008$ N.m.s/rd

**Table 1:** The Parameters of the Five-Phase Induction Machine.

## 7 Conclusion

In this paper, the sensorless control of the five-phase induction motor using the direct torque control combined with space vector modulations (DTC-SVM) is presented and analyzed. Indeed, the main aim of the application of this control is to ensure the accurate

control of the rotor speed with improved dynamic performances following an imposed reference rotor speed profile which includes speed variation and direction inversion under torque load variation. This paper investigates the use of two different speed techniques for the estimation of the rotor speed used in the applied DTC-SVM, namely, the adaptive flux and speed observer and the model reference adaptive system (MRAS). Both sensorless control approaches are tested in this work based on the proposed profile of the rotor speed using simulation. The obtained results show that the application of both approaches has ensured the desired control performance and it can be said that their dynamic behaviors are the same as at their application to the three-phase induction machine. However, the analysis of the application of both estimation approaches shows that the sensorless control approach based on the MRAS has rather simple structure, easy implementation and requires less time of computation compared to the adaptive flux and speed observer, these features make the MRAS more advantageous in practical implementation and industrial applications for the sensorless control of the five-phase induction motor.

## References

- [1] Z. Liu, Y. Li and Z. Zheng. A review of drive techniques for multiphase machines. *CES Transactions on Electrical Machines and Systems* **2** (2) (2018) 243–251.
- [2] I. Takahashi and T. Noguchi. A new quick response and high efficiency control strategy of an induction motor. *IEEE Trans. ind. Applicat.* **IA** (22) (1986) 820–827.
- [3] M. Depenbrock. Direct self control of inverter-fed induction machines. *IEEE Trans. Power Electron.* **3** (1988) 420–429.
- [4] Y. Tatte and M. Aware. Direct Torque Control of Five-Phase Induction Motor with Common-Mode Voltage and Current Harmonics Reduction. *IEEE Transactions on Power Electronics* **32** (11) (2017) 8644–8654.
- [5] Y. Chedni, D.J. Boudana, A. Moualdia, L. Nezli and P. Wira. Sensorless Two Series Connected Quasi Six-Phase IM Based Direct Torque Control for Torque Ripples Minimization. *Nonlinear Dynamics and Systems Theory* **20** (2) (2020) 153–167.
- [6] T. Djellouli, S. Moulahoum, A. Moualdia, M.S. Bouchrit and P. Wira. Speed Sensorless Direct Torque Control Strategy of a Doubly Fed Induction Motor Using an ANN and an EKF. *Nonlinear Dynamics and Systems Theory* **20** (4) (2020) 374–387.
- [7] H. Xu and H. A. Toliyat. A novel direct torque control (DTC) method for five-phase induction machines. In: *Proc. Applied Power Electron. Conf. Exp., APEC* **1** (2000) 162–168.
- [8] Y.S. Lai and J.H. Chen. A new approach to direct torque control of induction motor drives for constant inverter switching frequency and torque ripple reduction. *IEEE Transactions on Energy Conversion* **16** (3) (2001) 220–227.
- [9] B.S. Khaldi, H. Abu-Rub, A. Iqbal, R. Kennel, M.O. Mahmoudi and D. Boukhetala. Comparison study between a simple sensorless method and adaptive observer for DTC-SVM five-phase induction motor drive. *IEEE International Conference on Industrial Technology, Athens*, (2012) 743–748.
- [10] H. Echeikh, R. Trabelsi, A. Iqbal, R. Alammari and M. F. Mimouni. Sensorless indirect rotor flux oriented control of a five-phase induction motor based on sliding mode observer. In: *International Conference on Sciences and Techniques of Automatic Control and Computer Engineering* (2015) 471–479.
- [11] O. González, J. Rodas, R. Gregor, M. Ayala and M. Rivera. Speed sensorless predictive current control of a five-phase induction machine. In: *IEEE Conference on Industrial Electronics and Applications*, (2017) 343–348.

- [12] M. Morawiec and F Wilczyński. Sensorless Control of Five-phase Machine Supplied by the Current Source Inverter. *International Conference on Electrical Power Drive Systems.*, (2020) 1-6.
- [13] A. S. Morsy, A. S. Abdel-Khalik, S. Ahmed and A. Massoud. Sensorless V/f control with MRAS speed estimator for a five-phase induction machine under open-circuit phase faults. *7th IEEE GCC Conference and Exhibition*, Doha, (2013) 268–273.
- [14] H. Abu-Rub, M. R. Khan, A. Iqbal and S. M. Ahmed. MRAS-based sensorless control of a five-phase induction motor drive with a predictive adaptive model. In: *IEEE International Symposium on Industrial Electronics*, Bari, (2010) 3089–3094.
- [15] S. Khadar, A. Kouzou, A. Hafaifa and A. Iqbal. Investigation on SVM-Backstepping sensorless control of five-phase open-end winding induction motor based on model reference adaptive system and parameter estimation. *Engineering Science and Technology, an International Journal* **22** (4) (2019) 1013–1026.
- [16] E. Levi, M. Jones, S. N. Vukosavic and H. A. Toliyat. A novel concept of a multiphase, multimotor vector controlled drive system supplied from a single voltage source inverter. *IEEE Trans. Power Electron.* **19** (2) (2004) 320–335.
- [17] D. Casadei, F. Profumo, G. Serra and A. Tani. FOC and DTC: two viable schemes for induction motors torque control. *IEEE Trans. Power Electron.* **17** (5) (2002) 779–787.
- [18] A. Iqbal and S Moinuddin. Comprehensive Relationship Between Carrier-Based PWM and Space Vector PWM in a Five-Phase VSI. *IEEE Trans. Power Electron.* **24** (10) (2009) 2379–2390.
- [19] P. Vas. *Sensorless Vector and Direct Torque Control*. London: Oxford Univ. Press. 2003.
- [20] A. Pal, S. Das and A. K. Chattopadhyay. An improved rotor flux space vector based MRAS for field-oriented control of induction motor drives. *IEEE Trans. Power Electron.* **33** (6) (2018) 5131–5141.



# A Dynamic Contact Problem for Elasto-Viscoplastic Piezoelectric Materials with Normal Compliance, Normal Damped Response and Damage

L. Maiza<sup>1</sup>, T. Hadj Ammar<sup>2\*</sup> and M. Said Ameer<sup>2</sup>

<sup>1</sup> *Department of Mathematics, Laboratory of Applied Mathematics, Kasdi Merbah University, BP 511, Ouargla 30000, Algeria.*

<sup>2</sup> *Departement of Mathematics, El Oued University, 39000 El Oued, Algeria.*

Received: March 23, 2021; Revised: May 29, 2021

**Abstract:** This work studies a mathematical model involving a dynamic contact between two elasto-viscoplastic piezoelectric bodies with damage. The contact is modelled with a combination of a normal compliance and a normal damped response law associated with friction. We derive a variational formulation of the problem and we prove an existence and uniqueness result for the weak solution. The proof is based on the classical existence and uniqueness result for parabolic inequalities, differential equations and fixed-point arguments.

**Keywords:** *dynamic process; elastic-viscoplastic piezoelectric materials; damage; normal compliance; normal damped; fixed point.*

**Mathematics Subject Classification (2010):** 35Q74, 47H10, 49J40, 74D10.

## 1 Introduction

In this paper we study a contact problem which involves viscous friction of Tresca type described in [1]. A nonlinear elasto-viscoplastic constitutive law is used to model the piezoelectric material. The piezoelectricity can be described as follows: when mechanical pressure is applied to a certain class of crystalline materials (e.g., ceramics  $BaTiO_3$ ,  $BiFeO_3$ ), the crystalline structure produces a voltage proportional to the pressure. Conversely, when an electric field is applied, the structure changes its shape producing dimensional modifications in the material. Different models have been developed to describe the interaction between the electrical and mechanical fields, see, for example, [5, 17] and the

---

\* Corresponding author: <mailto:hadjammam-tedjani@univ-eloued.dz>

references therein. For contact problems involving elasto-piezoelectric materials see [15]. Different models of viscoelastic piezoelectric problems have been studied in [3, 14, 20], contact problems for electro-elasto-viscoplastic materials were studied in [5, 11].

The damage is an extremely important topic in engineering since it affects directly the useful life of the designed structure or component. There exists a very large engineering literature on it. Models taking into account the influence of the internal damage of the material on the contact process have been investigated mathematically. General models for damage were derived in [6] from the virtual power principle. The models of mechanical damage, which were derived from thermodynamical considerations and the principle of virtual work, can be found in [8]. The new idea of [7] was the introduction of the damage function  $\beta^\ell = \beta^\ell(x, t)$ , which is the ratio between the elastic moduli of the damage and damage-free materials. In an isotropic and homogeneous elastic material, let  $E_Y^\ell$  be the Young modulus of the original material and  $E_{eff}^\ell$  be the current modulus, then the damage function is defined by  $\beta^\ell = E_{eff}^\ell/E_Y^\ell$ . Clearly, it follows from this definition that the damage function  $\beta^\ell$  is restricted to have values between zero and one. When  $\beta^\ell = 1$ , there is no damage in the material, when  $\beta^\ell = 0$ , the material is completely damaged, when  $0 < \beta^\ell < 1$ , there is partial damage and the system has a reduced load carrying capacity. Contact problems with damage have been investigated in [12]. The differential inclusion used for the evolution of the damage field is

$$\dot{\beta}^\ell - \kappa^\ell \Delta \beta^\ell + \partial_{k^\ell}(\beta^\ell) \ni S^\ell(\sigma^\ell - \mathcal{A}^\ell \varepsilon(\dot{u}^\ell) - (\mathcal{E}^\ell)^* \nabla \varphi^\ell(s), \varepsilon(u^\ell), \beta^\ell),$$

where  $K^\ell$  denotes the set of admissible damage functions defined by

$$K^\ell = \{\xi \in V^\ell; 0 \leq \xi \leq 1, \text{ a.e. in } \Omega^\ell\}, \tag{1}$$

$\kappa^\ell$  is a positive coefficient,  $\partial\varphi_{K^\ell}$  represents the subdifferential of the indicator function of the set  $K^\ell$ , and  $S^\ell$  is a given constitutive function which describes the sources of the damage in the system. The paper is structured as follows. In Section 2, we present the physical setting and describe the mechanical problem. In Section 3, we introduce some notation, list the assumptions on the problems data, and derive the variational formulation of the model. In Section 4, we state our main existence and uniqueness result, Theorem 4.1. The proof of the theorem is based on the arguments of nonlinear evolution equations with monotone operators, a classical existence and uniqueness result for parabolic inequalities and fixed-point arguments.

## 2 The Model

We describe the model for the process and we present its variational formulation. We consider the following physical setting. Let us consider two electro-elastic-viscoplastic bodies, occupying two bounded domains  $\Omega^1, \Omega^2$  of the space  $\mathbb{R}^d (d = 2, 3)$ . For each domain  $\Omega^\ell$ , the boundary  $\Gamma^\ell$  is assumed to be Lipschitz continuous, and is partitioned into three disjoint measurable parts  $\Gamma_1^\ell, \Gamma_2^\ell$  and  $\Gamma_3^\ell$ , on one hand, and into two measurable parts  $\Gamma_a^\ell$  and  $\Gamma_b^\ell$ , on the other hand, such that  $meas\Gamma_1^\ell > 0, meas\Gamma_a^\ell > 0$ . Let  $T > 0$  and let  $[0, T]$  be the time interval of interest. The  $\Omega^\ell$  body is subject to  $f_0^\ell$  forces and volume electric charges of density  $q_0^\ell$ . The bodies are assumed to be clamped on  $\Gamma_1^\ell \times [0, T]$ . The surface tractions  $f_2^\ell$  act on  $\Gamma_2^\ell \times [0, T]$ . We also assume that the electrical potential vanishes on  $\Gamma_a^\ell \times [0, T]$  and a surface electric charge of density  $q_2^\ell$  is prescribed

on  $\Gamma_b^\ell \times [0, T]$ . The two bodies can enter in contact along the common part  $\Gamma_3^1 = \Gamma_3^2 = \Gamma_3$ . We use an electro-elastic-viscoplastic constitutive law with damage given by

$$\begin{aligned} \boldsymbol{\sigma}^\ell &= \mathcal{A}^\ell \boldsymbol{\varepsilon}(\dot{\mathbf{u}}^\ell) + \mathcal{G}^\ell \boldsymbol{\varepsilon}(\mathbf{u}^\ell) + (\mathcal{E}^\ell)^* \nabla \varphi^\ell + \\ &\int_0^t \mathcal{F}^\ell \left( \boldsymbol{\sigma}^\ell(s) - \mathcal{A}^\ell \boldsymbol{\varepsilon}(\dot{\mathbf{u}}^\ell(s)) - (\mathcal{E}^\ell)^* \nabla \varphi^\ell, \boldsymbol{\varepsilon}(\mathbf{u}^\ell(s)) \right) ds, \end{aligned} \quad (2)$$

$$\mathbf{D}^\ell = \mathcal{E}^\ell \boldsymbol{\varepsilon}(\mathbf{u}^\ell) - \mathcal{B}^\ell \nabla \varphi^\ell, \quad (3)$$

where  $\mathbf{D}^\ell$  is the electric displacement field,  $\mathbf{u}^\ell$  is the displacement field,  $\boldsymbol{\sigma}^\ell$  and  $\boldsymbol{\varepsilon}(\mathbf{u}^\ell)$  represent the stress and the linearized strain tensor, respectively. Here  $\mathcal{A}^\ell$  is a given nonlinear function,  $\mathcal{F}^\ell$  is the relaxation tensor, and  $\mathcal{G}^\ell$  represents the elasticity operator.  $E(\varphi^\ell) = -\nabla \varphi^\ell$  is the electric field,  $\mathcal{E}^\ell = (e_{ijk})$  represents the third order piezoelectric tensor,  $(\mathcal{E}^\ell)^*$  is its transposition. It follows from (2) that at each time moment, the stress tensor  $\boldsymbol{\sigma}^\ell(t)$  is split into three parts:  $\boldsymbol{\sigma}^\ell(t) = \boldsymbol{\sigma}_V^\ell(t) + \boldsymbol{\sigma}_E^\ell(t) + \boldsymbol{\sigma}_R^\ell(t)$ , where  $\boldsymbol{\sigma}_V^\ell(t) = \mathcal{A}^\ell \boldsymbol{\varepsilon}(\dot{\mathbf{u}}^\ell(t))$  represents the purely viscous part of the stress,  $\boldsymbol{\sigma}_E^\ell(t) = (\mathcal{E}^\ell)^* \nabla \varphi^\ell(t)$  represents the electric part of the stress and  $\boldsymbol{\sigma}_R^\ell(t)$  satisfies a rate-type elastic-viscoplastic relation

$$\boldsymbol{\sigma}_R^\ell(t) = \mathcal{G}^\ell \boldsymbol{\varepsilon}(\mathbf{u}^\ell(t)) + \int_0^t \mathcal{F}^\ell(\boldsymbol{\sigma}_R^\ell(s), \boldsymbol{\varepsilon}(\mathbf{u}^\ell(s))) ds. \quad (4)$$

Various results, examples and mechanical interpretations in the study of elastic-viscoplastic materials of the form (4) can be found in [6, 9] and the references therein. Note also that when  $\mathcal{F}^\ell = 0$ , the constitutive law (2) becomes the Kelvin-Voigt electro-viscoelastic constitutive relation

$$\boldsymbol{\sigma}^\ell(t) = \mathcal{A}^\ell \boldsymbol{\varepsilon}(\dot{\mathbf{u}}^\ell(t)) + \mathcal{G}^\ell \boldsymbol{\varepsilon}(\mathbf{u}^\ell(t)) + (\mathcal{E}^\ell)^* \nabla \varphi^\ell(t). \quad (5)$$

Dynamic contact problems with the Kelvin-Voigt materials of the form (5) can be found in [3]. The normal compliance contact condition was first considered in [12] in the study of dynamic problems with linearly elastic and viscoelastic materials and then it was used in various references, see, e.g., [11, 17]. This condition allows the interpenetration of the body's surface into the obstacle and it was justified by considering the interpenetration and deformation of surface asperities.

We need to introduce some notation and preliminary material. Here and below,  $\mathbb{S}^d$  represents the space of the second-order symmetric tensors on  $\mathbb{R}^d$ . We recall that the inner products and the corresponding norms on  $\mathbb{S}^d$  and  $\mathbb{R}^d$  are given by

$$\begin{aligned} \mathbf{u}^\ell \cdot \mathbf{v}^\ell &= u_i^\ell \cdot v_i^\ell, & |\mathbf{v}^\ell| &= (\mathbf{v}^\ell \cdot \mathbf{v}^\ell)^{\frac{1}{2}}, & \forall \mathbf{u}^\ell, \mathbf{v}^\ell \in \mathbb{R}^d, \\ \boldsymbol{\sigma}^\ell \cdot \boldsymbol{\tau}^\ell &= \sigma_{ij}^\ell \cdot \tau_{ij}^\ell, & |\boldsymbol{\tau}^\ell| &= (\boldsymbol{\tau}^\ell \cdot \boldsymbol{\tau}^\ell)^{\frac{1}{2}}, & \forall \boldsymbol{\sigma}^\ell, \boldsymbol{\tau}^\ell \in \mathbb{S}^d. \end{aligned}$$

Here and below, the indices  $i$  and  $j$  run between 1 and  $d$ , and the summation convention over repeated indices is adopted. With these assumptions, the classical formulation of the dynamic problem for the friction contact with normal compliance and normal damped response between two elasto-viscoplastic piezoelectric bodies with damage is the following.

**Problem P.** For  $\ell = 1, 2$ , find a displacement field  $\mathbf{u}^\ell : \Omega^\ell \times [0, T] \rightarrow \mathbb{R}^d$ , a stress field  $\boldsymbol{\sigma}^\ell : \Omega^\ell \times [0, T] \rightarrow \mathbb{S}^d$ , an electric potential field  $\varphi^\ell : \Omega^\ell \times [0, T] \rightarrow \mathbb{R}$ , a damage

field  $\beta^\ell : \Omega^\ell \times [0, T] \rightarrow \mathbb{R}$  and an electric displacement field  $D^\ell : \Omega^\ell \times [0, T] \rightarrow \mathbb{R}^d$  such that

$$\sigma^\ell = \mathcal{A}^\ell \varepsilon(\dot{\mathbf{u}}^\ell) + \mathcal{B}^\ell \varepsilon(\mathbf{u}^\ell) + (\mathcal{E}^\ell)^* \nabla \varphi^\ell + \int_0^t \mathcal{G}^\ell \left( \sigma^\ell(s) - \mathcal{A}^\ell \varepsilon(\dot{\mathbf{u}}^\ell(s)) - (\mathcal{E}^\ell)^* \nabla \varphi^\ell(s), \varepsilon(\mathbf{u}^\ell(s)), \beta^\ell(s) \right) ds \quad \text{in } \Omega^\ell \times (0, T), \quad (6)$$

$$D^\ell = \mathcal{E}^\ell \varepsilon(\mathbf{u}^\ell) - \mathcal{B}^\ell \nabla \varphi^\ell \quad \text{in } \Omega^\ell \times (0, T), \quad (7)$$

$$\dot{\beta}^\ell - \kappa^\ell \Delta \beta^\ell + \partial_{k^\ell}(\beta^\ell) \ni \mathbf{S}^\ell(\sigma^\ell - \mathcal{A}^\ell \varepsilon(\dot{\mathbf{u}}^\ell) - (\mathcal{E}^\ell)^* \nabla \varphi^\ell(s), \varepsilon(\mathbf{u}^\ell), \beta^\ell), \quad (8)$$

$$\rho^\ell \ddot{\mathbf{u}}^\ell = \text{Div } \sigma^\ell + \mathbf{f}_0^\ell \quad \text{in } \Omega^\ell \times (0, T), \quad (9)$$

$$\text{div } D^\ell - q_0^\ell = 0 \quad \text{in } \Omega^\ell \times (0, T), \quad (10)$$

$$\mathbf{u}^\ell = 0 \quad \text{on } \Gamma_1^\ell \times (0, T), \quad (11)$$

$$\sigma^\ell \nu^\ell = \mathbf{f}_2^\ell \quad \text{on } \Gamma_2^\ell \times (0, T), \quad (12)$$

$$\begin{cases} \sigma_\nu^1 = \sigma_\nu^2 \equiv \sigma_\nu, \\ -\sigma_\nu = p_\nu([u_\nu] - g) + q_\nu([i_\nu]) \end{cases} \quad \text{on } \Gamma_3 \times (0, T), \quad (13)$$

$$\begin{cases} \sigma_\tau^1 = -\sigma_\tau^2 \equiv \sigma_\tau, \\ \|\sigma_\tau\| \leq p_\tau([u_\tau] - g) + q_\tau([i_\tau]) \end{cases} \quad \text{on } \Gamma_3 \times (0, T), \quad (14)$$

$$[i_\tau] \neq 0 \Rightarrow \sigma_\tau = -(p_\tau([u_\tau] - g) + q_\tau([i_\tau])) \cdot \frac{[i_\tau]}{[u_\tau]} \quad \text{on } \Gamma_3 \times (0, T), \quad (15)$$

$$\frac{\partial \beta^\ell}{\partial \nu^\ell} \quad \text{on } \Gamma^\ell \times (0, T), \quad (16)$$

$$\varphi^\ell = 0 \quad \text{on } \Gamma_a^\ell \times (0, T), \quad (17)$$

$$D^\ell \cdot \nu^\ell = q_2^\ell \quad \text{on } \Gamma_b^\ell \times (0, T), \quad (18)$$

$$\begin{cases} D^1 \cdot \nu^1 = D^2 \cdot \nu^2 = D, \\ D = \psi([u_\nu] - g) \phi_i(\varphi^1 + \varphi^2 - \varphi_0) \end{cases} \quad \text{on } \Gamma_3 \times (0, T), \quad (19)$$

$$\mathbf{u}^\ell(0) = \mathbf{u}_0^\ell, \quad \beta^\ell(0) = \beta_0^\ell \quad \text{in } \Omega^\ell. \quad (20)$$

First, equations (6) and (7) represent the electro-elastic-viscoplastic constitutive law with damage, the evolution of the field is governed by the inclusion of parabolic type given by the relation (8), where  $\mathbf{S}^\ell$  is the mechanical source of the damage growth, assumed to be a rather general function of the strains, and the damage itself,  $\partial \varphi_{k^\ell}$ , is the sub differential of the indicator function of the admissible damage functions set  $K^\ell$ . Next, equations (9) and (10) are the steady equations for the stress and electric-displacement field, respectively, in which "Div" and "div" denote the divergence operator for tensor

and vector-valued functions, i.e.,

$$\text{Div } \boldsymbol{\sigma}^\ell = (\sigma_{ij,j}^\ell), \quad \text{div } \mathbf{D}^\ell = (D_{i,i}^\ell).$$

We use these equations since the process is assumed to be mechanically dynamic and electrically quasi-static. Conditions (11) and (12) are the displacement and traction boundary conditions, whereas (17) and (18) represent the electric boundary conditions; the displacement field and the electrical potential vanish on  $\Gamma_1^\ell$  and  $\Gamma_a^\ell$ , respectively, while the forces and free electric charges are prescribed on  $\Gamma_2^\ell$  and  $\Gamma_b^\ell$ , respectively.

We turn to the boundary conditions (13) and (14) which describe the mechanical and electrical conditions on the potential contact surface  $\Gamma_3$ . The normal compliance function  $p_\nu$  in (13) is described below, and  $g$  represents the gap in the reference configuration between  $\Gamma_3$  and the foundation, measured along the direction of  $\boldsymbol{\nu}^\ell$ . When positive,  $[u_\nu] - g$  represents the interpenetration of the surface asperities into those of the foundation. This condition was first introduced in [10] and used in a large number of papers, see, for instance, [4, 7, 8, 14] and the references therein. Condition (14) is the associated friction law, where  $p_\tau$  is a given function. According to (14), the tangential shear cannot exceed the maximum frictional resistance  $p_\tau([u_\nu] - g)$ , the so-called friction bound. Moreover, when sliding commences, the tangential shear reaches the friction bound and opposes the motion. Frictional contact conditions of the form (13), (14) have been used in various papers, see, e.g., [5, 6, 17] and the references therein.

The relation (16) describes a homogeneous Neumann boundary condition, where  $\partial\boldsymbol{\beta}^\ell|\partial\nu^\ell$  is the normal derivative of  $\boldsymbol{\beta}^\ell$ . (17) and (18) represent the electric boundary conditions. Next, (19) is the electrical contact condition on  $\Gamma_3$ , introduced in [11]. It may be obtained as follows. First, unlike the previous papers on the piezoelectric contact, we assume that the contact surface is electrically conductive and its potential is maintained at  $\varphi_0$ . When there is no contact at a point on the surface (i.e.,  $[u_\nu] < g$ ), the gap is assumed to be an insulator (say, it is filled with air), there are no free electrical charges on the surface and the normal component of the electric displacement field vanishes. Thus,

$$[u_\nu] < g \Rightarrow \mathbf{D}^\ell \cdot \boldsymbol{\nu}^\ell = 0. \quad (21)$$

During the process of contact (i.e., when  $[u_\nu] \geq g$ ) the normal component of the electric displacement field or the free charge is assumed to be proportional to the difference between the potential of the foundation and the body's surface potential, with  $\mathbf{k}$  as the proportionality factor. Thus

$$[u_\nu] \geq g \Rightarrow \mathbf{D}^\ell \cdot \boldsymbol{\nu}^\ell = \mathbf{k}(\varphi^1 + \varphi^2 - \varphi_0). \quad (22)$$

We combine (21), (22) to obtain

$$\mathbf{D}^\ell \cdot \boldsymbol{\nu}^\ell = \mathbf{k}\chi_{[0,\infty)}([u_\nu] - g)(\varphi^1 + \varphi^2 - \varphi_0), \quad (23)$$

where  $\chi_{[0,\infty)}$  is the characteristic function of the interval  $[0, \infty)$ ; that is,

$$\chi_{[0,\infty)}(r) = \begin{cases} 0 & \text{if } r < 0, \\ 1 & \text{if } r \geq 0. \end{cases}$$

Condition (23) describes the perfect electrical contact and is somewhat similar to the well-known Signorini contact condition. Both conditions may be over idealizations in

many applications. To make it more realistic, we regularize condition (23) and write it as (19), in which  $\mathbf{k}_{\chi_{[0,\infty)}}([\mathbf{u}_v] - g)$  is replaced with  $\psi$  which is a regular function and which will be described below, and  $\phi_l$  is the truncation function

$$\phi_l(s) = \begin{cases} -l & \text{if } s < -l, \\ s & \text{if } -l \leq s \leq l, \\ l & \text{if } s > l, \end{cases}$$

where  $l$  is a large positive constant. We note that this truncation does not pose any practical limitations on the applicability of the model, since  $l$  may be arbitrarily large, higher than any possible peak voltage in the system, and therefore in applications  $\phi_l(\varphi^1 + \varphi^2 - \varphi_0) = \varphi^1 + \varphi^2 - \varphi_0$ . The reasons for the regularization (19) of (23) are mathematical. First, we need to avoid the discontinuity in the free electric charge when the contact is established and, therefore, we regularize the function  $\mathbf{k}_{\chi_{[0,\infty)}}$  in (23) with a Lipschitz continuous function  $\psi$ . A possible choice is

$$\psi(r) \begin{cases} 0 & \text{if } r < 0, \\ k\delta r & \text{if } 0 \leq r \leq l/\delta, \\ k & \text{if } r > \delta, \end{cases} \tag{24}$$

where  $\delta > 0$  is a small parameter. This choice means that during the process of contact the electrical conductivity increases as the contact among the surface asperities improves, and stabilizes when the penetration  $[\mathbf{u}_v] - g$  reaches the value  $\delta$ . Secondly, we need the term  $\phi_l(\varphi^1 + \varphi^2 - \varphi_0) = \varphi^1 + \varphi^2 - \varphi_0$  to control the boundedness of  $[\varphi] - \varphi_0$ . Note that  $\psi \equiv 0$  in (19), then

$$\mathbf{D}^\ell \cdot \boldsymbol{\nu}^\ell = 0 \quad \text{on } \Gamma_3 \times (0, T), \tag{25}$$

which decouples the electrical and mechanical problems on the contact surface. Condition (25) models the case when the obstacle is a perfect insulator and was used in [3, 14, 19, 20]. Condition (19), instead of (25), introduces a strong coupling between the mechanical and the electric boundary conditions and leads to a new and non-standard mathematical model. Because of the friction condition (14), which is non-smooth, we do not expect the problem to have, in general, any classical solutions. Finally, in equation (20)  $\mathbf{u}_0^\ell$  is the initial displacement, and  $\beta_0^\ell$  is the initial damage. To obtain the variational formulation of the problem (6), we introduce for the bonding field the set

$$\mathcal{Z} = \{ \theta \in L^\infty(0, T; L^2(\Gamma_3)); 0 \leq \theta(t) \leq 1 \quad \forall t \in [0, T], \text{ a.e. on } \Gamma_3 \}.$$

For this reason, we derive in the next section a variational formulation of the problem and investigate its solvability. Moreover, variational formulations are also starting points for the construction of finite element algorithms for this type of problems.

### 3 Variational Formulation and the Main Result

We use the standard notation for the  $L^p$  and the Sobolev spaces associated with  $\Omega^\ell$  and  $\Gamma^\ell$  and, for a function  $\zeta^\ell \in H^1(\Omega^\ell)$ , we still write  $\zeta^\ell$  to denote its trace on  $\Gamma^\ell$ . We recall that the summation convention applies to a repeated index. For the electric displacement field we use two Hilbert spaces

$$\mathcal{W}^\ell = L^2(\Omega^\ell)^d, \quad \mathcal{W}_1^\ell = \{ \mathbf{D}^\ell \in \mathcal{W}^\ell : \text{div } \mathbf{D}^\ell \in L^2(\Omega^\ell) \},$$

endowed with the inner products

$$(\mathbf{D}^\ell, \mathbf{E}^\ell)_{\mathcal{W}^\ell} = \int_{\Omega^\ell} \mathbf{D}_i^\ell \cdot \mathbf{E}_i^\ell dx, \quad (\mathbf{D}^\ell, \mathbf{E}^\ell)_{\mathcal{W}_1^\ell} = (\mathbf{D}^\ell, \mathbf{E}^\ell)_{\mathcal{W}^\ell} + (\operatorname{div} \mathbf{D}^\ell, \operatorname{div} \mathbf{E}^\ell)_{L^2(\Omega^\ell)},$$

and the associated norms  $\|\cdot\|_{\mathcal{W}^\ell}$  and  $\|\cdot\|_{\mathcal{W}_1^\ell}$ , respectively. The electric potential field is to be found in

$$W^\ell = \{\boldsymbol{\xi}^\ell \in H^1(\Omega^\ell) : \boldsymbol{\xi}^\ell = 0 \text{ on } \Gamma_a^\ell\}.$$

Since  $\operatorname{meas} \Gamma_a^\ell > 0$ , the Friedrichs-Poincaré inequality holds, thus,

$$\|\nabla(\boldsymbol{\xi}^\ell)\|_{\mathcal{W}^\ell} \geq c_F \|\boldsymbol{\xi}^\ell\|_{H_1^\ell(\Omega^\ell)} \quad \forall \boldsymbol{\xi}^\ell \in W^\ell, \tag{26}$$

where  $c_F > 0$  is a constant which depends only on  $\Omega^\ell$  and  $\Gamma_a^\ell$ . On  $W^\ell$ , we use the inner product

$$(\boldsymbol{\varphi}^\ell, \boldsymbol{\psi}^\ell)_{W^\ell} = (\nabla \boldsymbol{\varphi}^\ell, \nabla \boldsymbol{\psi}^\ell)_{\mathcal{W}^\ell}$$

and let  $\|\cdot\|_{W^\ell}$  be the associated norm. It follows from (26) that  $\|\cdot\|_{H^1(\Omega^\ell)}$  and  $\|\cdot\|_{W^\ell}$  are equivalent norms on  $W^\ell$  and therefore  $(W^\ell, \|\cdot\|_{W^\ell})$  is a real Hilbert space. Moreover, by the Sobolev trace theorem, there exists a constant  $c_0$  depending only on  $\Omega^\ell$ ,  $\Gamma_a^\ell$  and  $\Gamma_a^\ell$  such that

$$\|\boldsymbol{\xi}^\ell\|_{L^2(\Gamma_3)} \leq c_0 \|\boldsymbol{\xi}^\ell\|_{W^\ell} \quad \forall \boldsymbol{\xi}^\ell \in W^\ell. \tag{27}$$

We also introduce the spaces

$$E_0^\ell = L^2(\Omega^\ell), \quad E_1^\ell = H^1(\Omega^\ell).$$

We recall that when  $\mathbf{D}^\ell \in \mathcal{W}_1^\ell$  is a sufficiently regular function, the Green type formula holds:

$$(\mathbf{D}^\ell, \nabla \boldsymbol{\xi}^\ell)_{\mathcal{W}^\ell} + (\operatorname{div} \mathbf{D}^\ell, \boldsymbol{\xi}^\ell)_{\mathcal{W}^\ell} = \int_{\Gamma^\ell} \mathbf{D}^\ell \cdot \boldsymbol{\nu}^\ell \boldsymbol{\xi}^\ell da, \quad \forall \boldsymbol{\xi}^\ell \in H^1(\Omega^\ell). \tag{28}$$

For the stress and strain variables, we use the real Hilbert spaces

$$\begin{aligned} Q^\ell &= \{\boldsymbol{\tau}^\ell = (\tau_{i,j}^\ell); \tau_{i,j}^\ell = \tau_{j,i}^\ell \in L^2(\Omega^\ell)\} = L^2(\Omega^\ell)_{sym}^{d \times d}, \\ Q_1^\ell &= \{\boldsymbol{\sigma}^\ell = (\sigma_{i,j}^\ell) \in Q^\ell : \operatorname{div} \boldsymbol{\sigma}^\ell = (\sigma_{ij,j}^\ell) \in \mathcal{W}^\ell\} \end{aligned}$$

endowed with the respective inner products

$$(\boldsymbol{\sigma}^\ell, \boldsymbol{\tau}^\ell)_{Q^\ell} = \int_{\Omega^\ell} \sigma_{i,j}^\ell \cdot \tau_{i,j}^\ell dx, \quad (\boldsymbol{\sigma}^\ell, \boldsymbol{\tau}^\ell)_{Q_1^\ell} = (\boldsymbol{\sigma}^\ell, \boldsymbol{\tau}^\ell)_{Q^\ell} + (\operatorname{div} \boldsymbol{\sigma}^\ell, \operatorname{Div} \boldsymbol{\tau}^\ell)_{\mathcal{W}^\ell}$$

and the associated norms  $\|\cdot\|_{Q^\ell}$  and  $\|\cdot\|_{Q_1^\ell}$ . For the displacement variable we use the real Hilbert space

$$H_1^\ell = \{\mathbf{u}^\ell = (u_i) \in \mathcal{W}^\ell : \boldsymbol{\varepsilon}(\mathbf{u}^\ell) \in Q^\ell\}$$

endowed with the inner product

$$(\mathbf{u}^\ell, \mathbf{v}^\ell)_{H_1^\ell} = (\mathbf{u}^\ell, \mathbf{v}^\ell)_{\mathcal{W}^\ell} + (\boldsymbol{\varepsilon}(\mathbf{u}^\ell), \boldsymbol{\varepsilon}(\mathbf{v}^\ell))_{Q^\ell}$$

and the norm  $\|\cdot\|_{H_1^\ell}$ . When  $\boldsymbol{\sigma}^\ell$  is a regular function, the following Green's type formula holds:

$$(\mathbf{v}^\ell, \boldsymbol{\varepsilon}(\mathbf{v}^\ell))_{Q^\ell} + (\operatorname{Div} \boldsymbol{\sigma}^\ell, \mathbf{v}^\ell)_{\mathcal{W}^\ell} = \int_{\Gamma^\ell} \boldsymbol{\sigma}^\ell \cdot \boldsymbol{\nu}^\ell \mathbf{V}^\ell da, \quad \forall \mathbf{v}^\ell \in H_1^\ell. \tag{29}$$

Next, we define the space

$$V^\ell = \{ \mathbf{v}^\ell \in H_1^\ell : \mathbf{v} = 0 \text{ on } \Gamma_1^\ell \}.$$

Since  $meas \Gamma_1^\ell > 0$ , Korn’s inequality (e.g., [5, pp. 16-17]) holds and

$$\| \varepsilon(\mathbf{v}^\ell) \|_{\mathbf{Q}^\ell} \geq c_K \| \mathbf{v}^\ell \|_{H_1^\ell} \quad \forall \mathbf{v}^\ell \in V^\ell, \tag{30}$$

where  $c_K$  is a constant which depends only on  $\Omega^\ell$ , and  $\Gamma_1^\ell$  is a constant which depends only on  $V^\ell$ , we use the inner product

$$(\mathbf{u}^\ell, \mathbf{v}^\ell)_{V^\ell} = (\varepsilon(\mathbf{u}^\ell), \varepsilon(\mathbf{v}^\ell))_{\mathbf{Q}^\ell}, \quad \| \mathbf{v}^\ell \|_{V^\ell} = \| \mathbf{v}^\ell \|_{\mathbf{Q}^\ell}, \tag{31}$$

and let  $\| \cdot \|_{V^\ell}$  be the associated norm. It follows from (30) that the norms  $\| \cdot \|_{H_1^\ell}$  and  $\| \cdot \|_{V^\ell}$  are equivalent on  $V^\ell$ . Then  $(V^\ell, (\cdot)_{V^\ell})$  is a real Hilbert space. Moreover, by the Sobolev trace theorem and (27), there exists a constant  $\tilde{c}_0 > 0$  depending only on  $\Omega^\ell$ ,  $\Gamma_1^\ell$  and  $\Gamma_3$  such that

$$\| \mathbf{v}^\ell \|_{L^2(\Gamma_3)^d} \leq \tilde{c}_0 \| \mathbf{v}^\ell \|_{V^\ell} \quad \forall \mathbf{v}^\ell \in V^\ell. \tag{32}$$

In order to simplify the notations, we define the product spaces

$$E_0 = E_0^1 \times E_0^2, \quad E_1 = E_1^1 \times E_1^2.$$

Finally, for a real Banach space  $(X, \| \cdot \|_X)$  we use the classical notation for the spaces  $L^p(0, T; X)$  and  $W^{k,p}(0, T; X)$ , where  $1 \leq p \leq \infty$ ,  $k = 1, 2, \dots$ ; denote by  $C(0, T; X)$  and  $C^1(0, T; X)$  the spaces of continuous and continuously differentiable functions on  $[0, T]$  with values in  $X$ , with the respective norms

$$\begin{aligned} \| x \|_{C(0, T; X)} &= \max_{t \in [0, T]} \| x(t) \|_X, \\ \| x \|_{C^1(0, T; X)} &= \max_{t \in [0, T]} \| x(t) \|_X + \max_{t \in [0, T]} \| \dot{x}(t) \|_X. \end{aligned}$$

We complete this section with the following version of the classical theorem of Cauchy-Lipschitz (see, e.g., [18, p. 48]).

**Theorem 3.1** *Assume that  $(X, \| \cdot \|_X)$  is a real Banach space and  $T > 0$ . Let  $F(t, \cdot) : X \rightarrow X$  is an operator defined a.e. on  $(0, T)$  satisfying the following conditions:*

1. *There exists a constant  $L_F > 0$  such that*

$$\| F(t, x) - F(t, y) \|_X \leq L_F \| x - y \|_X \quad \forall x, y \in X, \quad \text{a.e. } t \in (0, T).$$

2. *There exists  $p \geq 1$  such that  $t \mapsto F(t, x) \in L^p(0, T; X) \quad \forall x \in X$ .*

*Then for any  $x_0 \in X$ , there exists a unique function  $x \in W^{1,p}(0, T; X)$  such that*

$$\begin{aligned} \dot{x}(t) &= F(t, x(t)), \quad \text{a.e. } t \in (0, T), \\ x(0) &= x_0. \end{aligned}$$

Theorem 3.1 will be used in Section 3 to prove the unique solvability of the intermediate problem involving the bonding field. Moreover, if  $X_1$  and  $X_2$  are the real Hilbert spaces, then  $X_1 \times X_1$  denotes the product Hilbert space endowed with the canonical inner product  $(\cdot, \cdot)_{X_1 \times X_1}$ . Recall that the dot represents the time derivative.

In the study of the Problem **P**, we consider the following assumptions: we assume that the *viscosity operator*  $\mathcal{A}^\ell : \Omega^\ell \times \mathbb{S}^d \rightarrow \mathbb{S}^d$  satisfies:

$$\left\{ \begin{array}{l} \text{(a) There exists } L_{\mathcal{A}^\ell} > 0 \text{ such that} \\ \quad |\mathcal{A}^\ell(\mathbf{x}, \boldsymbol{\xi}_1) - \mathcal{A}^\ell(\mathbf{x}, \boldsymbol{\xi}_2)| \leq L_{\mathcal{A}^\ell} |\boldsymbol{\xi}_1 - \boldsymbol{\xi}_2| \\ \quad \forall \boldsymbol{\xi}_1, \boldsymbol{\xi}_2 \in \mathbb{S}^d, \text{ a.e. } \mathbf{x} \in \Omega^\ell. \\ \text{(b) There exists } m_{\mathcal{A}^\ell} > 0 \text{ such that} \\ \quad (\mathcal{A}^\ell(\mathbf{x}, \boldsymbol{\xi}_1) - \mathcal{A}^\ell(\mathbf{x}, \boldsymbol{\xi}_2)) \cdot (\boldsymbol{\xi}_1 - \boldsymbol{\xi}_2) \geq m_{\mathcal{A}^\ell} |\boldsymbol{\xi}_1 - \boldsymbol{\xi}_2|^2 \\ \quad \forall \boldsymbol{\xi}_1, \boldsymbol{\xi}_2 \in \mathbb{S}^d, \text{ a.e. } \mathbf{x} \in \Omega^\ell. \\ \text{(c) The mapping } \mathbf{x} \mapsto \mathcal{A}^\ell(\mathbf{x}, \boldsymbol{\xi}) \text{ is Lebesgue measurable on } \Omega^\ell, \\ \quad \text{for any } \boldsymbol{\xi} \in \mathbb{S}^d. \\ \text{(d) The mapping } \mathbf{x} \mapsto \mathcal{A}^\ell(\mathbf{x}, \mathbf{0}) \text{ belongs to } Q^\ell. \end{array} \right. \quad (33)$$

The *elasticity operator*  $\mathcal{B}^\ell : \Omega^\ell \times \mathbb{S}^d \rightarrow \mathbb{S}^d$  satisfies:

$$\left\{ \begin{array}{l} \text{(a) There exists } L_{\mathcal{B}^\ell} > 0 \text{ such that} \\ \quad |\mathcal{B}^\ell(\mathbf{x}, \boldsymbol{\xi}_1) - \mathcal{B}^\ell(\mathbf{x}, \boldsymbol{\xi}_2)| \leq L_{\mathcal{B}^\ell} |\boldsymbol{\xi}_1 - \boldsymbol{\xi}_2| \\ \quad \forall \boldsymbol{\xi}_1, \boldsymbol{\xi}_2 \in \mathbb{S}^d, \text{ a.e. } \mathbf{x} \in \Omega^\ell. \\ \text{(b) The mapping } \mathbf{x} \mapsto \mathcal{B}^\ell(\mathbf{x}, \boldsymbol{\xi}) \text{ is Lebesgue measurable on } \Omega^\ell, \\ \quad \text{for any } \boldsymbol{\xi} \in \mathbb{S}^d. \\ \text{(c) The mapping } \mathbf{x} \mapsto \mathcal{B}^\ell(\mathbf{x}, \mathbf{0}) \text{ belongs to } Q^\ell. \end{array} \right. \quad (34)$$

The *viscoplasticity operator*  $\mathcal{G}^\ell : \Omega^\ell \times \mathbb{S}^d \times \mathbb{S}^d \times \mathbb{R} \times \mathbb{R} \rightarrow \mathbb{S}^d$  satisfies:

$$\left\{ \begin{array}{l} \text{(a) There exists a constant } L_{\mathcal{G}^\ell} > 0 \text{ such that} \\ \quad \|\mathcal{G}^\ell(\mathbf{x}, \boldsymbol{\sigma}_1, \boldsymbol{\varepsilon}_1, \boldsymbol{\theta}_1, \boldsymbol{\varsigma}_1) - \mathcal{G}^\ell(\mathbf{x}, \boldsymbol{\sigma}_2, \boldsymbol{\varepsilon}_2, \boldsymbol{\theta}_2, \boldsymbol{\varsigma}_2)\| \leq \\ \quad L_{\mathcal{G}^\ell} (\|\boldsymbol{\sigma}_1 - \boldsymbol{\sigma}_2\| + \|\boldsymbol{\varepsilon}_1 - \boldsymbol{\varepsilon}_2\| + \|\boldsymbol{\theta}_1 - \boldsymbol{\theta}_2\| + \|\boldsymbol{\varsigma}_1 - \boldsymbol{\varsigma}_2\|), \\ \quad \forall \boldsymbol{\sigma}_1, \boldsymbol{\sigma}_2, \boldsymbol{\varepsilon}_1, \boldsymbol{\varepsilon}_2 \in \mathbb{S}^d, \forall \boldsymbol{\theta}_1, \boldsymbol{\theta}_2, \boldsymbol{\zeta}_1, \boldsymbol{\zeta}_2 \in \mathbb{R} \text{ a.e. } \mathbf{x} \in \Omega^\ell. \\ \text{(b) The mapping } \mathbf{x} \mapsto \mathcal{G}^\ell(\mathbf{x}, \boldsymbol{\sigma}, \boldsymbol{\varepsilon}, \boldsymbol{\theta}, \boldsymbol{\varsigma}) \text{ is Lebesgue measurable on } \Omega^\ell, \\ \quad \text{for } \boldsymbol{\sigma}, \boldsymbol{\varepsilon} \in \mathbb{S}^d, \text{ for all } \boldsymbol{\theta}, \boldsymbol{\zeta} \in \mathbb{R}. \\ \text{(c) The mapping } \mathbf{x} \mapsto \mathcal{G}^\ell(\mathbf{x}, \mathbf{0}, \mathbf{0}, \mathbf{0}, \mathbf{0}) \text{ belongs to } Q^\ell. \end{array} \right. \quad (35)$$

The *electric permittivity operator*  $\mathbf{B}^\ell = (b_{ij}^\ell) : \Omega^\ell \times \mathbb{R}^d \rightarrow \mathbb{R}^d$  verifies:

$$\left\{ \begin{array}{l} \text{(a) } \mathbf{B}^\ell(\mathbf{x}, \mathbf{E}) = (b_{ij}^\ell(\mathbf{x})E_j) \quad \forall \mathbf{E} = (E_i) \in \mathbb{R}^d, \text{ a.e. } \mathbf{x} \in \Omega^\ell. \\ \text{(b) } b_{ij}^\ell = b_{ji}^\ell, b_{ij}^\ell \in L^\infty(\Omega^\ell), \quad 1 \leq i, j \leq d. \\ \text{(c) There exists } m_{\mathbf{B}^\ell} > 0 \text{ such that } \mathbf{B}^\ell \mathbf{E} \cdot \mathbf{E} \geq m_{\mathbf{B}^\ell} |\mathbf{E}|^2 \\ \quad \forall \mathbf{E} = (E_i) \in \mathbb{R}^d, \text{ a.e. } \mathbf{x} \in \Omega^\ell. \end{array} \right. \quad (36)$$

The *piezoelectric tensor*  $\mathcal{E}^\ell : \Omega^\ell \times \mathbb{S}^d \rightarrow \mathbb{R}^d$  satisfies:

$$\left\{ \begin{array}{l} \text{(a) } \mathcal{E}^\ell(\mathbf{x}, \boldsymbol{\tau}) = (e_{ijk}^\ell(\mathbf{x})\tau_{jk}), \quad \forall \boldsymbol{\tau} = (\tau_{ij}) \in \mathbb{S}^d \text{ a.e. } \mathbf{x} \in \Omega^\ell. \\ \text{(b) } e_{ijk}^\ell = e_{ikj}^\ell \in L^\infty(\Omega^\ell), \quad 1 \leq i, j, k \leq d. \end{array} \right. \quad (37)$$

The damage source function  $\mathbf{S}^\ell : \Omega^\ell \times \mathbb{S}^d \times \mathbb{S}^d \times \mathbb{R} \times \mathbb{R} \rightarrow \mathbb{S}^d$  satisfies:

$$\left\{ \begin{array}{l} \text{(a) There exists a constant } M_{S^\ell} > 0 \text{ such that} \\ \quad \|\mathbf{S}^\ell(\mathbf{x}, \boldsymbol{\sigma}_1, \boldsymbol{\varepsilon}_1, \boldsymbol{\beta}_1) - \mathbf{S}^\ell(\mathbf{x}, \boldsymbol{\sigma}_2, \boldsymbol{\varepsilon}_2, \boldsymbol{\beta}_2)\| \leq M_{S^\ell} (\|\boldsymbol{\sigma}_1 - \boldsymbol{\sigma}_2\| + \|\boldsymbol{\varepsilon}_1 - \boldsymbol{\varepsilon}_2\| \\ \quad + \|\boldsymbol{\beta}_1 - \boldsymbol{\beta}_2\|), \quad \forall \boldsymbol{\sigma}_1, \boldsymbol{\sigma}_2, \boldsymbol{\varepsilon}_1, \boldsymbol{\varepsilon}_2 \in \mathbb{S}^d, \forall \boldsymbol{\beta}_1, \boldsymbol{\beta}_2 \in \mathbb{R} \text{ a.e. } \mathbf{x} \in \Omega^\ell. \\ \text{(b) The mapping } \mathbf{x} \mapsto \mathbf{S}^\ell(\mathbf{x}, \boldsymbol{\sigma}, \boldsymbol{\varepsilon}, \boldsymbol{\beta}) \text{ is Lebesgue measurable on } \Omega^\ell, \\ \quad \text{for any } \boldsymbol{\sigma}, \boldsymbol{\varepsilon} \in \mathbb{S}^d, \text{ and } \boldsymbol{\beta} \in \mathbb{R}. \\ \text{(c) The mapping } \mathbf{x} \mapsto \mathbf{S}^\ell(\mathbf{x}, \mathbf{0}, \mathbf{0}, \mathbf{0}) \text{ belongs to } L^2(\Omega^\ell). \end{array} \right. \quad (38)$$

The normal damped response function  $q_r : \Gamma_3 \times \mathbb{R} \rightarrow \mathbb{R}$ , ( $r = v, \tau$ ) satisfies:

$$\left\{ \begin{array}{l} \text{(a) There exists a constant } C_1^r, C_2^r \text{ such that} \\ \quad |q_r(x, \mathbf{d})| \leq C_1^r |\mathbf{d}| + C_2^r, \quad \forall d \in \mathbb{R}^d \text{ a.e. } x \in \Gamma_3. \\ \text{(b) } (q_r(x, \mathbf{d}_1) - q_r(x, \mathbf{d}_2))(\mathbf{d}_1 - \mathbf{d}_2) \geq 0, \quad \forall \mathbf{d}_1, \mathbf{d}_2 \in \mathbb{R}^d \text{ a.e. } x \in \Gamma_3. \\ \text{(c) The mapping } \mathbf{x} \mapsto q_r(x, d) \text{ is measurable on } \Gamma_3 \text{ for any } d \in \mathbb{R}^d. \\ \text{(d) The mapping } \mathbf{x} \mapsto q_r(x, d) \text{ is continuous on } \mathbb{R}^d \text{ a.e. } x \in \Gamma_3. \end{array} \right. \quad (39)$$

The normal compliance functions  $p_r : \Gamma_3 \times \mathbb{R} \rightarrow \mathbb{R}_+$ , ( $r = v, \tau$ ) satisfies:

$$\left\{ \begin{array}{l} \text{(a) There exists a constant } C_1^r, C_2^r \text{ such that} \\ \quad |p_r(x, \mathbf{d})| \leq C_1^r |\mathbf{d}| + C_2^r, \quad \forall d \in \mathbb{R}^d \text{ a.e. } x \in \Gamma_3. \\ \text{(b) } (p_r(x, \mathbf{d}_1) - p_r(x, \mathbf{d}_2))(\mathbf{d}_1 - \mathbf{d}_2) \geq 0, \quad \forall \mathbf{d}_1, \mathbf{d}_2 \in \mathbb{R}^d \text{ a.e. } x \in \Gamma_3. \\ \text{(c) The mapping } \mathbf{x} \mapsto p_r(x, d) \text{ is measurable on } \Gamma_3 \text{ for any } d \in \mathbb{R}^d. \\ \text{(d) The mapping } \mathbf{x} \mapsto p_r(x, d) \text{ is continuous on } \mathbb{R}^d \text{ a.e. } x \in \Gamma_3. \end{array} \right. \quad (40)$$

An example of a normal compliance function  $p_\nu$ , which satisfies conditions (40), is  $p_\nu(u) = c_\nu u_+$ , where  $c_\nu \in L^\infty(\Gamma_3)$  is a positive surface stiffness coefficient, and  $u_+ = \max\{0, u\}$ . The choices  $p_\tau = \mu p_\nu$  and  $p_\tau = \mu p_\nu(1 - \delta p_\nu)_+$  in (14), where  $\mu \in L^\infty(\Gamma_3)$  and  $\delta \in L^\infty(\Gamma_3)$  are positive functions, lead to the usual or modified Coulomb’s law of dry friction, respectively, see [5,6,21] for details. Here,  $\mu$  represents the coefficient of friction and  $\delta$  is a small positive material constant related to the wear and hardness of the surface. We note that if  $p_\nu$  satisfies condition (40), then  $p_\tau$  satisfies it too, in both examples. Therefore, we conclude that the results below are valid for the corresponding piezoelectric frictional contact models. The surface electrical conductivity function  $\psi : \Gamma_3 \times \mathbb{R} \rightarrow \mathbb{R}_+$  satisfies

$$\left\{ \begin{array}{l} \text{(a) } \exists L_\psi > 0 \text{ such that } \|\psi(\mathbf{x}, u_1) - \psi(\mathbf{x}, u_2)\| \leq L_\psi \|u_1 - u_2\| \\ \quad \forall u_1, u_2 \in \mathbb{R}, \text{ a.e. } \mathbf{x} \in \Gamma_3. \\ \text{(b) } \exists M_\psi > 0 \text{ such that } \|\psi(\mathbf{x}, u)\| \leq M_\psi \|u\|, \quad \forall u \in \mathbb{R}, \text{ a.e. } \mathbf{x} \in \Gamma_3. \\ \text{(c) The mapping } \mathbf{x} \mapsto \psi(\mathbf{x}, u) \text{ is measurable on } \Gamma_3, \forall u \in \mathbb{R}. \\ \text{(d) } \psi(\mathbf{x}, u) = 0, \text{ for all } u \leq 0, \text{ a.e. } \mathbf{x} \in \Gamma_3. \end{array} \right. \quad (41)$$

An example of a conductivity function, which satisfies condition (41), is given by (24), in which case  $M_\psi = k$ . Another example is provided by  $\psi \equiv 0$ , which models the contact with an insulated foundation, as noted in Section 2. We conclude that our results below are valid for the corresponding piezoelectric contact models.

The microcrack diffusion coefficient verifies

$$K^\ell > 0, \quad (42)$$

and the initial damage field satisfies

$$\beta_0^\ell \in K^\ell. \quad (43)$$

Finally, we assume that the gap function, the given potential and the initial displacement satisfy

$$g \in L^2(\Gamma_3) \quad g \geq 0. \text{ a.e on } \Gamma_3, \quad (44)$$

$$\varphi_0 \in L^2(\Gamma_3), \quad (45)$$

$$\mathbf{u}_0 \in \mathbf{V}. \quad (46)$$

The forces, tractions, volume and surface free charge densities satisfy

$$\mathbf{f}_0^\ell \in W^{1,p}(0, T; W^\ell), \quad \mathbf{f}_2^\ell \in W^{1,p}(0, T; L^2(\Gamma_2^\ell)^d), \quad (47)$$

$$q_0^\ell \in W^{1,p}(0, T; L^2(\Omega^\ell)), \quad q_2^\ell \in W^{1,p}(0, T; L^2(\Gamma_b^\ell)). \quad (48)$$

Here,  $1 \leq p \leq \infty$ . We define the bilinear form  $a : H^1(\Omega^\ell) \times H^1(\Omega^\ell) \rightarrow \mathbb{R}$ ,

$$a(\xi^\ell, \varphi^\ell) = \sum_{\ell=1}^2 k^\ell \int_{(\Omega)^\ell} \nabla \xi^\ell \cdot \nabla \varphi^\ell dx. \quad (49)$$

Next, we define the four mappings  $j_1 : \mathbf{V} \times \mathbf{V} \rightarrow \mathbb{R}$ ,  $j_2 : \mathbf{V} \times \mathbf{V} \rightarrow \mathbb{R}$ ,  $h : \mathbf{V} \times W \rightarrow W$ ,  $\mathbf{f} : [0, T] \rightarrow \mathbf{V}$  and  $q : [0, T] \rightarrow W$ , respectively, by

$$j_1(\mathbf{u}, \mathbf{v}) = \int_{\Gamma_3} p_\nu([u_\nu] - g)[v_\nu] da + \int_{\Gamma_3} p_\tau([\mathbf{u}_\tau] - g)\|\mathbf{v}_\tau\| da, \quad (50)$$

$$j_2(\mathbf{u}, \mathbf{v}) = \int_{\Gamma_3} q_\nu([u_\nu])[v_\nu] da + \int_{\Gamma_3} q_\tau([\mathbf{u}_\tau])\|\mathbf{v}_\tau\| da, \quad (51)$$

$$(h(\mathbf{u}, \varphi), \xi)_W = \int_{\Gamma_3} \psi([\mathbf{u}_v] - g)\phi_l([\varphi] - \varphi_0)\xi da, \quad (52)$$

$$(\mathbf{f}(t), \mathbf{v})_{\mathbf{V}' \times \mathbf{V}} = \sum_{\ell=1}^2 \int_{\Omega^\ell} \mathbf{f}_0^\ell(t) \cdot \mathbf{v}^\ell dx + \sum_{\ell=1}^2 \int_{\Gamma_2^\ell} \mathbf{f}_2^\ell(t) \cdot \mathbf{v}^\ell da, \quad (53)$$

$$(q(t), \zeta)_W = \sum_{\ell=1}^2 \int_{\Omega^\ell} q_0^\ell(t)\zeta^\ell dx - \sum_{\ell=1}^2 \int_{\Gamma_b^\ell} q_2^\ell(t)\zeta^\ell da \quad (54)$$

for all  $\mathbf{u}^\ell, \mathbf{v}^\ell \in V^\ell$ ,  $\varphi^\ell, \xi^\ell \in W^\ell$  and  $t \in [0; T]$ . We note that the definitions of  $h, f$  and  $q$  are based on the Riesz representation theorem, moreover, it follows from assumptions (38)-(46) that the integrals in (50)-(51) and (54) are well-defined. Using Green's formulas (28) and (29), it is easy to see that if  $\{\mathbf{u}^\ell, \boldsymbol{\sigma}^\ell, \mathbf{D}^\ell\}$  are sufficiently regular functions which satisfy (9)-(15) and (17)-(19), then

$$(\ddot{u}, v)_{\mathbf{V}' \times \mathbf{V}} + \sum_{\ell=1}^2 (\boldsymbol{\sigma}^\ell(t), \boldsymbol{\varepsilon}(\mathbf{v}^\ell))_{Q^\ell} + j_1(\mathbf{u}(t), \mathbf{v}) + j_2(\dot{\mathbf{u}}(t), \mathbf{v}) = (\mathbf{f}, \mathbf{v})_V, \quad (55)$$

$$\sum_{\ell=1}^2 (\mathbf{D}^\ell(t), \nabla \xi^\ell)_{W^\ell} - (q(t), \xi)_W = (h(\mathbf{u}, \varphi), \xi)_W \quad (56)$$

for all  $\mathbf{u}^\ell, \mathbf{v}^\ell \in V^\ell, \varphi^\ell, \xi^\ell \in W^\ell$  and  $t \in [0; T]$ . We substitute (6) in (55), (7) in (56), we use the initial condition (20) and derive a variational formulation of Problem  $\mathcal{P}$ .

**Problem  $\mathcal{P}_V$ .** Find a displacement field  $\mathbf{u} = (\mathbf{u}^1, \mathbf{u}^2) : [0, T] \rightarrow \mathbf{V}$ , a stress field  $\boldsymbol{\sigma} = (\boldsymbol{\sigma}^1, \boldsymbol{\sigma}^2) : [0, T] \rightarrow \mathbf{Q}$ , an electric potential field  $\varphi = (\varphi^1, \varphi^2) : [0, T] \rightarrow W$ , a damage field  $\beta = (\beta^1, \beta^2) : [0, T] \rightarrow \mathbf{E}_1$ , and an electric displacement field  $\mathbf{D} = (\mathbf{D}^1, \mathbf{D}^2) : [0, T] \rightarrow \mathcal{W}$  such that

$$\boldsymbol{\sigma}^\ell(t) = \mathcal{A}^\ell \boldsymbol{\varepsilon}(\dot{\mathbf{u}}^\ell(t)) + \mathcal{B}^\ell \boldsymbol{\varepsilon}(\mathbf{u}^\ell) + (\mathcal{E}^\ell)^* \nabla \varphi^\ell + \int_0^t \mathcal{G}^\ell \left( \boldsymbol{\sigma}^\ell(s) - \mathcal{A}^\ell \boldsymbol{\varepsilon}(\dot{\mathbf{u}}^\ell(s)) - (\mathcal{E}^\ell)^* \nabla \varphi^\ell, \boldsymbol{\varepsilon}(\mathbf{u}^\ell(s)), \beta^\ell(s) \right) ds \quad \text{in } \Omega^\ell \times (0, T), \quad (57)$$

$$\mathbf{D}^\ell = \mathcal{E}^\ell \boldsymbol{\varepsilon}(\mathbf{u}^\ell) - \mathcal{B}^\ell \nabla \varphi^\ell \quad \text{in } \Omega^\ell \times (0, T), \quad (58)$$

$$(\ddot{u}, v)_{\mathbf{V}' \times \mathbf{V}} + \sum_{\ell=1}^2 (\boldsymbol{\sigma}^\ell, \boldsymbol{\varepsilon}(\mathbf{v}^\ell))_{\mathbf{Q}^\ell} + j_1(\mathbf{u}, \mathbf{v}) + j_2(\dot{\mathbf{u}}, \mathbf{v}) = (\mathbf{f}, \mathbf{v})_{\mathbf{V}' \times \mathbf{V}}, \quad \forall \mathbf{v} \in \mathbf{V}, \quad (59)$$

$$\sum_{\ell=1}^2 (\mathcal{B}^\ell \nabla \varphi^\ell, \nabla \xi^\ell)_{\mathcal{W}^\ell} - \sum_{\ell=1}^2 (\mathcal{E}^\ell \boldsymbol{\varepsilon}(\mathbf{u}^\ell), \nabla \xi^\ell)_{\mathcal{W}^\ell} + (h(\mathbf{u}, \varphi), \xi)_{\mathcal{W}^\ell} = (q, \xi)_W, \quad \xi \in W, \quad (60)$$

$$\beta(t) \in K, \quad \sum_{\ell=1}^2 (\dot{\beta}^\ell(t), \xi^\ell - \beta^\ell(t))_{L^2(\Omega^\ell)} + a(\beta(t), \xi - \beta(t)) \geq \quad (61)$$

$$\sum_{\ell=1}^2 (\mathcal{S}^\ell(\boldsymbol{\sigma}^\ell(t) - \mathcal{A}^\ell \boldsymbol{\varepsilon}(\dot{\mathbf{u}}^\ell(t)) - (\mathcal{E}^\ell)^* \nabla \varphi^\ell(t), \boldsymbol{\varepsilon}(\mathbf{u}^\ell(t)), \xi^\ell - \beta^\ell(t))_{L^2(\Omega^\ell)}, \quad \xi \in K,$$

$$\mathbf{u}^\ell(0) = \mathbf{u}_0^\ell, \quad \dot{\mathbf{u}}^\ell(0) = \mathbf{v}_0^\ell, \quad \beta^\ell(0) = \beta_0^\ell. \quad (62)$$

To study Problem  $\mathcal{P}_V$ , we use the smallness assumption

$$M_{\psi^\ell} < \frac{m_{\mathbf{B}^\ell}}{c_0^2}, \quad (63)$$

where  $M_{\psi^\ell}$ ,  $c_0$  and  $m_{\mathbf{B}^\ell}$  are given in (41), (27) and (36), respectively. We note that only the trace constant, the coercivity constant of  $\mathbf{B}^\ell$  and the bound of  $\psi^\ell$  are involved in (63); therefore, this smallness assumption involves only the geometry and the electrical part, and does not depend on the mechanical data of the problem. Moreover, it is satisfied when the obstacle is insulated since then  $\psi^\ell \equiv 0$  and so  $M_{\psi^\ell} = 0$ . Removing this assumption remains a task for future research since it is made for mathematical reasons, and does not seem to relate to any inherent physical constraints of the problem.

#### 4 Existence and Uniqueness Result

Now, we propose our existence and uniqueness result.

**Theorem 4.1** *Assume that (32)-(48) hold. Then there exists a unique solution*

$\{\mathbf{u}, \varphi, \boldsymbol{\sigma}, \mathbf{D}, \beta\}$  to Problem  $\mathcal{P}_V$ . Moreover, the solution satisfies

$$\mathbf{u} \in W^{2,p}(0, T; \mathbf{V}) \cap C^1(0, T; \mathbf{V}), \quad \dot{\mathbf{u}} \in W^{2,p}(0, T; \mathbf{V}'), \tag{64}$$

$$\varphi \in W^{1,p}(0, T; W), \tag{65}$$

$$\boldsymbol{\sigma} \in W^{1,p}(0, T; Q), \quad (\text{Div } \boldsymbol{\sigma}^1, \text{Div } \boldsymbol{\sigma}^2) \in W^{1,p}(0, T; \mathcal{W}), \tag{66}$$

$$\mathbf{D} \in W^{1,p}(0, T; \mathcal{W}), \tag{67}$$

$$\beta \in W^{1,2}(0, T; E_0) \cap L^2(0, T; E_1). \tag{68}$$

The functions  $\mathbf{u}, \varphi, \boldsymbol{\sigma}, \mathbf{D}$  and  $\beta$ , which satisfy (57)-(62), are called a weak solution to the contact Problem  $\mathcal{P}$ . We conclude that, under the assumptions (33)-(48) and (63), the mechanical problem (6) has a unique weak solution satisfying (64).

The regularity of the weak solution is given by(64), and in terms of electric displacement,

$$\mathbf{D} \in W^{1,p}(0, T; \mathcal{W}). \tag{69}$$

It follows from (80) and (47) that  $\text{div } \mathbf{D}^\ell(t) - q_0^\ell(t) = 0$  for all  $t \in [0, T]$ , and therefore the regularity (65) of  $\varphi$ , combined with (36), (37) and (48), implies (69). In this section we suppose that the assumptions of Theorem4.1 hold, and we consider that  $C$  is a generic positive constant which depends on  $\Omega^\ell, \Gamma_1^\ell, \Gamma_3, p_\nu, p_\tau, q_\nu, q_\tau$  and may change from place to place.

Let a  $\eta \in L^2(0, T; \mathbf{V}')$  be given. In the first step, we consider the following variational problem.

**Problem  $\mathcal{PV}_\eta^1$ .** Find a displacement field  $\mathbf{u}_\eta = (\mathbf{u}_\eta^1, \mathbf{u}_\eta^2) : [0, T] \rightarrow \mathbf{V}$  such that

$$(\ddot{\mathbf{u}}_\eta(t), v)_{\mathbf{V}' \times \mathbf{V}} + \sum_{\ell=1}^2 (\mathcal{A}^\ell \varepsilon(\dot{\mathbf{u}}^\ell(t)), \varepsilon(\mathbf{v}^\ell))_{\mathcal{H}^\ell} + j_2(\dot{\mathbf{u}}(t), \mathbf{v}) \tag{70}$$

$$+(\eta(t), v)_{\mathbf{V}' \times \mathbf{V}} = (\mathbf{f}(t), \mathbf{v})_{\mathbf{V}' \times \mathbf{V}} \quad \forall \mathbf{v} \in \mathbf{V}, \text{ a.e. } t \in (0, T),$$

$$\mathbf{u}^\ell(0) = \mathbf{u}_0^\ell, \quad \dot{\mathbf{u}}^\ell(0) = \mathbf{v}_0^\ell \quad \text{in } \Omega^\ell. \tag{71}$$

To solve Problem  $\mathcal{PV}_\eta^1$ , we apply an abstract existence and uniqueness result which we recall now, for the convenience of the reader. Let  $\mathbf{V}$  and  $H$  denote real Hilbert spaces such that  $\mathbf{V}$  is dense in  $H$  and the inclusion map is continuous,  $H$  is identified with its dual and with a subspace of the dual  $\mathbf{V}'$  of  $\mathbf{V}$ , i.e.,  $\mathbf{V} \subset H \subset \mathbf{V}'$ , and we say that the inclusions above define a Gelfand triple. The notations  $\|\cdot\|_{\mathbf{V}}, \|\cdot\|_{\mathbf{V}'}$  and  $(\cdot, \cdot)_{\mathbf{V}' \times \mathbf{V}}$  represent the norms on  $\mathbf{V}$  and on  $\mathbf{V}'$  and the duality pairing between them, respectively. The following abstract result may be found in [22, p.48].

**Theorem 4.2** *Let  $\mathbf{V}, H$  be as above, and let  $A : \mathbf{V} \rightarrow \mathbf{V}'$  be a hemicontinuous and monotone operator which satisfies*

$$(A\mathbf{v}, \mathbf{v})_{\mathbf{V}' \times \mathbf{V}} \geq w \|\mathbf{v}\|_{\mathbf{V}}^2 + \lambda \quad \forall \mathbf{v} \in \mathbf{V}, \tag{72}$$

$$\|A\mathbf{v}\|_{\mathbf{V}'} \leq C(\|\mathbf{v}\|_{\mathbf{V}} + 1) \quad \forall \mathbf{v} \in \mathbf{V}, \tag{73}$$

for some constants  $w > 0, C > 0$  and  $\lambda \in \mathbb{R}$ . Then, given  $\mathbf{u}_0 \in H$  and  $f \in L^2(0, T; \mathbf{V}')$ , there exists a unique function  $\mathbf{u}$  which satisfies

$$\mathbf{u} \in L^2(0, T; \mathbf{V}) \cap C(0, T; H), \quad \dot{\mathbf{u}} \in L^2(0, T; \mathbf{V}'),$$

$$\dot{\mathbf{u}}(t) + A\mathbf{u}(t) = \mathbf{f}(t) \quad \text{a.e. } t \in (0, T),$$

$$\mathbf{u}(0) = \mathbf{u}_0.$$

We have the following result for the problem.

**Lemma 4.1** *There exists a unique solution to Problem  $\mathcal{PV}_\eta^1$  and it has its regularity expressed in (64).*

**Proof.** We define the operator  $A : \mathbf{V} \rightarrow \mathbf{V}'$  by

$$(A\mathbf{u}, \mathbf{v})_{\mathbf{V}' \times \mathbf{V}} = \sum_{\ell=1}^2 (\mathcal{A}^\ell \varepsilon(\mathbf{u}^\ell), \varepsilon(\mathbf{v}^\ell))_{\mathcal{H}^\ell} + j_2(\mathbf{u}, \mathbf{v}) \quad \forall \mathbf{u}, \mathbf{v} \in \mathbf{V}. \tag{74}$$

Let  $\mathbf{u}_1, \mathbf{u}_2 \in \mathbf{V}$ , using (74) and (51), we find

$$\begin{aligned} (A\mathbf{u}_1 - A\mathbf{u}_2, \mathbf{u}_1 - \mathbf{u}_2)_{\mathbf{V}' \times \mathbf{V}} &= \sum_{\ell=1}^2 (\mathcal{A}^\ell \varepsilon(\mathbf{u}_1^\ell) - \mathcal{A}^\ell \varepsilon(\mathbf{u}_2^\ell), \varepsilon(\mathbf{u}_1^\ell - \mathbf{u}_2^\ell))_{\mathcal{H}^\ell} + \\ &\int_{\Gamma_3} (q_\nu([u_{1\nu}]) - q_\nu([u_{2\nu}])([u_{1\nu} - u_{2\nu}]) da + \int_{\Gamma_3} (q_\tau([\mathbf{u}_{1\tau}]) - q_\tau([\mathbf{u}_{2\tau}])) \|[\mathbf{u}_{1\tau} - \mathbf{u}_{2\tau}]\| da, \end{aligned}$$

and keeping in mind (33), (39), we obtain

$$(A\mathbf{u}_1 - A\mathbf{u}_2, \mathbf{u}_1 - \mathbf{u}_2)_{\mathbf{V}' \times \mathbf{V}} \geq m \|\mathbf{u}_1 - \mathbf{u}_2\|_{\mathbf{V}}^2 \quad \forall \mathbf{u}_1, \mathbf{u}_2 \in \mathbf{V}. \tag{75}$$

Use again (74) and (51), it follows that

$$\begin{aligned} (A\mathbf{u}_1 - A\mathbf{u}_2, \mathbf{v})_{\mathbf{V}' \times \mathbf{V}} &= \sum_{\ell=1}^2 (\mathcal{A}^\ell \varepsilon(\mathbf{u}_1^\ell) - \mathcal{A}^\ell \varepsilon(\mathbf{u}_2^\ell), \varepsilon(\mathbf{v}^\ell))_{\mathcal{H}^\ell} + \\ &\int_{\Gamma_3} (q_\nu([u_{1\nu}]) - q_\nu([u_{2\nu}])([v_\nu]) da + \int_{\Gamma_3} (q_\tau([\mathbf{u}_{1\tau}]) - q_\tau([\mathbf{u}_{2\tau}])) \|[\mathbf{v}_\tau]\| da, \quad \forall \mathbf{v} \in \mathbf{V}, \end{aligned}$$

and by (32) and (33), we deduce that

$$\begin{aligned} |A\mathbf{u}_1 - A\mathbf{u}_2|_{\mathbf{V}'} &\leq L_{\mathcal{A}^\ell} |\mathbf{u}_1 - \mathbf{u}_2|_{\mathbf{V}} + c_0 |q_\nu([u_{1\nu}]) - q_\nu([u_{2\nu}])|_{L^2(\Gamma_3)} \\ &\quad + c_0 |q_\tau([\mathbf{u}_{1\tau}]) - q_\tau([\mathbf{u}_{2\tau}])|_{L^2(\Gamma_3)^d}, \quad \forall \mathbf{u}_1, \mathbf{u}_2 \in \mathbf{V}, \end{aligned}$$

and keeping in mind the Krasnoselski theorem (see [10, p.60]), we deduce that  $A : \mathbf{V} \rightarrow \mathbf{V}'$  is a continuous operator. Now, by (74), (31) and (33), we find where the positive constant  $m = \min\{m_{\mathcal{A}^1}, m_{\mathcal{A}^2}\}$ . Choosing  $\mathbf{u}_2 = 0_{\mathbf{V}}$  in (75) we obtain

$$\begin{aligned} (A\mathbf{u}_1, \mathbf{u}_1)_{\mathbf{V}' \times \mathbf{V}} &\geq m \|\mathbf{u}_1\|_{\mathbf{V}}^2 - \|A0_{\mathbf{V}}\|_{\mathbf{V}'}^2 \|\mathbf{u}_1\|_{\mathbf{V}} \\ &\geq \frac{1}{2} m \|\mathbf{u}_1\|_{\mathbf{V}}^2 - \frac{1}{2m} \|A0_{\mathbf{V}}\|_{\mathbf{V}'}^2 \quad \forall \mathbf{u}_1 \in \mathbf{V}, \end{aligned}$$

which implies that  $A$  satisfies condition (72) with  $\omega = \frac{m}{2}$  and  $\lambda = -\frac{1}{2m} \|A0_{\mathbf{V}}\|_{\mathbf{V}'}^2$ . Moreover, by (74) and (33) we find

$$\|A\mathbf{u}_1\|_{\mathbf{V}'} \leq C^1 \|\mathbf{u}_1\|_{\mathbf{V}} + C^2 \quad \forall \mathbf{u}_1 \in \mathbf{V},$$

where  $C^1 = \max\{C_{\mathcal{A}^1}^1, C_{\mathcal{A}^2}^1\}$  and  $C^2 = \max\{C_{\mathcal{A}^1}^2, C_{\mathcal{A}^2}^2\}$ . This inequality and (31) imply that  $A$  satisfies condition (75). Finally, we recall that by (47) and (53) we have  $\mathbf{f} - \eta \in L^2(0, T; \mathbf{V}')$  and  $\mathbf{v}_0 \in H$ .

It follows now from Theorem 4.2 that there exists a unique function  $\mathbf{v}_\eta$  which satisfies

$$\mathbf{v}_\eta \in L^2(0, T; \mathbf{V}) \cap C(0, T; H), \quad \dot{\mathbf{v}}_\eta \in L^2(0, T; \mathbf{V}'), \tag{76}$$

$$\dot{\mathbf{v}}_\eta(t) + A\mathbf{v}_\eta(t) + \eta(t) = \mathbf{f}(t), \quad a.e. \ t \in [0, T], \tag{77}$$

$$\mathbf{v}_\eta(0) = \mathbf{v}_0. \tag{78}$$

Let  $\mathbf{u}_\eta : [0, T] \rightarrow \mathbf{V}$  be the function defined by

$$\mathbf{u}_\eta(t) = \int_0^t \mathbf{v}_\eta(s) ds + \mathbf{u}_0 \quad \forall t \in [0, T]. \tag{79}$$

It follows from (74) and (76)–(79) that  $\mathbf{u}_\eta$  is a unique solution of the variational Problem  $\mathcal{PV}_\eta^1$ , and it satisfies the regularity expressed in (64).

In the second step, let  $\eta \in L^2(0, T; \mathbf{V}')$ , we use the displacement field  $\mathbf{u}_\eta = (\mathbf{u}_\eta^1, \mathbf{u}_\eta^2)$  obtained in Lemma 4.1 and we consider the following variational problem.

**Problem  $\mathcal{PV}_\eta^2$ .** Find the electrical potential field  $\varphi_\eta = (\varphi_\eta^1, \varphi_\eta^2) : [0; T] \rightarrow W$  such that

$$\sum_{\ell=1}^2 (\mathcal{B}^\ell \nabla \varphi_\eta^\ell(t) - \mathcal{E}^\ell \varepsilon(\mathbf{u}_\eta^\ell(t)), \nabla \xi^\ell)_{W^\ell} + (h(\mathbf{u}_\eta(t), \varphi_\eta(t)), \xi)_W = (q(t), \xi)_W \tag{80}$$

for all  $\xi \in W, t \in [0, T]$ .

The well-posedness of Problem  $\mathcal{PV}_\eta^2$  follows.

**Lemma 4.2** *There exists a unique solution  $\varphi_\eta = (\varphi_\eta^1, \varphi_\eta^2) \in W^{1,p}(0, T; W)$  which satisfies (80). Moreover, if  $\varphi_{\eta_1}$  and  $\varphi_{\eta_2}$  are the solutions of (80) corresponding to  $\varphi_{\eta_1}, \varphi_{\eta_2} \in C(0, t; Q)$ , then there exists  $c > 0$  such that*

$$\|\varphi_{\eta_1}(t) - \varphi_{\eta_2}(t)\|_W \leq C \|\mathbf{u}_{\eta_1}(t) - \mathbf{u}_{\eta_2}(t)\|_{\mathbf{V}} \quad \forall t \in [0, T]. \tag{81}$$

**Proof.** We define a bilinear form  $b(., .) : W \times W \rightarrow \mathbb{R}$  such that

$$b(\varphi, \xi) = \sum_{\ell=1}^2 (\mathcal{B}^\ell \nabla \varphi^\ell, \nabla \xi^\ell)_{H^\ell} \quad \forall \varphi, \xi \in W. \tag{82}$$

We use (30), (36) and (71) to show that the bilinear form  $b(., .)$  is continuous, symmetric and coercive on  $W$ . Moreover, using the Riesz representation theorem, we may define an element  $q_\eta : [0, T] \rightarrow W$  such that

$$(q_\eta(t), \xi)_W = \sum_{\ell=1}^2 (\mathcal{E}^\ell \varepsilon(\mathbf{u}_\eta^\ell(t)), \nabla \xi^\ell)_{H^\ell} - (h(\mathbf{u}_\eta(t), \varphi_\eta(t)) + q(t), \xi)_W, \quad \forall \xi \in W, t \in (0, T).$$

We apply the Lax-Milgram theorem to deduce that there exists a unique element  $\varphi_\eta(t) \in W$  such that

$$b(\varphi_\eta(t), \xi) = (q_\eta(t), \xi)_W \quad \forall \xi \in W. \tag{83}$$

We conclude that  $\varphi_\eta(t)$  is a solution to Problem  $\mathcal{PV}_\eta^2$ . Let  $t_1, t_2 \in [0, T]$ , it follows from (80) that

$$\|\varphi_\eta(t_1) - \varphi_\eta(t_2)\|_W \leq C (\|\mathbf{u}_\eta(t_1) - \mathbf{u}_\eta(t_2)\|_{\mathbf{V}} + \|q(t_1) - q(t_2)\|_W),$$

and the previous inequality, the regularity of  $\mathbf{u}_\eta$  and  $q$  imply that  $\varphi_\eta \in C(0, T; W)$ . In the third step, we use the displacement field  $\mathbf{u}_\eta$  obtained in Lemma 4.1 and we consider the following initial-value problem.

In the third step, we let  $\theta = (\theta^1, \theta^2) \in L^2(0, T; E_0)$  be given and consider the following variational problem for the damage field.

**Problem  $\mathcal{PV}_\theta$ .** Find the damage field  $\beta_\theta = (\beta_\theta^1, \beta_\theta^2) : [0; T] \rightarrow E_1$  such that

$$\beta_\theta(t) \in K, \quad \sum_{\ell=1}^2 (\dot{\beta}_\theta^\ell(t), \xi^\ell - \beta_\theta^\ell)_{L^2(\Omega^\ell)} + a(\beta_\theta(t), \xi - \beta_\theta(t)) \geq \tag{84}$$

$$\sum_{\ell=1}^2 (\theta^\ell(t), \xi^\ell - \beta_\theta^\ell(t))_{L^2(\Omega^\ell)} \quad \forall \xi \in K, \text{ a.e. } t \in (0, T),$$

$$\beta_\theta^\ell(0) = \beta_0^\ell. \tag{85}$$

The following abstract result for parabolic variational inequalities (see, e.g., [18, p.48]) is valid.

**Theorem 4.3** *Let  $X \subset Y = Y' \subset X'$  be a Gelfand triple. Let  $F$  be a nonempty, closed, and convex set of  $X$ . Assume that  $a(\cdot, \cdot) : X \times X \rightarrow \mathbb{R}$  is a continuous and symmetric bilinear form such that for some constants  $\alpha > 0$  and  $c_0$ ,*

$$a(v, v) + c_0 \|v\|_Y^2 \geq \alpha \|v\|_X^2.$$

*Then, for every  $u_0 \in F$  and  $f \in L^2(0, T; Y)$ , there exists a unique function  $u \in H^1(0, T; Y) \cap L^2(0, T; X)$  such that  $u(0) = u_0$ ,  $u(t) \in F \quad \forall t \in (0, T)$ , and*

$$(\dot{u}(t), v - u(t))_{X' \times X} + a(u(t), v - u(t)) \geq (f(t), v - u(t))_Y \quad \forall v \in F \text{ a.e. } t \in (0, T).$$

We prove next the unique solvability of Problem  $\mathcal{PV}_\theta$ .

**Lemma 4.3** *There exists a unique solution  $\beta_\theta$  of Problem  $\mathcal{PV}_\theta$  and it satisfies*

$$\beta_\theta \in H^1(0, T; E_0) \cap L^2(0, T; E_1).$$

**Proof.** The inclusion mapping of  $(E_1, \|\cdot\|_{E_1})$  into  $(E_0, \|\cdot\|_{E_0})$  is continuous and its range is dense. We denote by  $E_1'$  the dual space of  $E_1$  and, identifying the dual of  $E_0$  with itself, we can write the Gelfand triple

$$E_1 \subset E_0 = E_0' \subset E_1'.$$

We use the notation  $(\cdot, \cdot)_{E_1' \times E_1}$  to represent the duality pairing between  $E_0$  and  $E_1$ . We have

$$(\beta, \xi)_{E_1' \times E_1} = (\beta, \xi)_{E_0} \quad \forall \beta \in E_0, \xi \in E_1$$

and we note that  $K$  is a closed convex set in  $E_1$ . Then, using (42), (49) and the fact that  $\beta_\theta \in K$  in (43), it is easy to see that Lemma 4.3 is a straight consequence of Theorem 4.3. Now we use the displacement field  $\mathbf{u}_\eta$  obtained in Lemma 4.1,  $\varphi_\eta$  obtained in Lemma 4.2 and  $\beta_\theta$  obtained in Lemma 4.3 to construct the following Cauchy problem for the stress field.

**Problem**  $\mathcal{PV}_{\eta,\theta}$ . Find the stress field  $\sigma_{\eta,\theta} = (\sigma_{\eta,\theta}^1, \sigma_{\eta,\theta}^2) : [0, T] \rightarrow Q$  which is a solution of the problem

$$\sigma_{\eta,\theta}^\ell(t) = \mathcal{B}^\ell \varepsilon(\mathbf{u}_\eta^\ell(t)) + \int_0^t \mathcal{G}^\ell(\sigma_{\eta,\theta}^\ell(s), \varepsilon(\mathbf{u}_\eta^\ell(s)), \beta_\theta^\ell(s)) ds, \quad \ell = 1, 2, \quad \text{a. e } t \in (0, T). \quad (86)$$

**Lemma 4.4** *There exists a unique solution of Problem  $\mathcal{PV}_{\eta,\theta}$  and it satisfies (66). Moreover, if  $\mathbf{u}_{\eta_i}^\ell, \beta_{\eta_i}^\ell$  and  $\sigma_{\eta_i, \theta_i}^\ell$  represent the solutions of problems  $\mathcal{PV}_{\eta_i}^1, \mathcal{PV}_{\theta_i}$  and  $\mathcal{PV}_{\eta_i, \theta_i}$ , respectively, for  $(\eta_i, \theta_i) \in W^{1,p}(0, T; Q \times E_0), i = 1, 2$ , then there exists  $C > 0$  such that*

$$\begin{aligned} \|\sigma_{\eta_1, \theta_1}(t) - \sigma_{\eta_2, \theta_2}(t)\|_Q^2 &\leq C(\|\mathbf{u}_{\eta_1}(t) - \mathbf{u}_{\eta_2}(t)\|_V^2 + \\ &\int_0^t \|\mathbf{u}_{\eta_1}(s) - \mathbf{u}_{\eta_2}(s)\|_V^2 ds + \int_0^t \|\beta_{\theta_1}(s) - \beta_{\theta_2}(s)\|_{E_0}^2 ds). \end{aligned} \quad (87)$$

**Proof.** Let  $\Lambda_{\eta,\theta}^\ell : W^{1,p}(0, T; Q^\ell) \rightarrow W^{1,p}(0, T; Q^\ell)$  be the operator given by

$$\Lambda_{\eta,\theta}^\ell \sigma^\ell(t) = \mathcal{B}^\ell \varepsilon(\mathbf{u}_\eta^\ell(t)) + \int_0^t \mathcal{G}^\ell(\sigma^\ell(s), \varepsilon(\mathbf{u}_\eta^\ell(s)), \beta_\theta^\ell(s)) ds, \quad \ell = 1, 2, \quad (88)$$

for all  $\sigma^\ell \in W^{1,p}(0, T; Q^\ell)$  and  $t \in (0, T)$ . For  $\sigma_1^\ell, \sigma_2^\ell \in W^{1,p}(0, T; Q^\ell)$  we use (35) and (88) to obtain for all  $t \in (0, T)$

$$\|\Lambda_{\eta,\theta}^\ell \sigma_1^\ell(t) - \Lambda_{\eta,\theta}^\ell \sigma_2^\ell(t)\|_Q \leq L_{\mathcal{G}^\ell} \int_0^t \|\sigma_1^\ell(s) - \sigma_2^\ell(s)\|_Q, \quad \ell = 1, 2. \quad (89)$$

It follows from this inequality that for  $n$  large enough, a power  $(\Lambda_{\eta,\theta}^\ell)^n$  is a contraction on the Banach space  $W^{1,p}(0, T; Q^\ell)$  and, therefore, there exists a unique element  $\sigma^\ell \in W^{1,p}(0, T; Q^\ell)$  such that  $\Lambda_{\eta,\theta}^\ell \sigma^\ell = \sigma^\ell$ . Moreover,  $\sigma$  is the unique solution to Problem  $\mathcal{PV}_{\eta,\theta}$  and, when using (86), the regularity of  $\mathbf{u}_\eta, \beta_\theta$  and the properties of the operators  $\mathcal{B}^\ell$  and  $\mathcal{G}^\ell$ , it follows that  $\sigma_i \in W^{1,p}(0, T; Q)$ . Consider now  $(\eta_1, \theta_1), (\eta_2, \theta_2) \in W^{1,p}(0, T; Q \times E_0)$  and, for  $i = 1, 2$ , denote  $\mathbf{u}_{\eta_i} = \mathbf{u}_i, \sigma_{\eta_i} = \sigma_i, \beta_{\theta_i} = \beta_i, \varphi_{\theta_i} = \varphi_i$ . We have

$$\sigma_i^\ell(t) = \mathcal{B}^\ell \varepsilon(\mathbf{u}_i^\ell(t)) + \int_0^t \mathcal{G}^\ell(\sigma_i^\ell(s), \varepsilon(\mathbf{u}_i^\ell(s)), \beta_i^\ell(s)) ds, \quad \ell = 1, 2, \quad \forall t \in (0, T), \quad (90)$$

and, using the properties (35) and (36) of  $\mathcal{G}^\ell$  and  $\mathcal{B}^\ell$ , we find

$$\begin{aligned} \|\sigma_1(t) - \sigma_2(t)\|_Q^2 &\leq C(\|\mathbf{u}_1(t) - \mathbf{u}_2(t)\|_V^2 + \int_0^t \|\sigma_1(s) - \sigma_2(s)\|_V^2 ds \\ &+ \int_0^t \|\mathbf{u}_1(s) - \mathbf{u}_2(s)\|_V^2 ds + \int_0^t \|\beta_1(s) - \beta_2(s)\|_{E_0}^2 ds), \quad \forall t \in (0, T). \end{aligned} \quad (91)$$

We use a Gronwall argument in the obtained inequality we deduced in (87), which concludes the proof of Lemma 4.4 Finally, as a consequence of these results and using the properties of the operator  $\mathcal{G}^\ell$ , the operator  $\mathcal{E}^\ell$ , the functional  $\mathcal{S}^\ell$  and the function for  $t \in [0, T]$ , we consider the element

$$\Lambda(\eta, \theta)(t) = (\Lambda^1(\eta, \theta)(t), \Lambda^2(\eta, \theta)(t)) \in Q \times E_0 \quad (92)$$

defined by the equations

$$\begin{aligned} (\Lambda^1(\eta, \theta)(t), \mathbf{v})_Q &= \sum_{\ell=1}^2 ((\mathcal{E}^\ell)^* \nabla \varphi_\eta^\ell(t) \varepsilon(\mathbf{v}^\ell))_{\mathcal{H}^\ell} + \\ &\sum_{\ell=1}^2 \left( \int_0^t \mathcal{G}^\ell(\boldsymbol{\sigma}_{\eta, \theta}^\ell(s), \varepsilon(\mathbf{u}_\eta^\ell(s)), \beta_\theta^\ell(s)) ds, \varepsilon(\mathbf{v}^\ell) \right)_Q + j_1(\mathbf{u}_\eta, \mathbf{v}) \quad \forall \mathbf{v} \in V, \end{aligned} \tag{93}$$

$$\Lambda^2(\eta, \theta)(t) = (\mathbf{S}^1(\boldsymbol{\sigma}_{\eta, \theta}^1(t), \varepsilon(\mathbf{u}_\eta^1(t)), \beta_\theta^1(t)), \mathbf{S}^2(\boldsymbol{\sigma}_{\eta, \theta}^2(t), \varepsilon(\mathbf{u}_\eta^2(t)), \beta_\theta^2(t))). \tag{94}$$

Here, for every  $(\eta, \theta) \in W^{1,p}(0, T; Q \times E_0)$  the element  $\Lambda(\eta, \theta) \in W^{1,p}(0, T; Q \times E_0)$ .  $\mathbf{u}_\eta$ ,  $\varphi_\theta$ ,  $\beta_\eta$  and  $\sigma_{\eta, \theta}$ , represent the displacement field, the potential field, the damage field and the stress field obtained in Lemmas 4.1, 4.2, 4.3, and 4.4.

**Lemma 4.5** *The mapping  $\Lambda$  has a unique fixed point  $(\eta^*, \theta^*) \in W^{1,p}(0, T; Q \times L^2(\Omega))$ .*

*Proof.* Let  $t \in (0, T)$  and  $(\eta_1, \theta_1), (\eta_2, \theta_2) \in W^{1,p}(0, T; Q \times E_0)$ . We use the notation  $\mathbf{u}_{\eta_i} = \mathbf{u}_i$ ,  $\dot{\mathbf{u}}_{\eta_i} = \dot{\mathbf{u}}_i$ ,  $\varphi_{\eta_i} = \varphi_i$  and  $\boldsymbol{\sigma}_{\eta_i, \theta_i} = \boldsymbol{\sigma}_i$  for  $i = 1, 2$ . Let us start by using (32), hypotheses, (35), (37) and (40) we have

$$\begin{aligned} \|\Lambda^1(\eta_1, \theta_1)(t) - \Lambda^1(\eta_2, \theta_2)(t)\|_Q^2 &\leq \sum_{\ell=1}^2 \|(\mathcal{E}^\ell)^* \nabla \varphi_1^\ell(t) - (\mathcal{E}^\ell)^* \nabla \varphi_2^\ell(t)\|_{Q^\ell}^2 \\ &+ \sum_{\ell=1}^2 \int_0^t \|\mathcal{G}^\ell(\boldsymbol{\sigma}_1^\ell(s), \varepsilon(\mathbf{u}_1^\ell(s)), \beta_1^\ell(s)) - \mathcal{G}^\ell(\boldsymbol{\sigma}_2^\ell(s), \varepsilon(\mathbf{u}_2^\ell(s)), \beta_2^\ell(s))\|_{\mathcal{H}^\ell}^2 ds \\ &\quad + C \|p_\nu([\mathbf{u}_{1\nu}(t)]([\mathbf{u}_{1\nu}(t)]) - p_\nu([\mathbf{u}_{2\nu}(t)]([\mathbf{u}_{2\nu}(t)]))\|_{L^2(\Gamma_3)}^2 \\ &\quad + C \|p_\tau([\mathbf{u}_{1\tau}(t)]([\mathbf{u}_{1\tau}(t)]) - p_\tau([\mathbf{u}_{2\tau}(t)]([\mathbf{u}_{2\tau}(t)]))\|_{L^2(\Gamma_3)}^2 \\ &\leq C \left( \|\varphi_1(t) - \varphi_2(t)\|_Q^2 + \int_0^t \|\mathbf{u}_1(s) - \mathbf{u}_2(s)\|_{\mathbf{V}}^2 ds \right. \\ &\left. + \int_0^t \|\boldsymbol{\sigma}_1(s) - \boldsymbol{\sigma}_2(s)\|_Q^2 ds + \int_0^t \|\beta_1(s) - \beta_2(s)\|_{E_0}^2 ds + \|\mathbf{u}_1(t) - \mathbf{u}_2(t)\|_{\mathbf{V}}^2 \right). \end{aligned} \tag{95}$$

We use estimates (81), (87) to obtain

$$\begin{aligned} \|\Lambda^1(\eta_1, \theta_1)(t) - \Lambda^1(\eta_2, \theta_2)(t)\|_Q^2 &\leq C \left( \|\mathbf{u}_1(t) - \mathbf{u}_2(t)\|_{\mathbf{V}}^2 \right. \\ &\left. + \int_0^t \|\mathbf{u}_1(s) - \mathbf{u}_2(s)\|_{\mathbf{V}}^2 ds + \int_0^t \|\beta_1(s) - \beta_2(s)\|_{E_0}^2 ds \right). \end{aligned} \tag{96}$$

By similar arguments, from (94), (87) and (38) we obtain

$$\begin{aligned} \|\Lambda^2(\eta_1, \theta_1)(t) - \Lambda^2(\eta_2, \theta_2)(t)\|_Q^2 &\leq C \left( \|\mathbf{u}_1(t) - \mathbf{u}_2(t)\|_{\mathbf{V}}^2 \right. \\ &\left. + \int_0^t \|\mathbf{u}_1(s) - \mathbf{u}_2(s)\|_{\mathbf{V}}^2 ds + \|\beta_1(t) - \beta_2(t)\|_{E_0}^2 + \int_0^t \|\beta_1(s) - \beta_2(s)\|_{E_0}^2 ds \right). \end{aligned} \tag{97}$$

Also, since

$$\mathbf{u}_i^\ell(t) = \int_0^t \mathbf{v}_i^\ell(s) ds + \mathbf{u}_0^\ell, \quad t \in [0, T], \quad \ell = 1, 2,$$

we have

$$\|\mathbf{u}_1(t) - \mathbf{u}_2(t)\|_{\mathbf{V}} \leq \int_0^t \|\mathbf{v}_1(s) - \mathbf{v}_2(s)\|_{\mathbf{V}} ds,$$

which implies

$$\|\mathbf{u}_1(t) - \mathbf{u}_2(t)\|_{\mathbf{V}}^2 + \int_0^t \|\mathbf{u}_1(s) - \mathbf{u}_2(s)\|_{\mathbf{V}}^2 ds \leq c \int_0^t \|\mathbf{v}_1(s) - \mathbf{v}_2(s)\|_{\mathbf{V}}^2 ds. \tag{98}$$

Therefore,

$$\begin{aligned} \|\Lambda(\eta_1, \theta_1)(t) - \Lambda(\eta_2, \theta_2)(t)\|_{\mathcal{Q} \times \mathbb{E}_0}^2 &\leq C \left( \|\mathbf{u}_1(t) - \mathbf{u}_2(t)\|_{\mathbf{V}}^2 + \right. \\ &\left. \int_0^t \|\mathbf{u}_1(s) - \mathbf{u}_2(s)\|_{\mathbf{V}}^2 ds + \|\beta_1(t) - \beta_2(t)\|_{\mathbb{E}_0}^2 + \int_0^t \|\beta_1(s) - \beta_2(s)\|_{\mathbb{E}_0}^2 ds \right). \end{aligned} \tag{99}$$

Moreover, from (70) we obtain

$$\begin{aligned} (\dot{\mathbf{v}}_1 - \dot{\mathbf{v}}_2, \mathbf{v}_1 - \mathbf{v}_2)_{\mathbf{V}' \times \mathbf{V}} + \sum_{\ell=1}^2 (\mathcal{A}^\ell \varepsilon(\mathbf{v}_1^\ell) - \mathcal{A}^\ell \varepsilon(\mathbf{v}_2^\ell), \varepsilon(\mathbf{v}_1^\ell - \mathbf{v}_2^\ell))_{\mathcal{H}^\ell} \\ + j_2(\mathbf{v}_1, \mathbf{v}_1 - \mathbf{v}_2) - j_2(\mathbf{v}_2, \mathbf{v}_1 - \mathbf{v}_2) + (\eta_1 - \eta_2, \mathbf{v}_1 - \mathbf{v}_2)_{\mathbf{V}' \times \mathbf{V}} = 0. \end{aligned} \tag{100}$$

We use (39) (51) to deduce that

$$j_2(\mathbf{v}_1, \mathbf{v}_1 - \mathbf{v}_2) - j_2(\mathbf{v}_2, \mathbf{v}_1 - \mathbf{v}_2) \geq 0. \tag{101}$$

It follows from (100) and (101) that

$$\begin{aligned} (\dot{\mathbf{v}}_1 - \dot{\mathbf{v}}_2, \mathbf{v}_1 - \mathbf{v}_2)_{\mathbf{V}' \times \mathbf{V}} + \sum_{\ell=1}^2 (\mathcal{A}^\ell \varepsilon(\mathbf{v}_1^\ell) - \mathcal{A}^\ell \varepsilon(\mathbf{v}_2^\ell), \varepsilon(\mathbf{v}_1^\ell - \mathbf{v}_2^\ell))_{\mathcal{H}^\ell} \\ \leq -(\eta_1 - \eta_2, \mathbf{v}_1 - \mathbf{v}_2)_{\mathbf{V}' \times \mathbf{V}}. \end{aligned} \tag{102}$$

We integrate this equality with respect to time, use the initial conditions  $\mathbf{v}_1(0) = \mathbf{v}_2(0) = \mathbf{v}_0$  and condition (33) to find

$$\begin{aligned} \min(m_{\mathcal{A}^1}, m_{\mathcal{A}^2}) \int_0^t \|\mathbf{v}_1(s) - \mathbf{v}_2(s)\|_{\mathbf{V}}^2 ds \leq \\ - \int_0^t (\eta_1(s) - \eta_2(s), \mathbf{v}_1(s) - \mathbf{v}_2(s))_{\mathbf{V}' \times \mathbf{V}} ds \end{aligned}$$

for all  $t \in [0, T]$ . Then, using the inequality  $2ab \leq \frac{a^2}{m} + mb^2$ , we obtain

$$\int_0^t \|\mathbf{v}_1(s) - \mathbf{v}_2(s)\|_{\mathbf{V}}^2 ds \leq C \int_0^t \|\eta_1(s) - \eta_2(s)\|_{\mathbf{V}'}^2 ds \quad \forall t \in [0, T]. \tag{103}$$

Form (84), we deduce that

$$(\dot{\beta}_1 - \dot{\beta}_2, \beta_1 - \beta_2)_{\mathbb{E}_0} + a(\beta_1 - \beta_2, \beta_1 - \beta_2) \leq (\theta_1 - \theta_1, \beta_1 - \beta_2)_{\mathbb{E}_0} \quad \forall t \in [0, T].$$

Integrating the previous inequality with respect to time, using the initial conditions  $\beta_1(0) = \beta_2(0) = \beta_0$  and inequality  $a(\beta_1 - \beta_2, \beta_1 - \beta_2) \geq 0$ , we find

$$\frac{1}{2} \|\beta_1(s) - \beta_2(s)\|_{E_0}^2 ds \leq \int_0^t (\theta_1(s) - \theta_2(s), \beta_1(s) - \beta_2(s))_{E_0} ds, \tag{104}$$

which implies

$$\|\beta_1(s) - \beta_2(s)\|_{E_0}^2 ds \leq \int_0^t \|\theta_1(s) - \theta_2(s)\|_{E_0}^2 ds + \int_0^t \|\beta_1(s) - \beta_2(s)\|_{L^2(\Omega)}^2 ds.$$

This inequality, combined with Gronwall’s inequality, leads to

$$\|\beta_1(s) - \beta_2(s)\|_{E_0}^2 ds \leq C \int_0^t \|\theta_1(s) - \theta_2(s)\|_{E_0}^2 ds \quad \forall [0, T]. \tag{105}$$

Form the previous inequality and estimates (103), (105) and (99) it follows now that

$$\|\Lambda(\eta_1, \theta_1)(t) - \Lambda(\eta_2, \theta_2)(t)\|_{Q \times E_0}^2 \leq C \int_0^t \|(\eta_1, \theta_1)(s) - (\eta_2, \theta_2)(s)\|_{Q \times E_0}^2 ds.$$

Reiterating this inequality  $n$  times we obtain

$$\|\Lambda^n(\eta_1, \theta_1) - \Lambda^n(\eta_2, \theta_2)\|_{W^{1,p}(0,T;Q \times E_0)}^2 \leq \frac{C^n T^n}{n!} \|(\eta_1, \theta_1) - (\eta_2, \theta_2)\|_{W^{1,p}(0,T;Q \times E_0)}^2.$$

Thus, for  $n$  sufficiently large,  $\Lambda^n$  is a contraction on  $W^{1,p}(0, T; Q \times E_0)$ , and so  $\Lambda$  has a unique fixed point in this Banach space.

Now, we have all the ingredients to prove Theorem 4.1.

**Existence.** Let  $(\eta^*, \theta^*) \in W^{1,p}(0, T; Q \times E_0)$  be the fixed point of  $\Lambda$  defined by (92)-(94), and denote

$$\mathbf{u}_* = \mathbf{u}_{\eta^*}, \quad \varphi_* = \varphi_{\eta^*}, \quad \beta_* = \beta_{\theta^*}, \tag{106}$$

$$\boldsymbol{\sigma}_*^\ell = \mathcal{A}^\ell \boldsymbol{\varepsilon}(\dot{\mathbf{u}}_*^\ell) + (\mathcal{E}^\ell)^* \nabla \varphi_*^\ell + \boldsymbol{\sigma}_{\eta^* \theta^*}^\ell, \quad \ell = 1, 2, \tag{107}$$

$$\mathbf{D}_*^\ell = \mathcal{E}^\ell \boldsymbol{\varepsilon}(\mathbf{u}_*^\ell) - \mathcal{B}^\ell \nabla \varphi_*^\ell, \quad \ell = 1, 2. \tag{108}$$

We prove that  $\{\mathbf{u}_*, \boldsymbol{\sigma}_*, \varphi_*, \beta_*, \mathbf{D}_*\}$  satisfies (57)–(62) and the regularities(64)–(67). Indeed, we write (70) for  $\eta^* = \eta$  and use (106) to find

$$\begin{aligned} & (\ddot{\mathbf{u}}_*(t), \mathbf{v})_{\mathbf{V}' \times \mathbf{V}} + \sum_{\ell=1}^2 (\mathcal{A}^\ell \boldsymbol{\varepsilon}(\dot{\mathbf{u}}_*^\ell(t)), \boldsymbol{\varepsilon}(\mathbf{v}^\ell))_{\mathcal{H}^\ell} + j_2(\dot{\mathbf{u}}_*(t), \mathbf{v}) \\ & + (\eta^*(t), \mathbf{v})_{\mathbf{V}' \times \mathbf{V}} = (\mathbf{f}(t), \mathbf{v})_{\mathbf{V}' \times \mathbf{V}} \quad \forall \mathbf{v} \in \mathbf{V}, a.e. t \in [0, T]. \end{aligned} \tag{109}$$

For the equalities  $\Lambda^1(\eta^*, \theta^*) = \eta^*$  and  $\Lambda^2(\eta^*, \theta^*) = \theta^*$  it follows that

$$\begin{aligned} (\eta^*(t), \mathbf{v})_{Q \times \mathbf{V}} = & \sum_{\ell=1}^2 (\mathcal{E}^\ell \boldsymbol{\varepsilon}(\mathbf{u}^\ell(t)), \boldsymbol{\varepsilon}(\mathbf{v}^\ell))_Q + \sum_{\ell=1}^2 \left( \int_0^t \mathcal{G}^\ell(\boldsymbol{\sigma}^\ell(s) - \mathcal{A}^\ell \boldsymbol{\varepsilon}(\dot{\mathbf{u}}^\ell(s)) \right. \\ & \left. - \mathcal{E}^\ell \nabla \varphi^\ell(s), \boldsymbol{\varepsilon}(\mathbf{u}^\ell(s)), \beta(s)) ds, \boldsymbol{\varepsilon}(\mathbf{v}^\ell) \right)_Q + j_1(\mathbf{u}_*(t), \mathbf{v}) \end{aligned} \tag{110}$$

$$\theta^*(t) = \sum_{\ell=1}^2 (\mathcal{S}^\ell(\boldsymbol{\sigma}^\ell(t) - \mathcal{A}^\ell \boldsymbol{\varepsilon}(\dot{\mathbf{u}}^\ell(t)) - (\mathcal{E}^\ell)^* \nabla \varphi^\ell(t), \boldsymbol{\varepsilon}(\mathbf{u}^\ell(t)), \beta^\ell(t)). \quad (111)$$

We now substitute (110) in (109) to obtain

$$\begin{aligned} & (\ddot{\mathbf{u}}_*(t), v)_{\mathbf{V}' \times \mathbf{V}} + \sum_{\ell=1}^2 (\mathcal{A}^\ell \boldsymbol{\varepsilon}(\dot{\mathbf{u}}_*^\ell(t)), \boldsymbol{\varepsilon}(\mathbf{v}^\ell))_{\mathcal{H}^\ell} + j_2(\dot{\mathbf{u}}_*(t), v) \\ & + \sum_{\ell=1}^2 (\mathcal{B}^\ell \boldsymbol{\varepsilon}(\mathbf{u}_*^\ell(t)), \boldsymbol{\varepsilon}(\mathbf{v}^\ell))_{\mathcal{H}^\ell} + \sum_{\ell=1}^2 ((\mathcal{E}^\ell)^* \nabla \varphi_*^\ell, \boldsymbol{\varepsilon}(\mathbf{v}^\ell))_{\mathcal{H}^\ell} \\ & + \sum_{\ell=1}^2 \left( \int_0^t \mathcal{G}^\ell(\boldsymbol{\sigma}_*^\ell(s) - \mathcal{A}^\ell \boldsymbol{\varepsilon}(\dot{\mathbf{u}}_*^\ell(s)) - (\mathcal{E}^\ell)^* \nabla \varphi_*^\ell(s), \boldsymbol{\varepsilon}(\mathbf{u}_*^\ell(s)), \beta_*^\ell(s)) ds, \boldsymbol{\varepsilon}(\mathbf{v}^\ell) \right)_{\mathcal{H}^\ell} \\ & + j_1(\mathbf{u}_*(t), v) = (\mathbf{f}(t), v)_{\mathbf{V}' \times \mathbf{V}}, \quad \forall v \in \mathbf{V}, \end{aligned} \quad (112)$$

and we substitute (111) in (84) to have

$$\begin{aligned} \beta_*(t) \in K, \quad & \sum_{\ell=1}^2 (\dot{\beta}_*^\ell(t), \xi^\ell - \beta_*^\ell(t))_{L^2(\Omega^\ell)} + a(\beta(t), \xi - \beta(t)) \geq \\ & \sum_{\ell=1}^2 \left( \phi^\ell(\boldsymbol{\sigma}_*^\ell(t) - \mathcal{A}^\ell \boldsymbol{\varepsilon}(\dot{\mathbf{u}}_*^\ell(t)) - (\mathcal{E}^\ell)^* \nabla \varphi^\ell(t), \boldsymbol{\varepsilon}(\mathbf{u}_*^\ell(t)), \beta_*^\ell(t)), \xi^\ell - \beta_*^\ell(t) \right)_{L^2(\Omega^\ell)}, \\ & \forall \xi \in K, \text{ a.e. } t \in [0, T]. \end{aligned} \quad (113)$$

We write now (80) for  $\eta = \eta^*$  and use (106) to see that

$$\begin{aligned} & \sum_{\ell=1}^2 (\mathcal{B}^\ell \nabla \varphi_*^\ell(t), \nabla \xi^\ell)_{H^\ell} - \sum_{\ell=1}^2 (\mathcal{E}^\ell \boldsymbol{\varepsilon}(\mathbf{u}_*^\ell(t)), \nabla \xi^\ell)_{H^\ell} = (q(t), \xi)_W, \\ & \forall \xi \in W, \text{ a.e. } t \in [0, T]. \end{aligned} \quad (114)$$

The relations (106)- (108), (112), (113), and (114) allow us to conclude now that  $\{\mathbf{u}_*, \boldsymbol{\sigma}_*, \varphi_*, \beta_*, \mathbf{D}_*\}$  satisfies (57). Next, (62) and the regularities (64), (65), (68) follow from Lemmas 4.1, 4.2 and 4.3. Since  $\mathbf{u}_*$  and  $\varphi_*$  satisfy (64) and (68), it follows from Lemma 4.4 and (107) that

$$\boldsymbol{\sigma}_* \in L^2(0, T; \mathcal{H}). \quad (115)$$

We choose  $v = (v^1, v^2)$  with  $v^\ell = \omega^\ell \in D(\Omega^\ell)^d$  and  $v^{3-\ell} = 0$  in (112) and by (106) and (53)

$$\rho^\ell \ddot{\mathbf{u}}_*^\ell = \text{Div } \boldsymbol{\sigma}_*^\ell + \mathbf{f}_0^\ell, \text{ a.e. } t \in [0, T], \quad \ell = 1, 2.$$

Also, by (47), (64) and (115) we have

$$(\text{Div } \boldsymbol{\sigma}_*^1, \text{Div } \boldsymbol{\sigma}_*^2) \in L^2(0, T; \mathbf{V}').$$

Let  $t_1, t_2 \in [0, T]$ , by (26), (36), (37) and (108), we deduce that

$$\|\mathbf{D}_*(t_1) - \mathbf{D}_*(t_2)\|_H \leq C (\|\varphi_*(t_1) - \varphi_*(t_2)\|_W + \|\mathbf{u}_*(t_1) - \mathbf{u}_*(t_2)\|_{\mathbf{V}}).$$

The regularity of  $\mathbf{u}_*$  and  $\varphi_*$  given by (64) and (65) implies

$$\mathbf{D}_* \in C(0, T; H). \quad (116)$$

We choose  $\phi = (\phi^1, \phi^2)$  with  $\phi^\ell \in D(\Omega^\ell)^d$  and  $\phi^{3-\ell} = 0$  in (114), and using (54), (108) we find

$$\operatorname{div} \mathbf{D}_*^\ell(t) = q_0^\ell(t) \quad \forall t \in [0, T], \quad \ell = 1, 2,$$

and, by (48), (116), we obtain

$$\mathbf{D}_* \in C(0, T; \mathcal{W}).$$

Finally, we conclude that the weak solution  $\{\mathbf{u}_*, \boldsymbol{\sigma}_*, \varphi_*, \beta_*, \mathbf{D}_*\}$  of the piezoelectric contact Problem **PV** has the regularities (64)–(67), which concludes the existence part of Theorem 4.1.

**Uniqueness.** The uniqueness of the solution is a consequence of the uniqueness of the fixed point of the operator  $\Lambda$  defined by (93)–(94) and the unique solvability of the Problems  $\mathcal{PV}_\eta^1$ ,  $\mathcal{PV}_\eta^2$ ,  $\mathcal{PV}_\theta$  and  $\mathcal{PV}_{\eta,\theta}$ .

## Conclusion

We presented a model for the dynamic process of frictional contact between two elasto-viscoplastic piezoelectric bodies with damage response. The contact was modeled with a normal compliance and a normal damped. The existence of the unique weak solution for the problem was established by using arguments from the parabolic inequalities, differential equations and fixed-point arguments.

## References

- [1] R. C. Batra and J.S. Yang. Saint Venant's principle in linear piezoelectricity. *Journal of Elasticity* **38** (1995) 209–218.
- [2] S. Barna. Existence results for hemivariational inequality involving  $p(x)$ -Laplacian. *Opuscula Math. Journal of Elasticity* **32** (2012) 439–454.
- [3] P. Bisenga, F. Lebon and F. Maceri. The unilateral frictional contact of a piezoelectric body with a rigid support, in *Contact Mechanics. J.A.C. Martins and Manuel D.P. Monteiro Marques (Eds)*, Dordrecht, 2002, 347–354.
- [4] W. Han and M. Sofonea. Evolutionary variational inequalities arising in viscoelastic contact problems. *SIAM Journal of Numerical Analysis* **38** (2000) 556–579.
- [5] W. Han and M. Sofonea. *Quasistatic Contact Problems in Viscoelasticity and Viscoplasticity*, Studies in Advanced Mathematics 30, American Mathematical Society, Providence, RI - Intl. Press, Sommerville, MA 2002.
- [6] M. Rochdi, M. Shillor and M. Sofonea. Quasistatic viscoelastic contact with normal compliance and friction. *Journal of Elasticity* **51** (1982) 105–126.
- [7] M. Frémond and B. Nedjar. Damage in concrete: the unilateral phenomenon. *Nuclear Engng. Design.* **156** (1995) 323–335.
- [8] M. Frémond and B. Nedja. Damage, Gradient of Damage and Principle of Virtual Work. *Int. J. Solids Structures* **33** (8) (1996) 1083–1103.

- [9] J. R. Fernández-García, M. Sofonea and J. M. Viano. A Frictionless Contact Problem for Elastic-Viscoplastic Materials with Normal Compliance. *Numerische Mathematik* **90** (2002) 689–719.
- [10] T. Ikeda. *Fundamentals of Piezoelectricity*. Oxford University Press, 1990.
- [11] Z. Lerguet, M. Shillor and M. Sofonea. A frictional contact problem for an electro-viscoelastic body. *Electronic Journal of Differential Equations* **170** (2007) 1–16.
- [12] R. D. Mindlin. Polarisation gradient in elastic dielectrics. *Int. J. Solids Structures* **4** (1968) 637–663.
- [13] R. D. Mindlin. Elasticity piezoelectricity and crystal lattice dynamics. *Journal of Elasticity* **4** (1972) 217–280.
- [14] F. Maceri and P. Bisegna. The unilateral frictionless contact of a piezoelectric body with a rigid support. *Math. Comp. Modelling* **28** (1998) 19–28.
- [15] V. Z. Patron and B. A. Kudryavtsev. *Electromagnetoelasticity, Piezoelectrics and Electrically Conductive Solids*. Gordon Breach, London, 1988.
- [16] M. Selmani and L. Selmani. Analysis of frictionless contact problem for elastic-viscoplastic materials. *Nonlinear Analysis, Modelling and control* **17** (1) (2012) 77–99.
- [17] M. Shillor, M. Sofonea and J. J. Telega. *Models and Analysis of Quasistatic Contact*. Lecture Notes in Physics 655, Springer-Berlin, 2004.
- [18] M. Sofonea, W. Han and M. Shillor. *Analysis and Approximation of Contact Problems with Adhesion or Damage*. Pure and Applied Mathematics Vol. 276, Chapman, Hall/CRC Press, New York, 2006.
- [19] M. Sofonea and El H. Essoufi. A Piezoelectric contact problem with slip dependent coefficient of friction. *Mathematical Modelling and Analysis* **9** (2004) 229–242.
- [20] M. Sofonea and El H. Essoufi. Quasistatic frictional contact of a viscoelastic piezoelectric body. *Adv. Math. Sci. Appl.* **14** (2004) 613–631.
- [21] N. Stromberg, L. Johansson and A. Klarbring. Derivation and analysis of a generalized standard model for contact friction and wear. *Int. J. Solids Structures* **33** (1996) 1817–1836.
- [22] L. Zhor, Z. Zellagui, H. Benseridi and S. Drabla. Variational analysis of an electro-viscoelastic contact problem with friction. *J. Assoc. Arab Univ. Basic Appl. Sci.* **14** (2013) 93–100.



# Trajectory Tracking of Coordinated Multi-Robot Systems using Nonlinear Model Predictive Control

H. Purnawan, S. Subchan \*, D. Adzkiya and T. Asfihani

*Control and Optimization Group, Modeling and Simulation Laboratory,  
Department of Mathematics, Institut Teknologi Sepuluh Nopember, Surabaya, Indonesia*

Received: November 10, 2020; Revised: June 3, 2021

**Abstract:** This paper proposes a centralized and decentralized nonlinear model predictive control (NMPC) for multiple robots in the trajectory tracking problem with collision avoidance. The kinematic model of mobile robot is employed to implement these concepts. The path of each robot is constructed such that there exist some intersections between some paths of the robots. Additionally, the initial conditions and parameters of the model are taken so that the robots will collide on the intersections of their paths. Based on the simulation results, both centralized and decentralized schemes can avoid collision between one robot and another one by satisfying the inequality constraints. All solutions of the optimization problems in both schemes are feasible as well, so this indicates that local minimum solutions are found. According to the simulations, the decentralized scheme is better than the centralized scheme in terms of the computational complexity and error tracking.

**Keywords:** *nonlinear optimization; multiple robots dynamics; nonlinear model predictive control; centralized and decentralized schemes.*

**Mathematics Subject Classification (2010):** 65K10, 70E60, 90B15, 49M37.

## 1 Introduction

During the last years, the research interests in robotics area have grown exponentially from some publications (refer to [1–3]), but are not limited to those. Nowadays, to employ a robot for many kinds of tasks is very common in various fields such as agriculture, logistics, and even service for some of Covid-19 patients in hospital [4–6]. In those applications, it is expected that the robot can be navigated in different situations and environments [7]. The strategy can be done by controlling its position, so that it can

---

\* Corresponding author: <mailto:subchan@matematika.its.ac.id>

move from its current position to the final destination. This concept is usually called the point stabilization control. When the robot has to follow the given path, it is commonly known as the trajectory tracking.

To address many ways in controlling the robot, several techniques have been implemented such as the PID controller [8], sliding mode control [3], sliding PID [9] and others. Two mentioned methods specifically do not use multivariable controls, whereas most robots are a system with multivariable inputs and states usually called the multi-input-multi-output (MIMO) type. Especially for these cases, we have to design many controllers for each input and state by assuming a decoupling control. Through this approach, the system can be treated as the single-input-single-output (SISO) type, so a single loop controller can be developed as well [10].

One of the controllers having a capability to deal with the MIMO systems is a model predictive control (MPC). A version of the MPC for nonlinear systems is a nonlinear model predictive control (NMPC). Because of its ability to handle the limitation of a system, this controller becomes the most popular control method in some sectors such as chemical processes [11], autonomous vehicles [12], and others. As time goes by, the NMPC was also implemented for multi-object systems. Some approaches were proposed, namely, centralized [13], decentralized [14,15], and distributed [13]. Based on the previous study, in this paper, we implement the centralized and decentralized scheme-based NMPC in trajectory tracking, where each path of the robots has some intersections. The aim is to examine our proposed method by defining collision avoidance constraint in the optimization problem of NMPC.

This paper is constructed as follows. The kinematic model of nonholonomic robots in terms of a MIMO system is defined in Section 2. Next, Section 3 explains the centralized and decentralized scheme-based NMPC for multi-agent systems. In this section, the collision avoidance constraint is defined to avoid collision among the robots. Then, Section 4 contains some discussions based on our simulation results. Lastly, Section 5 is the conclusion and development of the future research.

## 2 Kinematic Model of Mobile Robot

Kinematics is the fundamental study that learns about how an object can move from one position to other positions without considering the forces working on the object. In order to design mobile robots for some purpose, it is essential to understand the mechanical behavior of a robot [16]. The behavior of a mobile robot can be expressed in the following mathematical model [16]:

$$\begin{aligned}\dot{x} &= v \cos \psi, \\ \dot{y} &= v \sin \psi, \\ \dot{\psi} &= \omega,\end{aligned}\tag{1}$$

where  $(x, y)$  represents the position of a mobile robot in the X-axis and Y-axis, respectively,  $\psi$  is the heading angle of a mobile robot,  $v$  and  $\omega$ , respectively, denote the linear and angular velocity.

Model (1) is a nonlinear system and it can be written in a state space form as follows:

$$\dot{\chi} = \mathbf{f}(\chi, \mathbf{u}),\tag{2}$$

where  $\boldsymbol{\chi} = [x, y, \psi]^T$  denotes the state variables and  $\mathbf{u} = [v, \omega]^T$  indicates the input or control variables for the system. Equation (2) is a continuous-time system, so it can be converted into a discrete-time system using a discretization method. Based on the Euler approach, equation (2) is stated as

$$\boldsymbol{\chi}(k+1) = \boldsymbol{\chi}(k) + T_s \mathbf{f}(\boldsymbol{\chi}(k), \mathbf{u}(k)), \tag{3}$$

where  $T_s$  is the sampling time used to transform the continuous-time system into a discrete-time system.

### 3 Nonlinear Model Predictive Control

The NMPC is an optimization-based method for nonlinear systems [17]. Generally, the difference between the MPC and the NMPC lies in their systems. However, it is not limited to those, since the MPC can be implemented on the nonlinear systems by using the linearization method around operating points (refer to [18]). The idea of the NMPC is to predict the future system behavior by utilizing the model (3). The aim of the NMPC is to minimize an objective function subject to its constraints, so it is possible to obtain the optimal inputs along the prediction horizon.

Assuming that the prediction horizon is equal to the control horizon at every discrete-time  $k$ , the optimization formula of the NMPC can be written as follows:

$$V_N(k) = \sum_{i=1}^N \|\mathbf{r}_i(k) - \hat{\mathbf{y}}_i(k)\|_{\mathbf{Q}}^2 + \|\mathbf{u}_{i-1}(k)\|_{\mathbf{R}}^2 \tag{4}$$

subject to

$$\begin{aligned} \boldsymbol{\chi}_{i+1}(k) &= \mathbf{f}_d(\boldsymbol{\chi}_i(k), \mathbf{u}_i(k)), \quad i = 0, 1, \dots, N-1, \\ \hat{\mathbf{y}}_i(k) &= \mathbf{g}(\boldsymbol{\chi}_i(k)), \quad i = 1, 2, \dots, N, \\ \boldsymbol{\chi}_0(k) &= \boldsymbol{\chi}(k), \\ \boldsymbol{\chi}^{min} &\leq \boldsymbol{\chi}_i(k) \leq \boldsymbol{\chi}^{max}, \quad i = 0, 1, \dots, N, \\ \mathbf{u}^{min} &\leq \mathbf{u}_i(k) \leq \mathbf{u}^{max}, \quad i = 0, 1, \dots, N-1, \end{aligned}$$

where  $V_N$  is a quadratic cost function,  $N$  is the prediction horizon,  $\mathbf{Q}$  and  $\mathbf{R}$  are the weighting matrices being positive semi-definite and positive definite, where their sizes are appropriate to the dimension of outputs and inputs,  $\mathbf{r}$  is the reference or desired value,  $\hat{\mathbf{y}}$  is the predicted outputs of the system,  $\boldsymbol{\chi}^{min}$ ,  $\boldsymbol{\chi}^{max}$ ,  $\mathbf{u}^{min}$ ,  $\mathbf{u}^{max}$  are the lower and upper bounds for the states and inputs, respectively, and the notation in (4) is given as follows:

$$\begin{aligned} \|\mathbf{r}_i(k) - \hat{\mathbf{y}}_i(k)\|_{\mathbf{Q}}^2 &= [\mathbf{r}_i(k) - \hat{\mathbf{y}}_i(k)]^T \mathbf{Q} [\mathbf{r}_i(k) - \hat{\mathbf{y}}_i(k)], \\ \|\mathbf{u}_{i-1}(k)\|_{\mathbf{R}}^2 &= (\mathbf{u}_{i-1}(k))^T \mathbf{R} \mathbf{u}_{i-1}(k). \end{aligned}$$

By solving the optimization problem (4), we obtain a sequence of optimal inputs  $\{\mathbf{u}_0^*(k), \mathbf{u}_1^*(k), \dots, \mathbf{u}_{N-1}^*(k)\}$ , but only the first element of the sequence, i.e.,  $\mathbf{u}_0^*(k)$ , is injected to the system.

To implement the NMPC for multi-robot systems, it is important to formulate the constraints appropriately to avoid collision among the agents. The following approach is used to manifest the concept.

Collision avoidance among the robots: to ensure safety during the trajectory execution, it is necessary to formulate the following inequality constraints using the Euclidean distance in optimization problem (4). By considering the discrete system for each prediction window, we define the constraint as follows:

$$\sqrt{(x_i^j(k) - x_i^l(k))^2 + (y_i^j(k) - y_i^l(k))^2} \geq \frac{1}{2}(r_d^j + r_d^l), \quad j \neq l, \\ \forall j, l = 1, 2, \dots, N_r, \quad \forall i = 0, 1, \dots, N, \quad (5)$$

where  $(x_i(k), y_i(k))$  is the position of robots at time  $k$ ,  $r_d$  is the diameter of robots,  $N_r$  represents the number of robots, and the superscript denotes the robot index.

To design the NMPC controller for multiple robots, some schemes that can be utilized are the centralized and decentralized schemes. The explanation about the schemes is discussed in the following subsection.

### 3.1 Centralized NMPC

The centralized scheme is a classical control scheme, where the whole system is controlled by one controller [13]. Since we treat all robots as a single entity, the system can be written as a large-scale system as follows:

$$\bar{\chi}(k+1) = \begin{bmatrix} \mathbf{f}_d^1(\boldsymbol{\chi}^1(k), \mathbf{u}^1(k)) \\ \mathbf{f}_d^2(\boldsymbol{\chi}^2(k), \mathbf{u}^2(k)) \\ \vdots \\ \mathbf{f}_d^{N_r}(\boldsymbol{\chi}^{N_r}(k), \mathbf{u}^{N_r}(k)) \end{bmatrix} = \bar{\mathbf{f}}_d(\bar{\boldsymbol{\chi}}(k), \bar{\mathbf{u}}(k)), \quad (6)$$

where the state and input variables are defined as  $\bar{\boldsymbol{\chi}}(k) = [\boldsymbol{\chi}^1(k), \boldsymbol{\chi}^2(k), \dots, \boldsymbol{\chi}^{N_r}(k)]^T$  and  $\bar{\mathbf{u}}(k) = [\mathbf{u}^1(k), \mathbf{u}^2(k), \dots, \mathbf{u}^{N_r}(k)]^T$ , respectively. These changes also influence the formula of objective function and constraints for our optimization problem. The new objective function and constraints can be stated as

$$\bar{V}_N(k) = \sum_{i=1}^N \|\bar{\mathbf{r}}_i(k) - \bar{\mathbf{y}}_i(k)\|_{\bar{\mathbf{Q}}}^2 + \|\bar{\mathbf{u}}_{i-1}(k)\|_{\bar{\mathbf{R}}}^2 \quad (7)$$

subject to

$$\begin{aligned} \bar{\boldsymbol{\chi}}_{i+1}(k) &= \bar{\mathbf{f}}_d(\bar{\boldsymbol{\chi}}_i(k), \bar{\mathbf{u}}_i(k)), \quad i = 0, 1, \dots, N-1, \\ \bar{\mathbf{y}}_i(k) &= \bar{\mathbf{g}}(\bar{\boldsymbol{\chi}}_i(k)), \quad i = 1, 2, \dots, N, \\ \bar{\boldsymbol{\chi}}_0(k) &= \bar{\boldsymbol{\chi}}(k), \\ \bar{\boldsymbol{\chi}}^{min} &\leq \bar{\boldsymbol{\chi}}_i(k) \leq \bar{\boldsymbol{\chi}}^{max}, \quad i = 0, 1, \dots, N, \\ \bar{\mathbf{u}}^{min} &\leq \bar{\mathbf{u}}_i(k) \leq \bar{\mathbf{u}}^{max}, \quad i = 0, 1, \dots, N-1, \\ \sqrt{(x_i^j(k) - x_i^l(k))^2 + (y_i^j(k) - y_i^l(k))^2} &\geq \frac{1}{2}(r_d^j + r_d^l), \quad j \neq l, \forall j, l = 1, 2, \dots, N_r, \\ &\forall i = 0, 1, \dots, N, \end{aligned}$$

where  $\bar{\mathbf{r}}(k) = [\mathbf{r}^1(k), \dots, \mathbf{r}^{N_r}(k)]^T$ ,  $\bar{\mathbf{y}}(k) = [\mathbf{y}^1(k), \dots, \mathbf{y}^{N_r}(k)]^T$  and the weighting matrices  $\bar{\mathbf{Q}}$  and  $\bar{\mathbf{R}}$  are defined as  $\bar{\mathbf{Q}} = \text{diag}(\mathbf{Q}, \mathbf{Q}, \dots, \mathbf{Q})$  and  $\bar{\mathbf{R}} = \text{diag}(\mathbf{R}, \mathbf{R}, \dots, \mathbf{R})$  with respect to the size of  $\bar{\mathbf{y}}$  and  $\bar{\mathbf{u}}$ , respectively.

At each sampling time, Algorithm 3.1 is used to obtain the optimal input in the case of the centralized NMPC scheme.

**Algorithm 3.1** The Centralized NMPC for Multi-Agent Systems.

- 1: Predict future outputs  $\bar{\mathbf{y}}_i(k)$ ,  $i = 1, 2, \dots, N$ , as a function of future inputs  $\bar{\mathbf{u}}_i(k)$ ,  $i = 0, 1, \dots, N - 1$ , using the current states  $\bar{\mathbf{x}}(k)$ .
- 2: Solve the optimization problem (7) using a *fmincon* MATLAB function by utilizing an anonymous function to obtain the sequence of optimal inputs  $\{\bar{\mathbf{u}}_0(k), \bar{\mathbf{u}}_1(k), \dots, \bar{\mathbf{u}}_{N-1}(k)\}$ .
- 3: Only the first element of the optimal input sequence  $\bar{\mathbf{u}}_0(k)$  is applied to the systems by extracting it into  $\{\mathbf{u}_0^1(k), \mathbf{u}_0^2(k), \dots, \mathbf{u}_0^{N_r}(k)\}$  for each system.
- 4: Save the data and update the current states.
- 5: At time- $k + 1$ , repeat step 1.

The drawback of this scheme is the computational complexity that grows significantly when the number of agents increases, so it is not suitable for the case with too many agents. Next, the alternative scheme will be presented to control multi-agent systems.

### 3.2 Decentralized NMPC

In this architecture, the optimization problem is solved in parallel, i.e., each robot solves the optimization separately [15]. As in (5), to avoid collision among robots, each optimizer needs other robots' future states information. By using communication, this study assumes that all robots can share required information such as the current states and optimal inputs over the prediction horizon in the previous calculation at every sampling time [14]. If the communication is failed, the current and one-step previous states are used by each optimizer to estimate the last input commands of other robots, then it is used to predict other robots' future state information by reduplicating it over the prediction horizon [15]. The illustration of this method can be seen in [13, 15]. In the decentralized control, there are multiple NMPCs for each robot. Algorithm 3.2 shows the process to obtain the sequence of optimal inputs for each agent by using information from other agents.

**Algorithm 3.2** The Decentralized NMPC for Multi-Agent Systems.

- 1: Guess the suitable initial inputs over the prediction horizon to check the inequality constraints (5) for collision avoidance by using current states information from other agents via communication.
- 2: Predict future outputs  $\hat{\mathbf{y}}_i^j(k)$ ,  $i = 1, 2, \dots, N$ , as a function of future inputs  $\mathbf{u}_i^j(k)$ ,  $i = 0, 1, \dots, N - 1$ , using the current states  $\mathbf{x}^j(k)$  for the  $j$ -th agent.
- 3: Solve the optimization problem (4) by adding (5) for every agent using *fmincon* MATLAB by utilizing an anonymous function to obtain a sequence of optimal inputs  $\{\mathbf{u}_0^j(k), \mathbf{u}_1^j(k), \dots, \mathbf{u}_{N-1}^j(k)\}$ .
- 4: Only the first element of the optimal input sequence  $\mathbf{u}_0^j(k)$  is applied to the system of the  $j$ -th agent.
- 5: Save the data and update the current states.

- 6: At time- $k + 1$ , the obtained optimal input over the prediction horizon from (3) and updated current states are needed to check the inequality constraints by other agents via communication.
- 7: Repeat step 2.

Algorithm 3.2 is used by every agent to obtain its optimal inputs. This scheme is more efficient than the centralized one w.r.t both computational time and control design.

#### 4 Simulation Results and Discussion

In this paper, both centralized and decentralized NMPC use the same prediction horizon  $N$  and sampling time  $T_s$ . The weighting matrices in the objective function and simulation time for each robot are given by  $\mathbf{Q} = \begin{bmatrix} 1 & 0 \\ 0 & 1 \end{bmatrix}$ ,  $\mathbf{R} = \begin{bmatrix} 0.5 & 0 \\ 0 & 0.5 \end{bmatrix}$  and  $t_{end} = 400$  s. The initial conditions and references of all simulations are shown in Table 1, the diameter of all robots is assumed 0.3 m and the upper and lower bounds of the inputs are defined as  $v \in [-0.6, 0.6]$  for linear velocity and for angular velocity  $\omega \in [-\frac{\pi}{4}, \frac{\pi}{4}]$ , respectively.

**Table 1:** The initial conditions and references of each robot.

Robot	Initial conditions	References	
		$x_{ref}(t)$	$y_{ref}(t)$
1	$[-2, 3.5, 0]^T$	$-1 + 2 \sin(0.02t)$	$1 + 2 \cos(0.02t)$
2	$[-2, -3.5, 0]^T$	$-1 + 2 \sin(0.02t)$	$-1 - 2 \cos(0.02t)$
3	$[2, 3.5, \pi]^T$	$1 - 2 \sin(0.02t)$	$1 + 2 \cos(0.02t)$
4	$[2, -3.5, \pi]^T$	$1 - 2 \sin(0.02t)$	$-1 - 2 \cos(0.02t)$

All simulations are performed in MATLAB 2019b on a computer with 8GB RAM and a core i5-1035G4. For the first running simulation, we use  $T_s = 0.5$  s and  $N = 8$  (equal to 4 s) with the initial conditions as in Table 1. The simulation result of the centralized scheme to follow the specified references can be seen in Figure 1 while for the decentralized scheme it is shown in Figure 2.

Figures 1 and 2 show all robots can follow their references using both centralized and decentralized schemes from the initial conditions of each robot. The tracking errors of each robot are caused by avoiding the collision among them, so these results are appropriate to our desire. From the figures, we can see the decentralized scheme is better than the centralized one if it is seen from the tracking error between their trajectories and references. The intersections among references are constructed to verify whether the proposed approach through the algorithms can work perfectly.

To ensure that the inequality constraints for collision avoidance are satisfied by each robot, we show the distance between one robot and other robots. The results of our simulation about this idea are presented in Figures 3 and 4 for each proposed scheme.

In Figures 3 and 4, the requested minimum distance so that the collision does not occur is a half of the total diameter of each robot, i.e., 0.3 m. The symbol of  $D_{jl}(k)$  represents the distance between the  $i$ -th and  $j$ -th robot at time  $k$  computed by the following formula:

$$D_{jl}(k) = \sqrt{(x^j(k) - x^l(k))^2 + (y^j(k) - y^l(k))^2}, \quad j \neq l, \quad j, l = 1, 2, 3, 4.$$

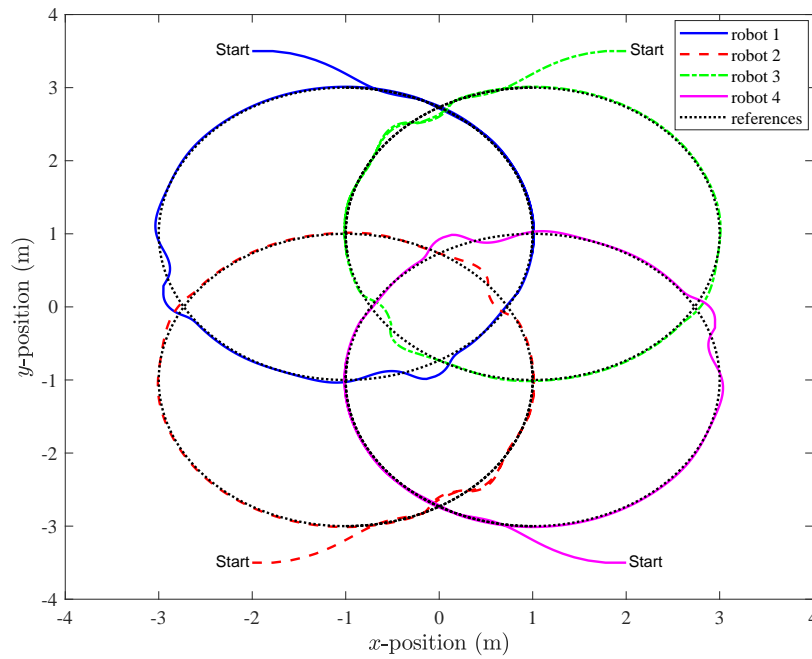


**Figure 1:** Trajectory Tracking for Each Robot using the Centralized NMPC.

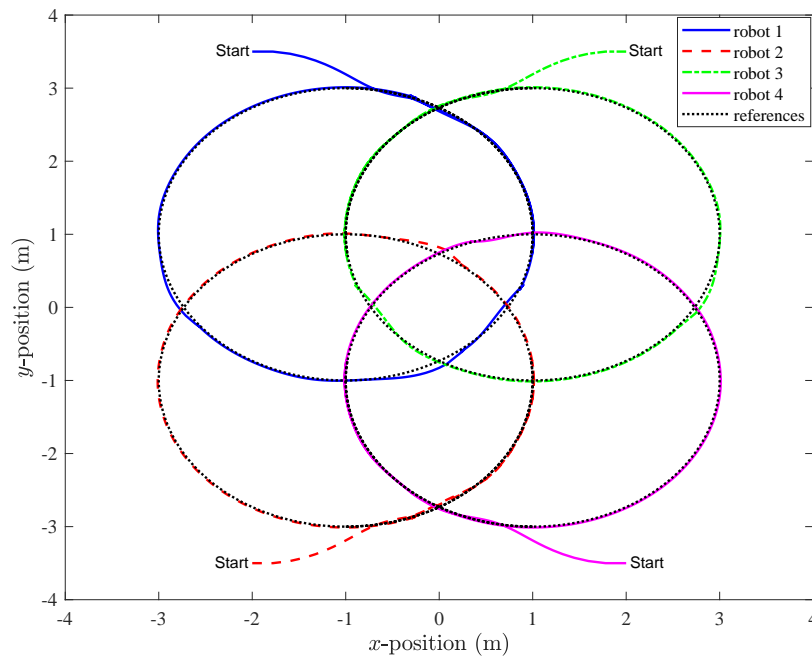


**Figure 2:** Trajectory Tracking for Each Robot using the Decentralized NMPC.

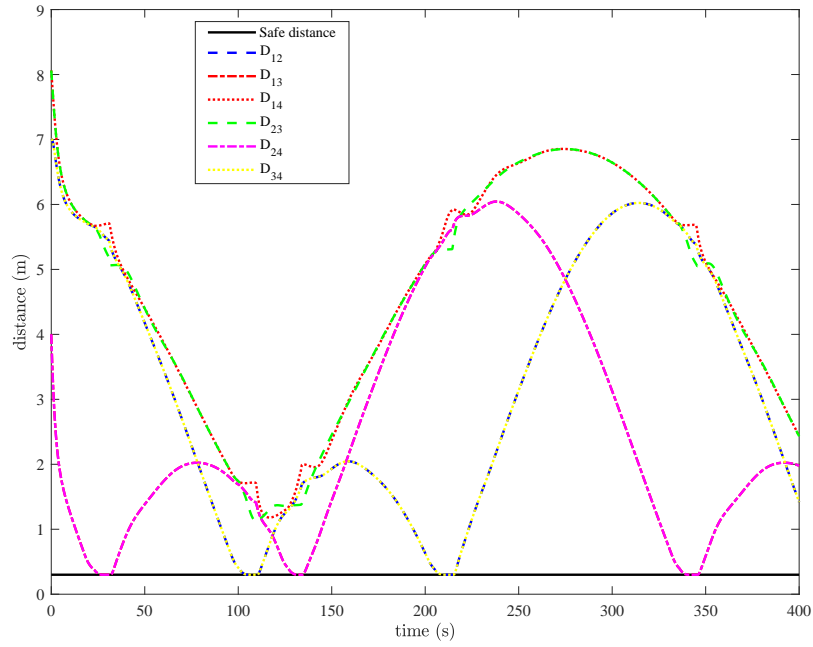


**Figure 3:** The Distance Between One Robot and Other Robots Based on the Centralized Scheme.

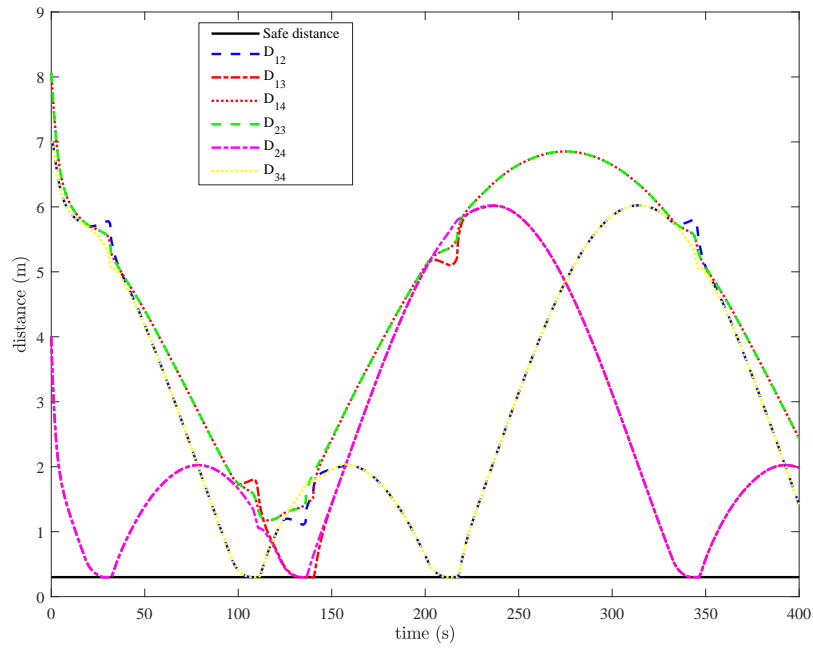


**Figure 4:** The Distance Between One Robot and Other Robots Based on the Decentralized Scheme.

Based on Figures 3 and 4, it can be seen that the distance among the robots satisfies the safe distance to avoid collision. It can be realized since we defined inequality constraint (5) in our optimization problem based on the NMPC approach at every discrete-time  $k$ . The optimal inputs of each robot shown in Figures 5 and 6 also satisfy the lower and upper bounds that we defined previously. This indicates that the solutions of our optimization problem are feasible at every discrete-time  $k$ . Figures 5 and 6 also inform that the NMPC tries to keep the inputs to be convergent to 0 in order to minimize costs when the robots move away from each other.

To compare the computational time for the centralized and decentralized schemes, the different groups of prediction horizon and sampling time ( $N, T_s$ ) are shown in Table 2. This is used to show which method is more effective to control and guide all robots in order that they are on their trajectories.

**Table 2:** Parameters for different simulations.

Parameters	Scenario 1	Scenario 2
Prediction horizon ( $N$ )	5	8
Sampling time ( $T_s$ )	1 s	0.5 s

Based on Table 2, the complexity of computational time for both proposed schemes in the case of controlling 4 robots can be investigated. The results of this idea are presented in Table 3.

**Table 3:** The computational time between the centralized and decentralized schemes.

Scenario	Centralized	Decentralized
1	59.7629 s	39.3990 s
2	244.6630 s	184.7699 s

Based on Table 3, it is clear that the increase of prediction horizon implies the increase of computational time for both centralized and decentralized schemes. The suggestion of this issue is needed to choose an appropriate prediction horizon and sampling time to reduce the complexity time while satisfying a desired performance. Table 3 also gives an information that the decentralized scheme is more effective than the centralized one in terms of computational time since the decentralized scheme provides fast computational time with good performance as shown in the previous simulation in Figures 2 and 4.

## 5 Conclusion

In this study, two different schemes are proposed, namely, a centralized and decentralized NMPC to control multi-robot systems. These schemes are implemented for the trajectory tracking problem where there are some intersections among the robot paths. Based on our simulation, both schemes give satisfying results as all robots can follow their references without a collision between one robot and another robot. In addition, the distance between one robot and another robot is greater than or equal to the safe distance, so this ensures that all robots can avoid collision between each other. For control inputs, the NMPC also guarantees that the actuator saturation limits are satisfied. In our simulation, it can be concluded that the decentralized scheme is better than the centralized scheme.

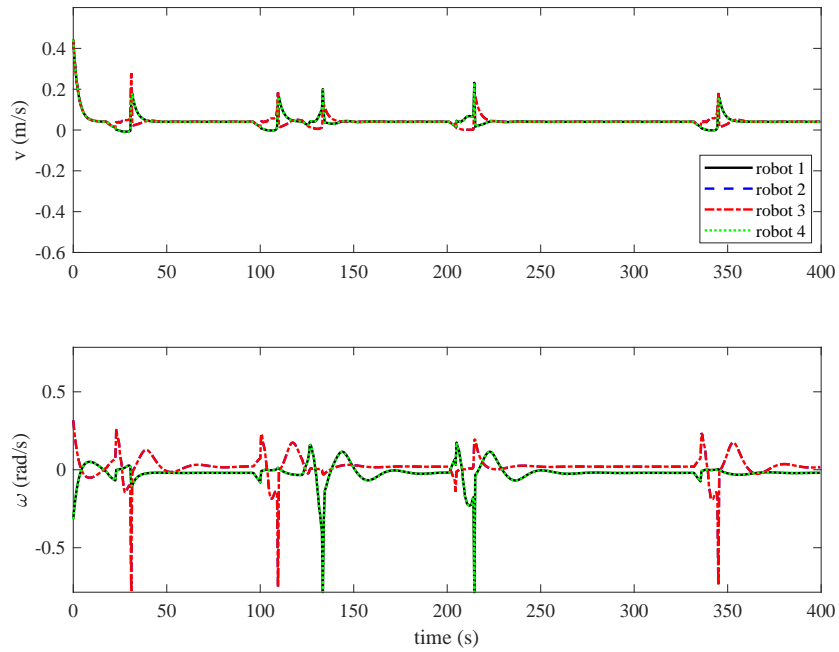


**Figure 5:** The Control Inputs of Each Robot Based on the Centralized Scheme.

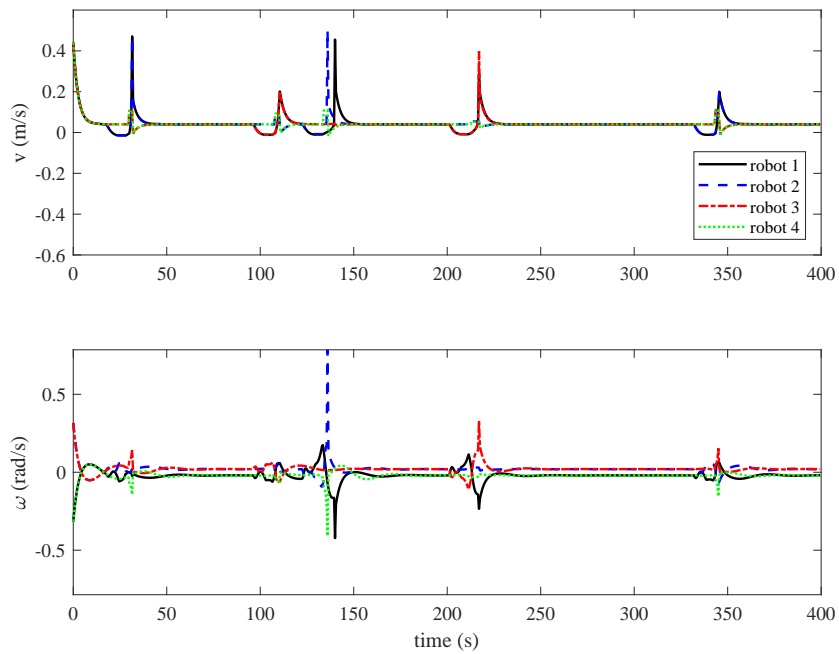


**Figure 6:** The Control Inputs of Each Robot Based on the Decentralized Scheme.

This is shown in the computational complexity that gives the fast computational time as the prediction horizon increases. For the future research, we will include disturbance and consider some obstacles in the more complex cases such as unmanned aerial vehicles (UAVs) and autonomous surface vehicles (ASVs).

### Acknowledgment

The authors would like to thank DRPM RISTEKDIKTI (No. 3/E1/KP.PTNBH/2021) for funding this research by Doctoral Dissertation Research (Penelitian Disertasi Doktor) scheme with contract No. 851/PKS/ITS/2021.

### References

- [1] J. Alonso-Mora, P. Beardsley and R. Siegwart. Cooperative collision avoidance for nonholonomic robots. *IEEE Transactions on Robotics* **34** (2) (2018) 404–420.
- [2] M. Mendili and F. Bouani. Predictive control of mobile robot using kinematic and dynamic models. *Journal of Control Science and Engineering* **2017** (2017).
- [3] F. G. Rossomando, C. Soria and R. Carelli. Sliding mode neuro adaptive control in trajectory tracking for mobile robots. *Journal of Intelligent & Robotic Systems* **74** (3-4) (2014) 931–944.
- [4] A. Bechar and C. Vigneault. Agricultural robots for field operations. Part 2: Operations and systems. *Biosystems Engineering* **153** (2017) 110–128.
- [5] L. Haiming, L. Weidong, Z. Mei and C. An. Algorithm of Path Planning Based on Time Window for Multiple Mobile Robots in Warehousing System. In: *2019 Chinese Control Conference (CCC) 2019*, 2193–2199.
- [6] M. Tavakoli, J. Carriere and A. Torabi. Robotics For COVID-19: How Can Robots Help Health Care in the Fight Against Coronavirus, 03, 2020.
- [7] G. Farias, G. Garcia, G. Montenegro, E. Fabregas, S. Dormido-Canto and S. Dormido. Reinforcement Learning for Position Control Problem of a Mobile Robot. *IEEE Access* **8** (2020) 152941–152951.
- [8] F. Ouendi, S. Houti and M. Tadjine. Comparison of Quadrotor Performance Using Forwarding and PID-Backstepping Control. *Nonlinear Dynamics and System Theory* **19** (3) (2019) 427–443.
- [9] T. Herlambang, S. Subchan, H. Nurhadi and D. Adzkiya. Motion Control Design of UN-USAITS AUV Using Sliding PID. *Nonlinear Dynamics and System Theory* **20** (1) (2020) 51–60.
- [10] G. He, J. Li and P. Cui. Decoupling control design for the module suspension control system in maglev train. *Mathematical Problems in Engineering* **2015** (2015).
- [11] J. A. Paulson, E. A. Buehler, R. D. Braatz and A. Mesbah. Stochastic model predictive control with joint chance constraints. *International Journal of Control* **93** (1) (2020) 126–139.
- [12] I. B. Nascimento, A. Ferramosca, L. C. Piment and G. V. Raffo. NMPC Strategy for a Quadrotor UAV in a 3D Unknown Environment. In: *2019 19th International Conference on Advanced Robotics (ICAR) 2019*, 179–184.
- [13] S. S. Mansouri, G. Nikolakopoulos and T. Gustafsson. Distributed model predictive control for unmanned aerial vehicles. In: *2015 Workshop on Research, Education and Development of Unmanned Aerial Systems (RED-UAS) 2015*, 152–161.

- [14] S. Kim, H. Oh and A. Tsourdos. Nonlinear model predictive coordinated standoff tracking of a moving ground vehicle. *Journal of Guidance, Control and Dynamics* **36** (2) (2013) 557–566.
- [15] J. Shin and H. J. Kim. Nonlinear model predictive formation flight. *IEEE Transactions on Systems, Man, and Cybernetics-Part A: Systems and Humans* **39** (5) (2009) 1116–1125.
- [16] R. Siegwart, I.R. Nourbakhsh and D. Scaramuzza. *Introduction to Autonomous Mobile Robots*. MIT press, 2011.
- [17] L. Grüne and J. Pannek. *Nonlinear Model Predictive Control*. Springer, 2017.
- [18] A. Franco and V. Santos. Short-term path planning with multiple moving obstacle avoidance based on adaptive MPC. In: *2019 IEEE International Conference on Autonomous Robot Systems and Competitions (ICARSC)* 2019, 1–7.



# Flow and Heat Transfer of a Non-Newtonian Power-Law Fluid over a Non-Linearly Stretching Sheet with Thermal Radiation and Aligned Magnetic Field

A. Rani<sup>1\*</sup>, P. Singh<sup>2</sup> and Mani Mala<sup>1</sup>

<sup>1</sup> School of Engineering & Technology, Ansal University, Gurgaon, 122003, Haryana, India.

<sup>2</sup> Department of Mathematics, School of Engineering & Technology, Central University, Mahendergarh, 123031, Haryana, India.

Received: January 16, 2019; Revised: June 7, 2021

**Abstract:** In the present paper the effect of a non-linearly permeable stretching sheet on the solution profile in the presence of thermal radiation and aligned magnetic field has been investigated. A drive has been undertaken to thus highlight the effects of heat and mass transfer of a non-Newtonian power-law fluid over a stretching sheet when the equations are transformed into ordinary differential equations using similarity variables. The transformed equations have been solved numerically using the Runge-Kutta method coupled with the shooting technique. These results are presented graphically for various values of power-law index and for different parameters, viz the stretching parameter, suction parameter, Prandtl number radiation parameter etc.

**Keywords:** *MHD, non-Newtonian power law fluids; stretching sheet; thermal radiation.*

**Mathematics Subject Classification (2010):** 76A05, 85A30.

---

\* Corresponding author: <mailto:anjukaushik2001@gmail.com>

## 1 Introduction

The study of the heat and mass transfer of a fluid over a stretching sheet has attracted many researchers these days due to its various applications in industry, for example, manufacturing of rubber sheet and plastic sheet. Fluids are used in making polymers, blowing of glass, petroleum productions, polymer extrusion, crystal growing fiber spinning and many more. Schowalter [17] was the first one who applied the boundary layer theory to the power-law pseudo-plastic fluid. After that, Schowalter and Collins [9] studied the behaviour of non-Newtonian fluid in the entry region of pipe. Crane [8] was the first to study the fluid flow past a stretching plate. Crane and Carragher [12] have studied the heat transfer on a stretching sheet instead of a plate.

After that, various researchers studied the effect of a fluid flow on a stretching sheet. Gupta and Gupta [1] studied the heat and mass transfer on a stretching sheet with suction or blowing. Vajravelu and Hadjinicolaou [7] analysed the heat transfer on a stretching sheet in the presence of dissipation and heat generation. Dandapat and Gupta [4] studied the flow and heat transfer in a viscoelastic fluid over a stretching sheet. Mahapatra and Gupta [16] have contributed on the heat transfer in the stagnation point flow towards a stretching sheet. Many researcher applied MHD flow and heat transfer over a stretching sheet due to its applications in the industries. Andersson [5] first of all studied the effect of MHD flow of a viscoelastic fluid. Andersson, Bech and Dandapat [5] studied a magneto-hydrodynamic flow of a power-law fluid over a stretching sheet. Siddheshwar and Mahabaleswar [13] studied the effects of radiation and heat source on the MHD flow of a viscoelastic liquid and heat transfer over a stretching sheet. Cortell [14] researched on a viscous flow and heat transfer over a nonlinearly stretching sheet. Fang et al. [15] found out about a slip MHD viscous flow over a stretching sheet.

Researchers discussed several models to analyse the non-Newtonian behaviour of fluids. Among these models the power-law model gained much popularity due to its successful applications of boundary layer assumptions. Till date, the power-law fluid model is the most widely used model to describe non-Newtonian fluids behaviour. Andersson [5] was the first to study the MHD flow on the power-law fluid model.

Various researchers have discussed the power-law fluid model to study various effects on a continuously stretching sheet under different circumstances. However, all of them discussed the presence of magnetic field in transverse direction. But to the best of the authors' knowledge no one has studied the effect of aligned magnetic field on the power-law model. Zhong et. al. discussed explicit solutions of a class of linear partial difference equations with constant coefficients. Aleksandrov and Platonov [2] studied the conditions of ultimate boundedness of solutions for a class of nonlinear systems.

Based on the review of the above studies, the main objective of this paper is to analyze the effects of variable thermal conductivity on the power-law fluid flow and heat transfer over a non-linearly stretching sheet in the presence of aligned magnetic field and considering suction and radiation.

## 2 Formulation of the Problem

The model being considered here consists of a steady two-dimensional flow of an incompressible non-Newtonian fluid following the power law over a permeable stretching sheet. The origin is located at the slit, through which the sheet is drawn through the fluid medium. The velocity of the model is denoted by  $u_w$ .

Equations related to the power-law model for the non-Newtonian fluid, with allowance for the viscous dissipation and aligned magnetic field, are given by

$$\frac{\partial u}{\partial x} + \frac{\partial v}{\partial y} = 0, \tag{1}$$

$$u \frac{\partial u}{\partial x} + v \frac{\partial v}{\partial y} = -\frac{1}{\rho} \frac{\partial p}{\partial x} + \frac{K}{\rho} \frac{\partial}{\partial y} \left( \frac{\partial u}{\partial y} \right)^n - \frac{\sigma(B_0 \sin \alpha)^2 u}{\rho}, \tag{2}$$

$$\rho C_p \left( u \frac{\partial T}{\partial x} + v \frac{\partial T}{\partial y} \right) = k \frac{\partial^2 T}{\partial y^2} + K \left( \frac{\partial u}{\partial y} \right)^{n+1} - \frac{\partial q_r}{\partial y}. \tag{3}$$

Here  $u$  and  $v$  are the components of fluid velocity in  $x$  and  $y$  directions, respectively.  $\rho, k$  and  $K$  represent the density of fluid, thermal conductivity and consistency coefficient,  $n$  is the power law index,  $B_0$  is the magnetic parameter,  $T$  is the temperature of the fluid,  $C_p$  is the specific heat at constant pressure,  $\sigma$  is electrical conductivity,  $\sigma_s$  is the Stefan-Boltzmann constant and  $q_r$  is the radiative heat flux approximated by the Rosseland approximation as

$$q_r = \frac{-4\sigma_s \partial T^4}{\partial y}. \tag{4}$$

Boundary conditions for the model are

$$\begin{aligned} u = u_w(x) = cx^m + u_{sl}, T = T_w, \text{ when } y = 0, \\ u \rightarrow U = bx^m, T \rightarrow T_\infty, \text{ when } y \rightarrow \infty. \end{aligned} \tag{5}$$

Applying the boundary conditions in (5) to the model equation (2), we get

$$U \frac{dU}{dx} = \frac{-1}{\rho} \frac{\partial p}{\partial x} - \frac{\sigma(B_0 \sin \alpha)^2 u}{\rho}. \tag{6}$$

Eliminating  $\frac{-1}{\rho} \frac{\partial p}{\partial x}$  from equations (2) and (6), we get

$$u \frac{\partial u}{\partial x} + v \frac{\partial v}{\partial y} = U \frac{\partial u}{\partial x} + \frac{K}{\rho} \frac{\partial}{\partial y} \left( \frac{\partial u}{\partial y} \right)^n - \frac{\sigma(B_0 \sin \alpha)^2 (u - U)}{\rho}. \tag{7}$$

For further analysis we introduce similarity variable  $\eta$  with dimensionless variables  $f$  and  $\theta$  as

$$\eta = \left[ \frac{c^{2-n}}{\frac{K}{\rho}} \right]^{\frac{1}{n+1}} x^{\frac{m(2-n)-1}{n+1}} y, \Psi(\eta) = \left( \frac{K}{\rho} \right)^{\frac{1}{n+1}} C^{\frac{2n-1}{n+1}} x^{\frac{m(2n-1)+1}{n+1}} f(\eta), \theta(\eta) = \frac{T - T_\infty}{T - T_w}. \tag{8}$$

With all the above similarity variables, the equations (7) and (3) reduce to

$$(f'')^{n-1} f''' + \left[ \frac{m(2n-1)+1}{n+1} \right] f f'' - m (f')^2 - H (\sin \alpha)^2 (f' - \lambda) + m\lambda^2 = 0, \tag{9}$$

$$\left( \frac{3+4R}{3} \right) \frac{\theta''}{P_R} + \left[ \frac{1+m(2n-1)}{n+1} \right] f \theta' - r f' \theta + E_C (f'')^{n+1} = 0. \tag{10}$$

The transformed boundary conditions are

$$f(0) = s, f'(0) = 1, +af''(0), \theta(0) = 1 \text{ when } \eta = 0, \tag{11}$$

$$f'(\infty) \rightarrow \lambda, \theta(\infty) \rightarrow 1 \text{ when } \eta \rightarrow \infty, \quad (12)$$

where  $P_R = \frac{\rho C_p}{k} \left( \left( \frac{K}{\rho} \right)^2 c^{(3m-1)(n-1)} \right)^{\frac{1}{n+1}}$  is the non-Newtonian Prandtl number and  $E_C = \frac{c^2 x^{2m}}{A x^r C_p}$  is the Eckert number and  $H = \sigma \frac{B_0^2}{\rho c x^{1-m}}$ ,  $s$  is the suction parameter,  $a$  is the constant and  $\lambda$  is the ratio of free stream velocity parameter and stretching parameter.

### 3 Solution of the Problem

To analyze the above flow model for the equations (9) and (10) along with boundary conditions (11) and (12), the fourth-order Runge-Kutta method with the shooting technique is used. With the help of the Newton-Raphson shooting method estimates for  $f''(0)$  and  $\theta(0)$  have been done so that the equations can be integrated with the help of the fourth-order Runge-Kutta method. The process of these iterations does not stop until the boundary conditions at infinity become zero. This iteration process has been performed for each value.

### 4 Results and Discussion

In this section the fourth-order Runge-Kutta method with the help of shooting method has been used to solve equations (9) and (10) for the various values of  $P_r, n, m, r, R, \lambda, a, s, \alpha$  and  $H$ . Values of  $f''(0)$  and  $\theta(0)$  have been evaluated correctly up to 8 decimal places so that stability and accuracy of the study can be shown. It is observed from Table 1 that the numerical values of  $f''(0)$  in the present paper for different values of power-law index  $n$ , when  $\lambda = 0, a = 0, s = 0, s = 0, m = 1$ , are in good agreement with the results obtained by Andersson and Kumaran [6], Mahmoud and Megahed [11] and Megahed [10].

By considering the numerical solutions for the various values of power-law index in the range  $0.5 \leq n \leq 1.5$ , the effects of various parameters on the velocity and the temperature distributions are studied.

$n$	Andersson and Kumaran[24]	Mahmoud and Megahed[32]	Megahed[35]	Present Paper
0.5	1.1605	1.1604	1.1604	1.16065620
0.6	1.0951	1.0951	1.0951	1.9512419
0.7	1.545	1.544	1.544	1.054660
0.8	1.0284	1.0284	1.0284	1.02841233
0.9	1.0113	1.0112	1.0112	1.01133117
1.0	1.0000	1.000	1.00000	1.000000
1.1	0.9924	0.9922	0.9922	0.992426994
1.2	0.9874	0.9874	0.9874	0.98737207
1.3	0.9840	0.9841	0.9841	0.9840342
1.4	0.9819	0.9819	0.9819	0.9818837043
1.5	0.9806	0.9806	0.9806	0.98056261
1.6	0.9798	0.9799	0.9799	0.979825441
1.7	0.979501	0.979503	0.979503	0.975007899
1.8	0.979468	0.979467	0.979467	0.971189942
1.9	0.9796	0.9796	0.9796	0.971189943
2.0	0.9800	0.97995	0.97995	0.97912466089

**Table 1:** Comparison of the values of  $f''(0)$  for the various values of  $n$  with the parameters' values  $\lambda = 0, a = 0, s = 0, s = 0, m = 1$ .

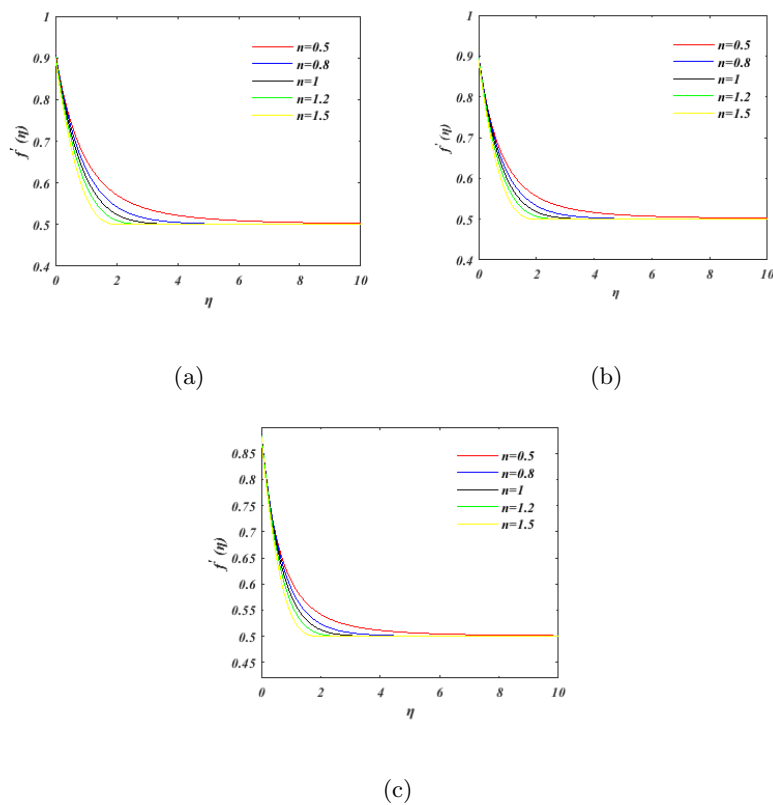


**Figure 1:** Figure (a), (b), (c) show the effects of  $\alpha = \pi/8, \pi/4$  and  $\pi/2$  on the velocity profile for different values of power-law index ( $\eta$ ), respectively.

$n$	Value of $f'$ and $\theta'$ for different values of $\alpha$ with $Pr = 0.71, Ec = 0.1,$ $H = 1, R = 1, s = 0.2, r = 1, m = 0.5, \lambda = 0.5$					
	$f''$			$\theta'$		
	$\alpha = \pi/8$	$\alpha = \pi/4$	$\alpha = \pi/2$	$\alpha = \pi/8$	$\alpha = \pi/4$	$\alpha = \pi/2$
$n = 0.5$	-0.439502	-0.506112	-0.584217	-0.565743	-0.556586	-0.546898
$n = 0.8$	-0.445340	-0.499400	-0.563085	-0.569565	-0.562002	-0.553820
$n = 1$	-0.461656	-0.510364	-0.567860	-0.568936	-0.562320	-0.555068
$n = 1.2$	-0.480821	-0.525376	-0.578055	-0.567408	-0.561607	-0.555187
$n = 1.5$	-0.510534	-0.550243	-0.597283	-0.564679	-0.559882	-0.554400

**Table 2:** Values of  $f''(0)$  and  $\theta'(0)$  for different types of fluid and different angle of magnetic field.

$n$	Value of $f'$ and $\theta'$ for different values of $\lambda$ with $Pr = 0.71, Ec = 0.1,$ $H = 1, R = 1, s = 0.2, r = 1, m = 0.5, \lambda = 0.5$ and $\alpha = \pi/3$					
	$f''$			$\theta'$		
	$\lambda = 0.8$	$\lambda = 1.5$	$\lambda = 2$	$\lambda = 0.8$	$\lambda = 1.5$	$\lambda = 2$
$n = 0.5$	-0.1857688	0.6706540	1.685632	-0.6306510	-0.7615877	-0.854726
$n = 0.8$	-0.2913153	0.6308961	1.440967	-0.6360154	-0.7734705	-0.856978
$n = 1.0$	-0.2289438	0.6367480	1.352774	-0.676532	-0.7807228	-0.859495
$n = 1.2$	-0.2495882	0.6429972	1.292932	-0.6385992	-0.7871893	-0.862109
$n = 1.5$	-0.2803766	0.6575240	1.232879	-0.6394543	-0.7954666	-0.865779

**Table 3:** Values of  $f'$  and  $\theta'$  for various values of  $\lambda$ .

The effects of magnetic field angle  $\alpha$  on the velocity profiles by changing the values of power law index between the range  $0.5 \leq n \leq 1.5$  are shown in Figures 1(a)-1(c). It is seen that as the angle of magnetic field increases, velocity decreases for both values of the power-law index, i.e,  $n < 1$  and  $n \geq 1$ . But it can hardly make any difference for the temperature distribution profile which is shown in Table 2.

The effects of parameter  $\lambda$ , which is basically the ratio of free stream velocity to the stretching parameter, on the solution profile are shown in Figures 2(a)-2(c). It is seen that with the increase in the values of  $\lambda$ , the velocity increases tremendously for the power-law index between  $0.5 \leq n \leq 1.5$ . The downfall of the temperature profile with the increase in  $\lambda$  is shown in Table 3.

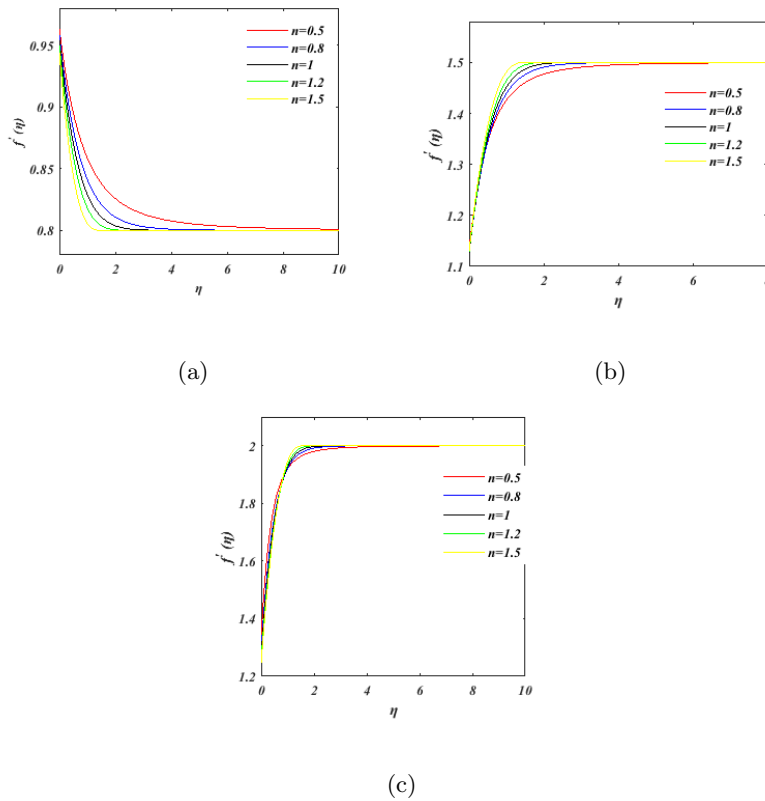


**Figure 2:** Figure (a), (b), (c) show the effects of  $\lambda = 0.8, 1.5$  and  $2$  on the velocity profile for different values of power-law index ( $\eta$ ), respectively.

Figures 3(a)–3(c) represent the velocity profile for the values of suction parameter  $s = 0, 1, 2$ , respectively.

The effects of the Hartmann number  $H$  on the velocity profile and temperature profile are shown in Figures 4(a)–4(b). It is seen from the figures that the velocity and temperature decrease with the increase of  $H$ .

The effect of the Prandtl number  $Pr$  on the dimensionless temperature profile is illustrated in Figure 5(a). It is seen that the increase in the Prandtl number  $Pr$  decreases the temperature distribution. Figure 5(b) shows the effect of change in the radiation parameter  $R$  on the temperature profile. It is seen from the figure that the temperature increases with the increase in radiation parameter for  $n = 0.5$ .

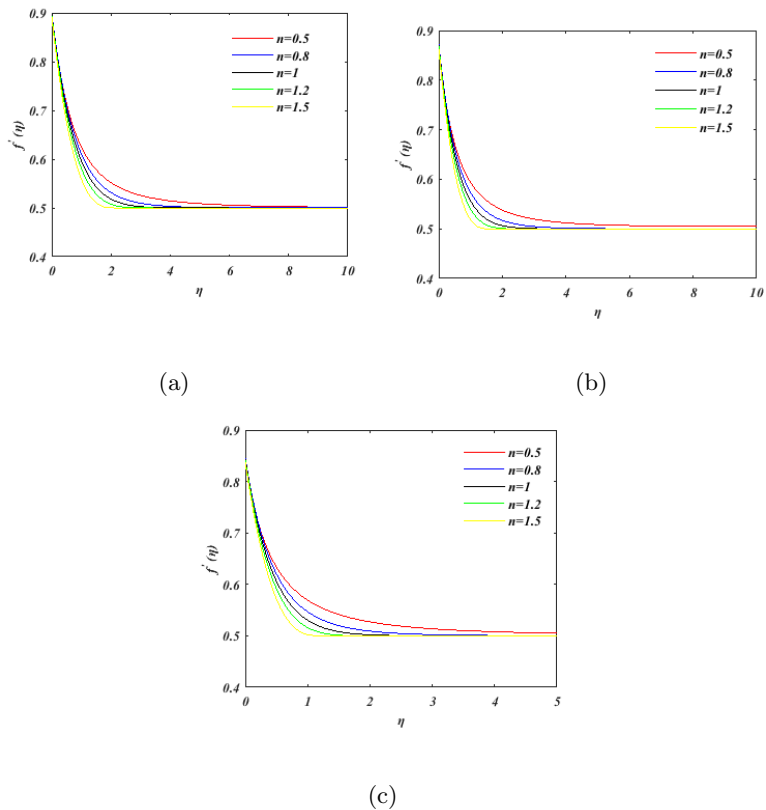


**Figure 3:** Figure (a), (b), (c) show the effects of  $s = 0, 1$  and  $2$  on the velocity profile for different values of power-law index ( $\eta$ ), respectively.

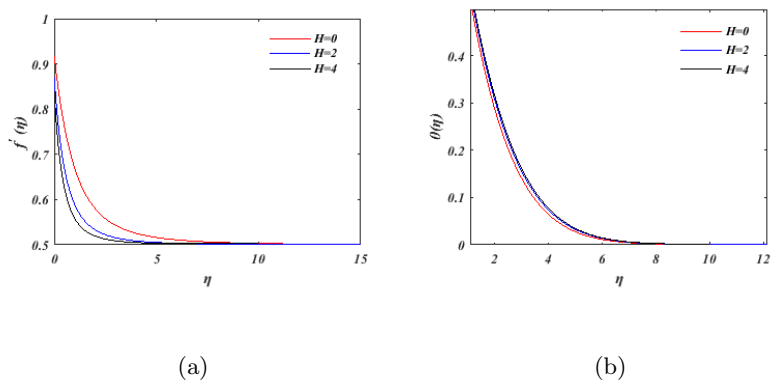


**Figure 4:** Figure (a), (b), (c) show the effects of different values of  $H$  on velocity profile and temperature profile, respectively.

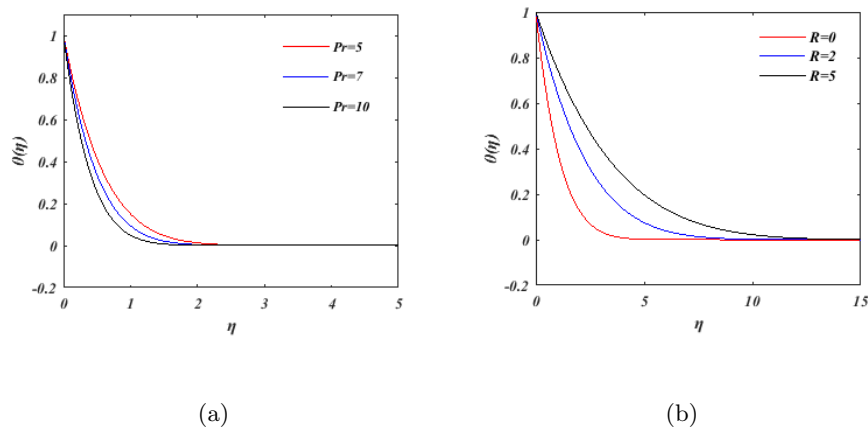


**Figure 5:** Figure (a), (b), (c) show the effects of different values of  $Pr$  and  $R$  on the temperature profile, respectively.

## 5 Conclusion

The first aim of the paper is the solution of the problem on a two dimensional flow of an incompressible non-Newtonian fluid following the power law over a permeable stretching sheet in the presence of thermal radiation. The second one is the transformation of the governing equations into a system of non-linear ordinary differential equations by using similarity transformations, which have been solved numerically using the fourth-order Runge-Kutta method coupled with the shooting technique. During the study the following observations have been achieved:

- Increase in the angle of magnetic field decreases the velocity of the fluid.
- Increase in the stretching parameter increases the velocity distribution but decreases the temperature distribution.
- As suction increases in the sheet, both velocity and temperature decrease.
- Temperature decreases with the increase in the Prandlt number.
- As the effect of magnetic field increases, the velocity decreases.
- The radiation parameter increases with the increase of temperature.

**Nomenclature**

$B_0$  = magnetic field intensity  
 $c$  = stretching sheet parameter  
 $C_p$  = specific heat at constant pressure  
 $K$  = consistency coefficient  
 $k'$  = permeability of the medium  
 $k$  = thermal conductivity  
 $H$  = Hartmann number  $\frac{\sigma B_0^2}{c\rho}$   
 $Pr$  = Prandtl number  
 $p_r$  = radiative heat flux  
 $q_r$  = rate of heat transfer  
 $R$  = radiation parameter  $(= 4\sigma_s T_\infty^3)/Kk$   
 $s$  = heat source/sink parameter  
 $T$  = fluid temperature  
 $T_\infty$  = free stream temperature  
 $T_w$  = temperature of stretching sheet  
 $u, v$  = velocity components along  $x$  and  $y$  axes, respectively  
 $u_w(x)$  = velocity of stretching sheet  
 $U(x)$  = free stream velocity  $(= bx^m)$   
 $x, y$  = Cartesian coordinates along  $x$  and  $y$  axes, respectively.

**Greek symbols**

$\eta$  = similarity variable  
 $\Psi$  = stream function  
 $\sigma$  = electrical conductivity  
 $\nu$  = kinematic viscosity  
 $\mu$  = coefficient of viscosity  
 $\sigma_s$  = Stefan-Boltzmann constant  
 $\Lambda$  = ratio of free stream velocity parameter to stretching sheet parameter.

**References**

- [1] A. Chakrabarti and A.S. Gupta. Hydromagnetic flow and heat transfer over a stretching sheet. *Quarterly of Applied Mathematics* **37** (1) (1979) 73–78.
- [2] A. Y. Aleksandrov and A.V. Platonov. Conditions of ultimate boundedness of solutions for a class of nonlinear systems. *Nonlinear Dynamics and Systems Theory* **8** (2) (2008) 109–122.
- [3] B.S. Dandapat and A.S. Gupta. Flow and heat transfer in a viscoelastic fluid over a stretching sheet. *International Journal of Non-Linear Mechanics* **24** (3) (1989) 215–219.
- [4] B.S. Dandapat and A.S. Gupta. Flow and heat transfer in a viscoelastic fluid over a stretching sheet. *International Journal of Non-Linear Mechanics* **24** (3) (1989) 215–219.
- [5] H.I. Andersson, K.H. Bech and B.S. Dandapat. Magnetohydrodynamic flow of a power-law fluid over a stretching sheet. *International Journal of Non-Linear Mechanics* **27** (6) (1992) 929–936.
- [6] HI Andersson and V Kumaran. On sheet-driven motion of power-law fluids. *International Journal of Non-Linear Mechanics* **41** (10) (2006) 1228–1234.
- [7] K. Vajravelu and A. Hadjinicolaou. Heat transfer in a viscous fluid over a stretching sheet with viscous dissipation and internal heat generation. *International Communications in Heat and Mass Transfer* **20** (3) (1993) 417–430.
- [8] L. J. Crane. Flow past a stretching plate. *Zeitschrift für angewandte Mathematik und Physik ZAMP* **21** (4) (1970) 645–647.

- [9] M. Collins and W. R. Schowalter. Behavior of non-newtonian fluids in the entry region of a pipe. *AIChE journal* **9** (6) (1963) 804–809.
- [10] M. A. A. Mahmoud and A. M. Megahed. Non-uniform heat generation effect on heat transfer of a non-newtonian power-law fluid over a non-linearly stretching sheet. *Meccanica* **47** (5) (2012) 1131–1139.
- [11] M. A. A. Mahmoud. Slip velocity effect on a non-newtonian power-law fluid over a moving permeable surface with heat generation. *Mathematical and Computer Modelling* **54** (5-6) (2011) 1228–1237.
- [12] P. Carragher and L. J. Crane. Heat transfer on a continuous stretching sheet. *ZAMM-Journal of Applied Mathematics and Mechanics/Zeitschrift für Angewandte Mathematik und Mechanik* **62** (10) (1982) 564–565.
- [13] P. G. Siddheshwar and U.S. Mahabaleswar. Effects of radiation and heat source on mhd flow of a viscoelastic liquid and heat transfer over a stretching sheet. *International Journal of Non-Linear Mechanics* **40** (6) (2005) 807–820.
- [14] R. Cortell. Viscous flow and heat transfer over a nonlinearly stretching sheet. *Applied Mathematics and Computation* **184** (2) (2007) 864–873.
- [15] T. Fang, J. Zhang, and S. Yao. Slip mhd viscous flow over a stretching sheet—an exact solution. *Communications in Nonlinear Science and Numerical Simulation* **14** (11) (2009) 3731–3737.
- [16] T. R. Mahapatra and A.S. Gupta. Heat transfer in stagnation-point flow towards a stretching sheet. *Heat and Mass transfer* **38** (6) (2002) 517–521.
- [17] W. R. Schowalter. The application of boundary-layer theory to power-law pseudoplastic fluids: Similar solutions. *AIChE Journal* **6** (1) (1960) 24–28.



# Mathematical Study of a Modified SEIR Model for the Novel SARS-Cov-2 Coronavirus

Abdelhamid Zaghdani \*

*Northern Border University, Faculty of Arts and Science, Rafha, P.O 840, Saudi Arabia.  
University of Tunis, Boulevard du 9 avril, 1939, Tunis. Department of Mathematics,  
Ensit, Taha Hussein Avenue, Montfleury, Tunis, Tunisia.*

Received: January 22, 2021; Revised: May 15, 2021

**Abstract:** In this paper, a modified SEIR mathematical model for the coronavirus infected disease-2019 (COVID-19) has studied. We named this model the SEIQR model and analyzed the stability mathematically. A qualitative analysis of the local and global stability of equilibrium points is carried out. It is shown that the disease-free equilibrium is globally asymptotically stable when the basic reproduction number  $\mathcal{R}_0 \leq 1$  and the disease-persistence equilibrium is globally asymptotically stable when  $\mathcal{R}_0 > 1$ .

**Keywords:** *COVID-19; coronavirus; SEIQR model; local and global stability; direct Lyapunov method; Lasalle's invariance principle.*

**Mathematics Subject Classification (2010):** 34D23, 35N25, 37B25, 49K40, 60H10, 65C30, 91B70.

## 1 Introduction

The novel Coronavirus was detected in China and a few months later it spreaded in the countries all over the world. Covid-19 contamination can be transmitted to a person from a contaminated person, a contaminated dry surface, through the nose or mouth. In March 2020, the World Health Organization declared the Covid-19 a global pandemic. For today, the novel Coronavirus caused tens of thousands of deaths and a few million cases of infections. It can be classified as the third highly pathogenic human Coronavirus appearing in the past two decades. Since its appearance, several scientific researchers have been interested in studies of various problems related to this novel Coronavirus [2, 7, 13].

---

\* Corresponding author: <mailto:hamido20042002@yahoo.fr>

In this paper, we study the following modified mathematical model of ODEs proposed first in [5]:

$$\begin{cases} \dot{S} = \mu N_T - \beta S I N_T - (\alpha + \mu)S, \\ \dot{E} = \beta S I N_T - (\gamma + \mu)E, \\ \dot{I} = \gamma E - (\delta + \mu)I, \\ \dot{Q} = \delta I - (\lambda + \mu)Q, \\ \dot{R} = \lambda Q - \mu R, \\ \dot{C} = \alpha S - \mu C \end{cases} \quad (1)$$

with the positive initial condition  $(S(0), E(0), I(0), Q(0), R(0), C(0)) \in \mathbb{R}_+^6$ , where  $S$  is the susceptible population,  $E$  is the exposed population,  $I$  is the infected population,  $Q$  is the population under quarantine (reported infected cases),  $R$  is the recovered population and  $C$  is the confined susceptible population.

The outline of this paper is as follows. In Section 2, some properties of the system (1) are given. Section 3 is devoted to the calculation of the basic reproduction number  $\mathcal{R}_0$  using the next generation matrix method to assess the transmissibility of the novel Coronavirus Covid-19. The analysis of the local and global stability of equilibrium points is presented in Sections 4 and 5, respectively. It is shown that the disease-persistence (endemic) equilibrium is globally asymptotically stable when  $\mathcal{R}_0 > 1$ . However, when  $\mathcal{R}_0 \leq 1$ , then the disease-free equilibrium is globally asymptotically stable. Finally, Section 6 is done to present some numerical tests confirming the obtained theoretical results.

## 2 Properties of the Mathematical Model

The parameters of the model (1) are the protection rate  $\alpha$ , the infection rate  $\beta$ , the incubation rate  $\gamma$ , the quarantine rate  $\delta$ , the natural mortality rate  $\mu$  (which is proportional to the birth rate) and the recovery rate  $\lambda$ . Define  $\bar{P} = (\frac{\mu N_T}{\alpha + \mu}, 0, 0, 0, 0, \frac{\alpha N_T}{\alpha + \mu})$  as the disease free equilibrium point.

### Proposition 2.1

1. For every given initial condition  $(S(0), E(0), I(0), Q(0), R(0), C(0))$  in  $\mathbb{R}_+^6$ , system (1) admits a bounded solution with positive components defined for all  $t > 0$ .
2. The set  $\Omega_1 = \{(S, E, I, Q, R, C) \in \mathbb{R}_+^6 / S + E + I + Q + R + C = N_T\}$  is a positively invariant attractor for system (1).

### Proof.

1. The solution is positive due to the fact that since  $S = 0$ , one has  $\dot{S} = \mu N_T > 0$ ; if  $E = 0$ , then  $\dot{E} = \beta S I N_T > 0$ ; once  $I = 0$ , then  $\dot{I} = \gamma E > 0$ ; if  $Q = 0$ , then  $\dot{Q} = \delta I > 0$ ; if  $R = 0$ , then  $\dot{R} = \lambda Q > 0$ ; and if  $C = 0$ , then  $\dot{C} = \alpha S > 0$ .

The boundedness of solutions of system (1) can be proved by adding all equations of system (1), and then one obtains, for  $T = S + E + I + Q + R + C - N_T$ , the following equation for the totality of individuals:

$$\dot{T} = \dot{S} + \dot{E} + \dot{I} + \dot{Q} + \dot{R} + \dot{C} = \mu N_T - \mu S - \mu E - \mu I - \mu Q - \mu R - \mu C = -\mu T.$$

Then

$$\begin{aligned} S(t) &+ E(t) + I(t) + Q(t) + R(t) + C(t) \\ &= N_T + (S(0) + E(0) + I(0) + Q(0) + R(0) + C(0) - N_T)e^{-\mu t}. \end{aligned} \quad (2)$$

Then the boundedness of the solution of system (1) holds since all compartments of  $T$  are positive.

2. One can easily deduce from (2) that the set  $\Omega_1$  is a positively invariant attractor for system (1).

### 3 Computation of the Basic Reproduction Number by the Next Generation Matrix Method

For determining the reproduction number of (1), we use the next generation matrix method proposed by Diekmann, et al. [3] and elaborated by van den Driessche and Watmough [6] for an ODE compartmental model.

In (1), the disease free-equilibrium is  $\bar{P} = (\frac{\mu N_T}{\alpha + \mu}, 0, 0, 0, 0, \frac{\alpha N_T}{\alpha + \mu})$  and the compartments containing infected individuals are  $X = (X_1, X_2, X_3) = (E, I, Q)$ . Using the generation matrix method [3, 6], consider these equations written in the form  $\dot{X}_i = \mathcal{F}_i(X) - \mathcal{V}_i(X)$  for  $i = 1, 2, 3$ .

Now define  $F = [\frac{\partial \mathcal{F}_i(\bar{P})}{X_j}]$  and  $V = [\frac{\partial \mathcal{V}_i(\bar{P})}{X_j}]$  for  $1 \leq i, j \leq 3$ . Thus the reproduction number  $\mathcal{R}_0$  is the spectral radius of the matrix  $FV^{-1}$  and we have

$$\mathcal{R}_0 = \rho(FV^{-1}).$$

As in [6], we have the following theorem.

**Theorem 3.1** *If  $\bar{P}$  is a DFE of the system  $\dot{X}_i = \mathcal{F}_i(X) - \mathcal{V}_i(X)$ , then  $\bar{P}$  is locally asymptotically stable if  $\mathcal{R}_0 = \rho(FV^{-1}) < 1$ , but unstable if  $\mathcal{R}_0 > 1$ .*

Now, we have the following theorem for the reproduction number  $\mathcal{R}_0$ .

**Theorem 3.2** *The reproduction number of (1) is given by*

$$\mathcal{R}_0 = N_T \sqrt{\frac{\gamma \beta \mu}{(\alpha + \mu)(\gamma + \mu)(\delta + \mu)}}. \quad (3)$$

**Proof.** According to the next generation matrix method, we have

$$F = \begin{pmatrix} 0 & \frac{\beta \mu}{\alpha + \mu} N_T^2 & 0 \\ \gamma & 0 & 0 \\ 0 & \delta & 0 \end{pmatrix} \quad \text{and} \quad V = \begin{pmatrix} \gamma + \mu & 0 & 0 \\ 0 & \delta + \mu & 0 \\ 0 & 0 & \lambda + \mu \end{pmatrix}.$$

Then

$$FV^{-1} = \begin{pmatrix} 0 & \frac{\beta \mu N_T^2}{(\alpha + \mu)(\delta + \mu)} & 0 \\ \frac{\gamma}{\alpha + \mu} & 0 & 0 \\ 0 & \frac{\delta}{\delta + \mu} & 0 \end{pmatrix}.$$

The basic reproduction number for model (1) is given by the spectral radius of the matrix  $FV^{-1}$  and so

$$\mathcal{R}_0 = N_T \sqrt{\frac{\gamma\beta\mu}{(\alpha + \mu)(\gamma + \mu)(\delta + \mu)}}.$$

#### 4 Local Stability

**Theorem 4.1 (1)** *If  $\mathcal{R}_0 < 1$ , then the disease free equilibrium  $\bar{P}$  is locally asymptotically stable.*

**(2)** *If  $\mathcal{R}_0 \geq 1$ , then the disease free equilibrium  $\bar{P}$  is unstable.*

**Proof.** The Jacobian matrix  $J$  evaluated at  $\bar{P} = (\frac{\mu N_T}{\alpha + \mu}, 0, 0, 0, 0, \frac{\alpha N_T}{\alpha + \mu})$  is given by

$$\bar{J} = \begin{pmatrix} -\alpha - \mu & 0 & -\frac{\beta}{\alpha + \mu} \mu N_T^2 & 0 & 0 & 0 \\ 0 & -\gamma - \mu & \frac{\beta}{\alpha + \mu} \mu N_T^2 & 0 & 0 & 0 \\ 0 & \gamma & -\delta - \mu & 0 & 0 & 0 \\ 0 & 0 & \delta & -\lambda - \mu & 0 & 0 \\ 0 & 0 & 0 & \lambda & -\mu & 0 \\ \alpha & 0 & 0 & 0 & 0 & -\mu \end{pmatrix}.$$

The characteristic equation is

$$\begin{aligned} \bar{P}(X) &= (X + \alpha + \mu)(X + \lambda + \mu)(X + \mu)^2 \begin{vmatrix} -\gamma - \mu - X & \frac{\beta}{\alpha + \mu} \mu N_T^2 \\ \gamma & -\delta - \mu - X \end{vmatrix} \\ &= (X + \alpha + \mu)(X + \lambda + \mu)(X + \mu)^2 \left( (\gamma + \mu + X)(\delta + \mu + X) - \frac{\gamma\beta}{\alpha + \mu} \mu N_T^2 \right) \\ &= (X + \alpha + \mu)(X + \lambda + \mu)(X + \mu)^2 \\ &\quad \times \left( X^2 + (\gamma + 2\mu + \delta)X + (\gamma + \mu)(\delta + \mu) - \frac{\gamma\beta}{\alpha + \mu} \mu N_T^2 \right) \\ &= (X + \alpha + \mu)(X + \lambda + \mu)(X + \mu)^2 \\ &\quad \times \left( X^2 + (\gamma + 2\mu + \delta)X + (\gamma + \mu)(\delta + \mu)(1 - \mathcal{R}_0)(1 + \mathcal{R}_0) \right) \\ &= (X + \alpha + \mu)(X + \lambda + \mu)(X + \mu)^2 \\ &\quad \times \left( X^2 + a_1X + a_0 \right), \end{aligned}$$

where  $a_1 = (\gamma + 2\mu + \delta) > 0$  and  $a_0 = (\gamma + \mu)(\delta + \mu)(1 - \mathcal{R}_0)(1 + \mathcal{R}_0) > 0$  if  $\mathcal{R}_0 < 1$ . By the Routh-Hurwitz criterion, we deduce that all eigenvalues have negative real parts and then  $\bar{P}$  is locally asymptotically stable if  $\mathcal{R}_0 < 1$ . If  $\mathcal{R}_0 \geq 1$ , then  $a_0 \leq 0$  and there exists at least one non negative eigenvalue  $\lambda$  of  $J^*$ , therefore  $\bar{P}$  is unstable.

**Theorem 4.2** *If  $\mathcal{R}_0 > 1$ , then the disease-persistence equilibrium  $P^*$  is locally asymptotically stable.*

**Proof.** Denote  $P^* = (S^*, E^*, I^*, Q^*, R^*, C^*)$ , then we have

$$\begin{aligned} E^* &= \frac{\mu N_T - (\alpha + \mu)S^*}{\gamma + \mu} = \frac{\mu N_T}{\gamma + \mu} - \frac{(\alpha + \mu)}{\gamma + \mu} S^*, \\ I^* &= \frac{\gamma}{\delta + \mu} E^* = \frac{\gamma \mu N_T}{(\delta + \mu)(\gamma + \mu)} - \frac{\gamma(\alpha + \mu)}{(\delta + \mu)(\gamma + \mu)} S^*, \\ Q^* &= \frac{\delta}{\lambda + \mu} I^* = \frac{\delta \gamma \mu N_T}{(\lambda + \mu)(\delta + \mu)(\gamma + \mu)} - \frac{\delta \gamma(\alpha + \mu)}{(\lambda + \mu)(\delta + \mu)(\gamma + \mu)} S^*, \\ R^* &= \frac{\lambda}{\mu} Q^* = \frac{\lambda \delta \gamma \mu N_T}{\mu(\lambda + \mu)(\delta + \mu)(\gamma + \mu)} - \frac{\lambda \delta \gamma(\alpha + \mu)}{\mu(\lambda + \mu)(\delta + \mu)(\gamma + \mu)} S^*, \\ C^* &= \frac{\alpha}{\mu} S^*. \end{aligned}$$

From the third equation in (1), we obtain

$$E^* = \frac{\delta + \mu}{\gamma} I^*.$$

Replacing this in the second equation of (1), we get

$$\begin{aligned} -(\gamma + \mu) \frac{\delta + \mu}{\gamma} I^* + \beta S^* I^* N_T = 0 &\implies (-(\gamma + \mu) \frac{\delta + \mu}{\gamma} + \beta S^* N_T) I^* = 0 \\ &\implies -(\gamma + \mu) \frac{\delta + \mu}{\gamma} + \beta S^* N_T = 0 \\ &\implies S^* = \frac{(\gamma + \mu)(\delta + \mu)}{\gamma \beta N_T}. \end{aligned}$$

From the system given previously, and the value of  $\mathcal{R}_0$ , we can write

$$\begin{aligned} I^* &= \frac{\gamma \mu N_T}{(\delta + \mu)(\gamma + \mu)} - \frac{\gamma(\alpha + \mu)}{(\delta + \mu)(\gamma + \mu)} S^* \\ &= \frac{\gamma \mu N_T}{(\delta + \mu)(\gamma + \mu)} - \frac{\alpha + \mu}{\beta N_T} \\ &= \frac{\alpha + \mu}{\beta N_T} (\mathcal{R}_0^2 - 1). \end{aligned}$$

Now, we compute the characteristic equation of the Jacobian matrix evaluated at  $P^*$ .

We have

$$\begin{aligned}
 P^*(X) &= -(X+\mu)^2(X+\lambda+\mu) \begin{vmatrix} -\alpha - \mu - \beta I^* N_T - X & 0 & -\beta S^* N_T \\ \beta I^* N_T & -\gamma - \mu - X & \beta S^* N_T \\ 0 & \gamma & -\delta - \mu - X \end{vmatrix} \\
 &= -(X+\mu)^2(X+\lambda+\mu) \begin{vmatrix} -\alpha - \mu - \beta I^* N_T - X & 0 & -\beta S^* N_T \\ -\alpha - \mu - X & -\gamma - \mu - X & 0 \\ 0 & \gamma & -\delta - \mu - X \end{vmatrix} \\
 &= -(X+\mu)^2(X+\lambda+\mu) \\
 &\quad \times ((-\alpha - \mu - \beta I^* N_T - X)(\gamma + \mu + X)(\delta + \mu + X) + \beta S^* N_T(\alpha + \mu + X)\gamma) \\
 &= -(X+\mu)^2(X+\lambda+\mu) \\
 &\quad \times ([-\alpha - \mu - \beta I^* N_T - X][X^2 + (\delta + \gamma + 2\mu)X + (\delta + \mu)(\gamma + \mu)] \\
 &\quad + \beta S^* N_T(\alpha + \mu + X)\gamma) \\
 &= (X+\mu)^2(X+\lambda+\mu)(X^3 + a_1X^2 + a_2X + a_3)
 \end{aligned}$$

with

$$\begin{aligned}
 a_1 &= \alpha + \mu + \beta I^* N_T + \delta + \gamma + 2\mu \\
 &= \alpha + \mu + (\alpha + \mu)(\mathcal{R}_0^2 - 1) + \delta + \gamma + 2\mu = (\alpha + \mu)\mathcal{R}_0^2 + \delta + \gamma + 2\mu, \\
 a_2 &= (\alpha + \mu + \beta I^* N_T)(\delta + \gamma + 2\mu) + (\delta + \mu)(\gamma + \mu) - \beta\gamma S^* N_T, \\
 a_3 &= (\alpha + \mu + \beta I^* N_T)(\delta + \mu)(\gamma + \mu) - \beta\gamma(\alpha + \mu)S^* N_T.
 \end{aligned}$$

Then

$$\begin{aligned}
 a_2 &= (\alpha + \mu + (\alpha + \mu)(\mathcal{R}_0^2 - 1))(\delta + \gamma + 2\mu) + (\delta + \mu)(\gamma + \mu) - (\gamma + \mu)(\delta + \mu) \\
 &= [\alpha + \mu + (\alpha + \mu)(\mathcal{R}_0^2 - 1)][\delta + \gamma + 2\mu] \\
 &= (\alpha + \mu)[\delta + \gamma + 2\mu]\mathcal{R}_0^2 > 0, \\
 a_3 &= (\alpha + \mu + (\alpha + \mu)(\mathcal{R}_0^2 - 1))(\delta + \mu)(\gamma + \mu) - (\alpha + \mu)(\gamma + \mu)(\delta + \mu) \\
 &= (\alpha + \mu)(\delta + \mu)(\gamma + \mu)\mathcal{R}_0^2 - (\alpha + \mu)(\gamma + \mu)(\delta + \mu) \\
 &= (\alpha + \mu)(\delta + \mu)(\gamma + \mu)(\mathcal{R}_0^2 - 1).
 \end{aligned}$$

Thus  $a_3 > 0$  if  $\mathcal{R}_0 > 1$ .

Now, we demonstrate that  $a_1a_2 > a_3$  if  $\mathcal{R}_0 > 1$ .

$$\begin{aligned}
 a_1a_2 - a_3 &= \left[ (\alpha + \mu)\mathcal{R}_0^2 + \delta + \gamma + 2\mu \right] \left[ (\alpha + \mu)[\delta + \gamma + 2\mu]\mathcal{R}_0^2 \right. \\
 &\quad \left. - (\alpha + \mu)(\delta + \mu)(\gamma + \mu)(\mathcal{R}_0^2 - 1) \right] \\
 &= (\alpha + \mu) \left[ [(\alpha + \mu)\mathcal{R}_0^2 + \delta + \gamma + 2\mu] (\delta + \gamma + 2\mu)\mathcal{R}_0^2 \right. \\
 &\quad \left. - (\alpha + \mu)(\delta + \mu)(\gamma + \mu)(\mathcal{R}_0^2 - 1) \right] \\
 &\geq (\alpha + \mu) \left[ \left( (\delta + \gamma + 2\mu)^2 \mathcal{R}_0^2 - (\delta + \mu)(\gamma + \mu)\mathcal{R}_0^2 + (\delta + \mu)(\gamma + \mu) \right) \right] \\
 &\geq (\alpha + \mu) \left[ \left( (\delta + \gamma + 2\mu)^2 - (\delta + \mu)(\gamma + \mu) \right) \mathcal{R}_0^2 + (\delta + \mu)(\gamma + \mu) \right].
 \end{aligned}$$

Since  $(\delta + \gamma + 2\mu)^2 - (\delta + \mu)(\gamma + \mu) > 0$  for every positive parameters  $\delta$ ,  $\gamma$  and  $\mu$ , we conclude that  $a_1 a_2 - a_3 > 0$  and the Routh-Hurwitz criterion permits to conclude.

## 5 Global Stability

**Lemma 5.1**  $\Omega_2 = \{(S, E, I, Q, R, C) \in \Omega_1; S \leq \frac{\mu N_T}{\alpha + \mu}\}$  is a positively invariant attractor for system (1).

**Proof.** It is proved in Proposition 2.1 that the bounded set  $\Omega_1$  is a positive invariant attractor set of all solutions of system (1). Now, since  $\dot{S}(t) < 0$  for  $S(t) > \frac{\mu N_T}{\alpha + \mu}$ , one has  $\liminf S(t) \leq \frac{\mu N_T}{\alpha + \mu}$ . This completes the proof.

**Theorem 5.1** If  $\mathcal{R}_0 \leq 1$ , then the disease-free equilibrium  $\bar{P}$  is globally asymptotically stable.

**Proof.** Consider the following Lyapunov function:  $L_1 = \gamma E + (\gamma + \mu)I$ . Therefore,

$$\begin{aligned} \dot{L}_1 &= \gamma \dot{E} + (\gamma + \mu) \dot{I} \\ &= \gamma (\beta S I N_T - (\gamma + \mu) E) + (\gamma + \mu) (\gamma E - (\delta + \mu) I) \\ &= \gamma \beta S I N_T - (\gamma + \mu) (\delta + \mu) I \\ &\leq \frac{\gamma \beta \mu}{\alpha + \mu} I N_T^2 - (\gamma + \mu) (\delta + \mu) I \text{ since } S \leq \frac{\mu N_T}{\alpha + \mu} \\ &= \left( \frac{\gamma \beta \mu}{\alpha + \mu} N_T^2 - (\gamma + \mu) (\delta + \mu) \right) I \\ &= (\gamma + \mu) (\delta + \mu) \left( \frac{\gamma \beta \mu}{(\alpha + \mu)(\gamma + \mu)(\delta + \mu)} N_T^2 - 1 \right) I \\ &= (\gamma + \mu) (\delta + \mu) (\mathcal{R}_0^2 - 1) I, \quad \forall (S, E, I, Q, R, C) \in \Omega_2. \end{aligned}$$

It follows that  $\dot{L}_1 \leq 0$  if  $\mathcal{R}_0 \leq 1$  with  $\dot{L}_1 = 0$  only if  $I = 0$ . Therefore,  $L_1$  is a Lyapunov function on  $\Omega_2$ . Moreover, Lemma 5.1 implies that  $\Omega_2$  is a compact, absorbing subset of  $\mathbb{R}_+^6$ , and the largest compact invariant set in  $\{(S, E, I, Q, R, C) \in \Omega_2 : \dot{L}_1 = 0\}$  is  $\{\bar{P}\}$ . Therefore, by the Lasalle invariance principle (see, for example, [11, Theorem 3.1] and [1, 4, 8–10, 14, 15] for other applications), we deduce that every solution of system (1) with the initial conditions in  $\mathbb{R}_+^6$  converges to  $\bar{P}$  as  $t \rightarrow +\infty$ .

Now, we give a result of global stability for the disease-persistence equilibrium  $P^*$ .

**Theorem 5.2** The disease-persistence equilibrium  $P^*$  is globally asymptotically stable if  $\mathcal{R}_0 > 1$ .

**Proof.** Consider the Lyapunov function

$$L_2 = \left( S - S^* \ln\left(\frac{S}{S^*}\right) \right) + \left( E - E^* \ln\left(\frac{E}{E^*}\right) \right) + \frac{(\gamma + \mu)}{\gamma} \left( I - I^* \ln\left(\frac{I}{I^*}\right) \right).$$

$P^*$  is the global minimum of  $L_2$ . Indeed,  $P^*$  is the unique internal stationary point of system (1) and the function  $L_2$  has its minimum value  $L_{2min} = S^* + E^* + \frac{(\gamma + \mu)}{\gamma} I^*$

when  $S = S^*$ ,  $E = E^*$ ,  $I = I^*$ ,  $Q = Q^*$ ,  $R = R^*$ ,  $C = C^*$ , and  $L_2(t) \rightarrow +\infty$  at the boundary of the positive quadrant.

Now, we compute the derivative of  $L_2(t)$  along the solutions of system (1):

$$\begin{aligned} \dot{L}_2 &= \left(1 - \frac{S^*}{S}\right)\dot{S} + \left(1 - \frac{E^*}{E}\right)\dot{E} + \frac{(\gamma + \mu)}{\gamma}\left(1 - \frac{I^*}{I}\right)\dot{I} \\ &= \left(1 - \frac{S^*}{S}\right)\left(\mu N_T - \beta S I N_T - (\alpha + \mu)S\right) + \left(1 - \frac{E^*}{E}\right)\left(\beta S I N_T - (\gamma + \mu)E\right) \\ &\quad + \frac{(\gamma + \mu)}{\gamma}\left(1 - \frac{I^*}{I}\right)\left(\gamma E - (\delta + \mu)I\right). \end{aligned}$$

Since  $\mu N_T = \beta S^* I^* N_T + (\alpha + \mu)S^*$  and  $(\gamma + \mu)E^* = \frac{(\delta + \mu)(\gamma + \mu)}{\gamma}I^* = \beta S^* I^* N_T$ , we can write

$$\begin{aligned} \dot{L}_2 &= \left(1 - \frac{S^*}{S}\right)\left(\beta S^* I^* N_T + (\alpha + \mu)S^* - \beta S I N_T - (\alpha + \mu)S\right) \\ &\quad + \beta S I N_T - (\gamma + \mu)E - \beta S I N_T \frac{E^*}{E} + (\gamma + \mu)E^* \\ &\quad + (\gamma + \mu)E - \frac{(\delta + \mu)(\gamma + \mu)}{\gamma}I - (\gamma + \mu)E \frac{I^*}{I} + \frac{(\delta + \mu)(\gamma + \mu)}{\gamma}I^* \\ &= \beta S^* I^* N_T + (\alpha + \mu)S^* - \beta S I N_T - (\alpha + \mu)S - \beta S^* I^* N_T \frac{S^*}{S} - (\alpha + \mu)S^* \frac{S^*}{S} \\ &\quad + \beta S^* I N_T + (\alpha + \mu)S^* + \beta S I N_T - \beta S I N_T \frac{E^*}{E} + \beta S^* I^* N_T - \beta S^* I^* N_T \frac{I^*}{I} \\ &\quad - \beta S^* I^* N_T \frac{E I^*}{E^* I} + \beta S^* I^* N_T \\ &= (\alpha + \mu)S^* \left(2 - \frac{S}{S^*} - \frac{S^*}{S}\right) + \beta S^* I^* N_T \left(3 - \frac{S^*}{S} - \frac{E I^*}{E^* I} - \frac{S I E^*}{S^* I^* E}\right). \end{aligned}$$

Using the fact that

$$\frac{S}{S^*} \frac{S^*}{S} = 1, \text{ and } \frac{S^*}{S} \frac{E I^*}{E^* I} \frac{S I E^*}{S^* I^* E} = 1$$

and the following inequality:

$$\sum_{i=1}^{i=n} x_i \geq n \left[ \prod_{i=1}^{i=n} x_i \right]^{\frac{1}{n}}, \quad x_1, x_2, x_3, \dots, x_n \geq 0, \tag{4}$$

we obtain the following inequalities:

$$2 - \frac{S^*}{S} - \frac{S}{S^*} \leq 0, \text{ and } 3 - \frac{S^*}{S} - \frac{E I^*}{E^* I} - \frac{S I E^*}{S^* I^* E} \leq 0.$$

Therefore,  $\dot{L}_2 \leq 0$ . With the help of the Lyapunov stability theorem, we deduce that  $P^* = (S^*, E^*, I^*, Q^*, R^*, C^*)$  is stable.

It remains to show that  $P^* = (S^*, E^*, I^*, Q^*, R^*, C^*)$  is asymptotically stable using the Lasalle invariance principle [11]. Denote

$$A_1 := 2 - \frac{S^*}{S} - \frac{S}{S^*} \quad \text{and} \quad A_2 := 3 - \frac{S^*}{S} - \frac{E I^*}{E^* I} - \frac{S I E^*}{S^* I^* E}.$$

Then one has  $\dot{L}_2(S, E, I, Q, R, C) = 0 \Leftrightarrow A_1 = A_2 = 0$ .

With the above equations, we obtain the following implications:

$$\begin{aligned} A_1 = 0 &\Rightarrow S = S^*, \\ (S = S^*, A_2 = 0) &\Rightarrow IE^* = I^*E. \end{aligned}$$

Finally, we get

$$\dot{L}_2(S, E, I, Q, R, C) = 0 \Leftrightarrow S = S^*, IE^* = I^*E. \tag{5}$$

Let  $e = \frac{E}{E^*} = \frac{I}{I^*}$ , then  $E = eE^*$  and  $I = eI^*$ . Replacing  $S, I$  in the first equation of (1) at equilibrium yields

$$\mu N_T = e\beta S^* I^* N_T + (\alpha + \mu)S^* = \beta S^* I^* N_T + (\alpha + \mu)S^*.$$

Therefore, we get  $e = 1$  and then  $I = I^*$  and  $E = E^*$ . Finally,

$$\dot{L}_2(S, E, I, Q, R, C) = 0 \Leftrightarrow (S = S^*, E = E^*, I = I^*, Q = Q^*, R = R^*, C = C^*).$$

Thus, the largest invariant set contained in  $\{(S, E, I, Q, R, C) \mid \dot{L}_2 = 0\}$  is  $\{(S^*, E^*, I^*, Q^*, R^*, C^*)\}$ . Then the global stability of the disease-persistence equilibrium  $P^* = (S^*, E^*, I^*, Q^*, R^*, C^*)$  follows according to the Lasalle invariance principle [12].

### 6 Numerical Simulations

We validate numerical simulations for system (1). We consider four cases; two of them (Figure 1) confirming the global stability of the disease-free equilibrium  $\bar{P}$  when  $\mathcal{R}_0 \leq 1$ . The other two tests (Figure 2) confirm the global stability of the disease-persistence equilibrium  $P^*$  when  $\mathcal{R}_0 > 1$ .

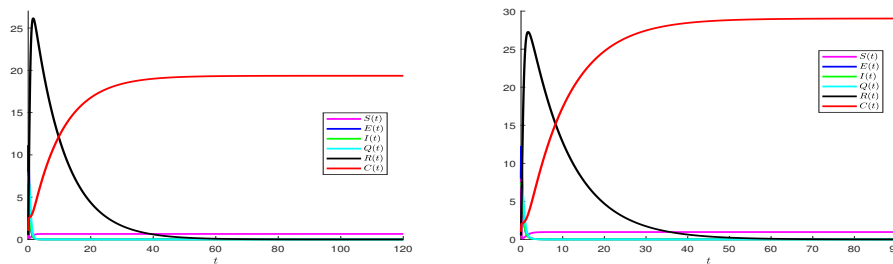


**Figure 1:**  $(S(t), E(t), I(t), Q(t), R(t), C(t))$  behaviours for (left)  $N_T = 20, \mu = 0.1, \beta = 0.1, \alpha = 3, \gamma = 3, \delta = 5, \lambda = 5, \mathcal{R}_0 = 0.49 \leq 1$  and for (right)  $N_T = 30, \mu = 0.1, \beta = 0.1, \alpha = 3, \gamma = 3, \delta = 5, \lambda = 5, \mathcal{R}_0 = 0.74 \leq 1$ .

We remark that the solution of (1) converges asymptotically to  $\bar{P}$ . Only susceptible and confined susceptible compartments persist, the other compartments vanish.

In this case, the solution of (1) converges asymptotically to  $P^*$  and all compartments persist.

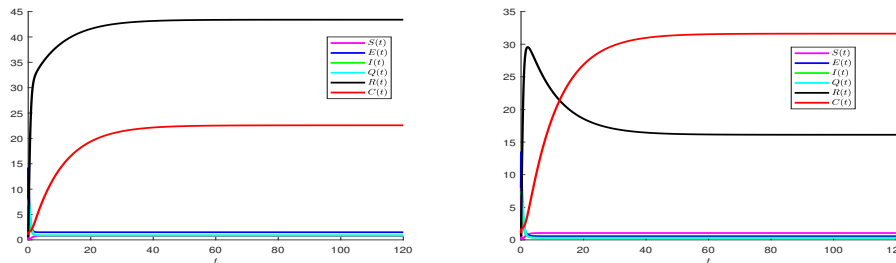


**Figure 2:**  $(S(t), E(t), I(t), Q(t), R(t), C(t))$  behaviours for (left)  $N_T = 70$ ,  $\mu = 0.1$ ,  $\beta = 0.1$ ,  $\alpha = 3$ ,  $\gamma = 3$ ,  $\delta = 5$ ,  $\lambda = 5$ ,  $\mathcal{R}_0 = 1.73 > 1$  and for (right)  $N_T = 50$ ,  $\mu = 0.1$ ,  $\beta = 0.1$ ,  $\alpha = 3$ ,  $\gamma = 3$ ,  $\delta = 5$ ,  $\lambda = 5$ ,  $\mathcal{R}_0 = 1.24 > 1$ .

### 7 Concluding Remarks

There is a dearth of epidemiological information on the rise of the coronavirus, which would be of critical importance to the structure and execution of auspicious, specially designated, sustainable general welfare intercessions, isolation and travel limitations. Infectious disease modelling is a tool that can be used to study the mechanisms by which diseases spread, predict the future course of the disease outbreaks and evaluate epidemic control strategies. A mathematical 6D dynamical system modelling an SEIQR model of transmissibility of the novel Covid-19 is studied. A profound study is given. The analysis of the local and global stability of equilibrium points is presented. It is shown that the disease-persistence equilibrium is globally asymptotically stable when  $\mathcal{R}_0 > 1$ . However, the disease-free equilibrium is globally asymptotically stable when  $\mathcal{R}_0 \leq 1$ .

### Acknowledgment

The author wish to thank the Editor and the anonymous Reviewers for their helpful feedback to improve the quality of this manuscript.

### References

- [1] S.A. Alharbi, A.S. Rambely and A. Othman Almatroud. Dynamic Modelling of Boosting the Immune System and Its Functions by Vitamins Intervention. *Nonlinear Dynamics and Systems Theory* **19** (2) (2019) 263–273.
- [2] T. Chen, J. Rui, Q. Wang, Z. Zhao, J.A. Cui and L. Yin. A mathematical model for simulating the phase-based transmissibility of a novel coronavirus. *Infectious Diseases of Poverty* **9** (24) (2020), 8pages.
- [3] O. Diekmann and J. Heesterbeek. On the definition and the computation of the basic reproduction ratio  $\mathcal{R}_0$  in models for infectious diseases in heterogeneous populations. *Journal of Mathematical Biology* **28** (4) (1990) 365–382.
- [4] E.F. Doungmo Goufo and G.M. Moremedi. Mathematical Analysis of a Differential Equation Modeling Charged Elements Aggregating in a Relativistic Zero-Magnetic Field. *Nonlinear Dynamics and Systems Theory* **19** (1-SI) (2019) 141–150.

- [5] L. Lopez and X. Rodo. A modified SEIR model to predict the COVID-19 outbreak in Spain and Italy: simulating control scenarios and multi-scale epidemics. *Results Phys* (2021) Feb; 21: 103746.
- [6] P. Van den Driessche and J. Watmough. Reproduction Numbers and Sub-Threshold Endemic Equilibria for Compartmental Models of Disease Transmission. *Math. Biosci.* **180** (2002) 29–48.
- [7] C. Huang, Y. Wang, X. Li, L. Ren, J. Zhao and Y. Hu Y. *Clinical Features of Patients Infected with 2019 Novel Coronavirus in Wuhan*. China. *Lancet*. 2020.
- [8] M. El Hajji. Modelling and optimal control for Chikungunya disease. *Theory Biosci* **140** (2021) 27–44.
- [9] M. El Hajji, S. Sayari and A. Zaghdani. Mathematical analysis of an "SIR" epidemic model in a continuous reactor - deterministic and probabilistic approaches. *J. Korean Math. Soc.* **58** (1) (2021) 45–67.
- [10] M. El Hajji. How can inter-specific interferences explain coexistence or confirm the competitive exclusion principle in a chemostat. *Int. J. Biomath.* **11** (8) (2018), 1850111.
- [11] J.K. Hale. *Ordinary Differential Equations*. John Wiley & Sons, New York. 1969.
- [12] J.P. LaSalle. *The Stability of Dynamical Systems*. SIAM, Philadelphia, 1976.
- [13] Q. Li, X. Guan, P. Wu, X. Wang, L. Zhou and Y. Tong Y. Early transmission dynamics in Wuhan, China, of novel coronavirus-infected pneumonia. *N. Engl. J. Med.* **382** (13) (2020) 1–9.
- [14] B. Labeled, S. Kaouache and M. S. Abdelouahab. Control of a Novel Class of Uncertain Fractional-Order Hyperchaotic Systems with External Disturbances via Sliding Mode Controller. *Nonlinear Dynamics and Systems Theory* **20** (2) (2020) 203–213.
- [15] M. Z. Ndi and A. K. Supriatna. Stochastic Dengue Mathematical Model in the Presence of Wolbachia: Exploring the Disease Extinction. *Nonlinear Dynamics and Systems Theory* **20** (2) (2020) 214–227.

CAMBRIDGE SCIENTIFIC PUBLISHERS

AN INTERNATIONAL BOOK SERIES  
STABILITY OSCILLATIONS AND OPTIMIZATION OF SYSTEMS

**Matrix Equations, Spectral Problems and Stability of Dynamic Systems**

*Stability, Oscillations and Optimization of Systems: Volume 2,*  
XX+270 pp, 2008 ISBN 978-1-904868-52-1 £55/\$100/€80

**A.G. Mazko**

*Institute of Mathematics, National Academy of Sciences of Ukraine, Kyiv, Ukraine*

This volume presents new matrix and operator methods of investigations in systems theory, related spectral problems, and their applications in stability analysis of various classes of dynamic systems. Providing new directions for future promising investigations, **Matrix Equations, Spectral Problems and Stability of Dynamic Systems**

- furnishes general methods for localization of eigenvalues of matrices, matrix polynomials and functions
- develops operator methods in a matrix space
- evolves the inertia theory of transformable matrix equations
- describes general spectral problems for matrix polynomials and functions in the form of matrix equations
- presents new Lyapunov type equations for various classes of dynamic systems as excellent algebraic approaches to solution of spectral problems
- demonstrates effective application of the matrix equations approaches in stability analysis of controllable systems
- gives new expression for the solutions of linear arbitrary order differential and difference systems
- advances the stability theory of positive and monotone dynamic systems in partially ordered Banach space
- systematizes comparison methods in stability theory
- and more!

Containing over 1200 equations, and references, this readily accessible resource is excellent for pure and applied mathematicians, analysts, graduate students and undergraduates specializing in stability and control theory, matrix analysis and its applications.

**CONTENTS**

**Preface • Preliminaries • Location of Matrix Spectrum with Respect to Plane Curves • Analogues of the Lyapunov Equation for Matrix Functions • Linear Dynamic Systems. Analysis of Spectrum and Solutions • Matrix Equations and Law of Inertia • Stability of Dynamic Systems in Partially Ordered Space • Appendix • References • Notation • Index**

---

Please send order form to:

**Cambridge Scientific Publishers**

PO Box 806, Cottenham, Cambridge CB4 8RT Telephone: +44 (0) 1954 251283  
Fax: +44 (0) 1954 252517 Email: [janie.wardle@cambridgescientificpublishers.com](mailto:janie.wardle@cambridgescientificpublishers.com)  
Or buy direct from our secure website: [www.cambridgescientificpublishers.com](http://www.cambridgescientificpublishers.com)

---